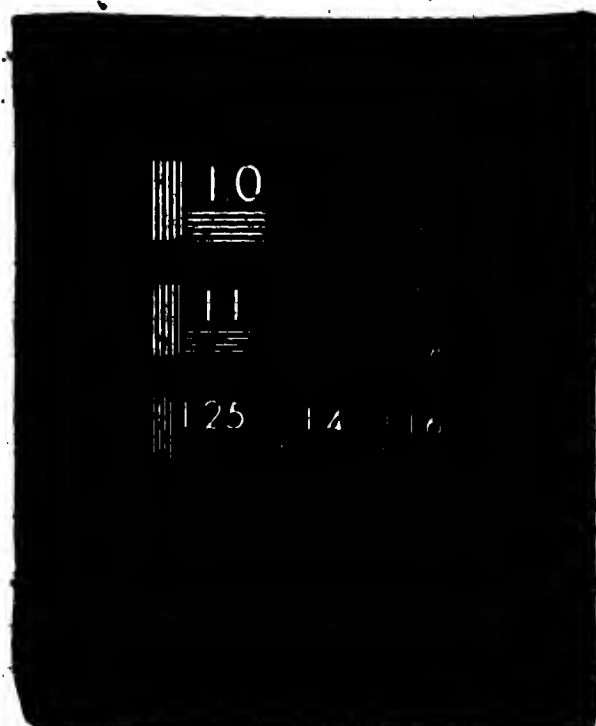


1 OF 2

N77 30474

UNCLAS



(NASA-CR-153411) BALL TO SEPARATOR CONTACT N77-30474  
FORCES IN ANGULAR CONTACT BALL BEARINGS  
UNDER THRUST AND RADIAL LOADS Status Report  
(California State Univ., Northridge.) 110 p Unclas  
HC AC6/MF A01 CSCL 131 G3/37 42008

**Study of Rolling Element Dynamic Interactions  
With Separators and Raceway Paths**

**Ball to Separator Contact Forces  
in  
Angular Contact Ball Bearings Under Thrust and Radial Loads**

**California State University, Northridge  
School of Engineering and Computer Science  
Northridge, California 91330**

**Prepared by Lester J. Nypan**

**July 30, 1977**

**Status Report MSG 3065  
Prepared for NASA Lewis Research Center  
Cleveland, Ohio 44135**

## Table of Contents

	Page
I Abstract	1
II Introduction	2
III Separator Study Machine	3
IV Test Bearings	6
V Separator Force Transducer	6
VI Force Transducer Calibration	8
VII Experimental Procedure	8
VIII Data Analysis	9
IX Results and Discussion	12
X Conclusion	17
XI References	19
Appendix I Computer Program	103

## List of Figures

Figure		Page
1	Separator Study Machine	19
2	Test Bearing in Separator Study Machine	22
3	Ball Contact Force Transducer	23
4	Sample Force Transducer Calibration	24
5	Example of Photographs Taken	25
6	Ball Contact Forces at 4000 rpm	26
7	Ball Contact Forces at 8000 rpm	44
8	Ball Contact Forces at 12000 rpm	65
9	Variation of Magnitude of Cage Forces with Speed-Radial Loads	74
10	Variation of Location of Cage Forces with Speed-Radial Loads	78
11	Variation of Magnitude of Cage Forces with Speed-Thrust Loads	83
12	Cage to Inner Race Land Contact Force	86
13	Cage to Inner Race Land Clearance Variation with Location	88
14	Cage to Shaft Speed Ratios	93

### List of Tables

Table		Page
1	Test Bearing Specifications	99
2	Speed, Load and Spring Constants	100
3	Spring Constants and Bearings Used	101
4	Calculated Number of Shaft Revolutions Between Photographs	102

### Abstract

Experimental data is reported on ball to cage contact forces in a 110 mm bore ball bearing operating at speeds to 12000 rpm under radial and thrust loads. Information is also reported on cage to inner race land contact force, cage to inner race land clearance, and cage to shaft speed ratios.

## II Introduction

Current developments in jet engine technology are placing more stringent demands on gas turbine design. There is a constantly increasing requirement for engines to develop greater thrust outputs. In addition to this increased loading the need to raise the thrust/weight ratio of engines and to improve the fuel consumption has led to higher rotor speeds and operating temperatures, lighter components and correspondingly increased structural flexibility. In anticipation of tomorrow's requirements, further advanced knowledge of engine component technology must be obtained.(1)\*

In the case of rolling contact bearings there is a need for a better understanding of cage and rolling element dynamics, particularly in ultra-high speed applications.(2,3,4,5)

Recently developed, advanced bearing theories have resulted in computerized optimization of rolling element bearing designs and in some cases accurate prediction of bearing performance. These developments and advances by no means substitute for testing of rolling element bearings which for many years was the basis for bearing development. To the contrary, the need for more refined data gathering methods has become obvious. Tests are needed to verify the theories which form the foundation of these computer programs. Also, performance tests and studies will always be needed to refine bearing designs for critical applications.

The interaction between the rolling elements of a bearing with the raceways and separators is particularly difficult to measure due

-----  
\*Numbers in parentheses designate references at end of report.



to the rapidity of their motion. The kinematic behavior and the resulting forces acting on a rolling element/separator/raceway assembly could in the past be measured only by tests where the operating conditions were drastically simplified.

### III Separator Study Machine

An optical bearing test rig has been constructed to operate the bearing and make photographic records of the rolling elements and separator behavior. Figure 1a shows an overall view of the machine as it is presently installed in the Dynamics Laboratory of the Engineering Building at California State University, Northridge. The machine was originally assembled by Industrial Tectonics, Inc., Compton, Calif., and has been used in industrial bearing research, and in a ball motion study reported in (6).

The bearing test rig is basically a shaft supported by a pair of preloaded ball bearings at one end and the test bearing at the other end. One face of the test bearing is exposed to allow free view of the balls and the separator. Radial load was applied to the test bearing by a hydraulic actuator through a cable loop over the bearing housing. The shaft was driven by a 75 hp hydraulic motor through a geared belt drive, giving speeds infinitely variable from 100 to 15,000 rpm. Figure 1b is a schematic of the shaft assembly.

Lubricating oil for under race cooling and test bearing lubrication is supplied through a series of orifices from the rear of the test bearing.

Due to the high tangential velocities present when a bearing is rotated at shaft speeds up to 15,000 rpm, conventional photograph techniques are inadequate. The difficulty lies in obtaining photo-

graphs having sufficient resolution for analysis when very short exposures are required to freeze the motion of the bearing elements. This problem has been overcome by eliminating the gross rotational motion using a derotation prism. The resulting image thus presents the differential motion between the separator and the rolling element, enabling observation and photographs to be made of an individual separator pocket. Derotation is accomplished by synchronizing the rotation of a Pechan prism at half-speed with the rotation of the ball separator, thus causing the apparent image rotation and the true separator rotation to coincide. This results in the derotated image of the area of interest being imaged on the film plane of a camera. Light rays from the illuminated bearing are collected through the front window of the instrument. This window is optically coated to reject ultraviolet energy produced by ultraviolet lamps, serving the circuit for the prism speed control. From the window, the rays travel through collimator lenses and the Pechan prism before they travel through the exit lenses. Their path is then deflected by mirrors which fold the image in different directions. Figure 1c shows light paths through the scanner.

One light trace travels to a beam splitter where approximately 15 % of the light is reflected to the eyepiece optics to provide an image observable to the operator. The balance of light enters the aperture of the pulse camera.

Alignment and positioning of the optical elements ensure that the eyepiece observes the same image quality and format as that which the film sees.

Another image is folded and demagnified in the transfer lens assembly before it enters the camera.

A derotated image of the luminous painted segment of the test bearing separator is optically folded out and directed toward an

image splitting mirror surface wedge which proportions the light entering two photomultiplier tube photocathodes. The electronic signals from these tubes are used by the tracking system to control the prism speed.

A tracking system holds the image of a selected point at the test bearing separator in the field of view. It will accommodate a variation of up to 10% of a fixed ratio of separator-to-shaft speed without loss of the ability to lock onto the proper position within one revolution of the bearing retainer.

It is necessary to sense the tracking error in angular position of the derotation prism to provide an input for the servo system. This error signal is provided in the form of the difference in output of two multiplier phototubes.

A sector on the bearing retainer is coated with fluorescent paint and illuminated with ultraviolet light. An image of the sector of arc is formed in a plane containing the apex of a mirror surface wedge. The light striking the two surfaces of the wedge is reflected and illuminates the photocathode of the photomultiplier tubes. Rotation of the prism results in a displacement of the image and a consequent increase in the output of one tube and decrease in the output of the other.

Electronic filtering is provided to discriminate between the steady signal due to the ultraviolet excitation of the phosphor and any intermittent excitation due to strobe lamps to reduce any interaction between the level of light striking the phosphor and the error signal produced by the photomultipliers.

Four Chadwick-Helmuth Strobex lamps are flashed at the 16-frame-per-second camera rate to illuminate the separator and to stop the images of the protractors on the inner and outer races of the bearing so that angular position information is recorded on the photographs.

Four mercury vapor spot lamps with ultraviolet filters illuminate the fluorescent patch for the tracking system.

The camera used was a Neyhard Enterprises model G-4. The camera film magazine accepts 100 or 200 foot reels of 35 mm film. The camera has a data box, the image of which is projected onto each film frame.

#### IV Test Bearings

The bearings used in the ball to separator contact force investigation were mainshaft thrust bearings used in the Pratt and Whitney TF 30 gas turbine engine, part numbers PWA 506110 and PWA 506111. Dimensions and other characteristics of these bearings are given in Table 1.

#### V Separator Force Transducer

A ball contact force transducer was constructed on the bearing separator by introducing a cantilever beam between two of the bearing balls. The cantilever beam replaced a rigid separating element so that cantilever beam deflection would give an indication of the ball contact force. A hole was drilled through one of the side rails of the separator to hold the fixed end of the cantilever beam. A notch to frame the deflected end of the cantilever was cut in the other side rail opposite the hole. Various beam cross sections were used depending on contact forces and deflections encountered. A Teflon

rubbing block was cemented to the center portion of the beam to make up the normal ball spacing dimension of the rigid separator element replaced by the ball force indicating beam. A duplicate modification was installed at 180° to the first to maintain separator balance.

With the shaft and test bearing operating at a speed and load condition to be investigated, the derotation prism was synchronized with the separator to produce a stationary image of the deflecting end of the cantilever beam as the balls and separator repeatedly moved through loaded and unloaded regions of the bearing. The 16 frame per second 35 mm instrumentation camera photographed the motions of the cantilever beam deflections relative to the notch in the separator. As ball contact forces may be expected to be a repetitive event from revolution to revolution the relatively slow framing rate can be extended to a very high effective framing rate by taking a large number of photographs over many revolutions of the bearing. This gives frames covering 0 to 360° to the applied load. The angle to the applied load was indicated by the position of the cantilever beam relative to a fixed protractor on the bearing outer race. Radial loads were applied vertically at the 360 (0) degree mark on the protractor. Static photographs with the cantilever beam at 90, 180, and 270 degrees to the vertical clearly indicated positive, zero, and negative deflections consistent with the weight of 19.05 mm (0.750 in) steel balls.

Figure 3 shows one of the ball contact force transducers as constructed.

## VI Force Transducer Calibration

The force transducing cantilever beam was assembled into the separator with epoxy resin with the Teflon spacing element also epoxied in place. The separator was held in a small vise and loaded with a wire hook positioned at the estimated ball contact location. A small weight pan and 6.35 mm (0.250 in.) balls were used to load the cantilever beam. Cantilever deflections were photographed. Figure 4 gives the force-deflection relation for the stiffest cantilever beam used (61.8 N/mm). The permanent deformation evident in Fig. 4 did not affect ball force measurements as forces encountered did not exceed 27.5 N (6.21 lb.). Table 3 gives values of spring constant and bearings used in the course of investigation.

## VII Experimental Procedure

The lubricating oil used throughout the tests was a 5-centistoke neopentyl polyol (tetra) ester. This is a type II oil which conforms to specification MIL-L-23699. Test bearing inlet oil was heated and controlled to 485° K (150±2°F).

The Separator Study Machine bearing rig was started with a 500 lb thrust load and brought up to speed, the desired load condition applied, the prism synchronized with the separator and 100 to 200 photographs taken. Film used was Kodak 2475 Recording Film. It was cut into lengths fitting stainless steel reels and developed in a small tank with HC 110 developer, dilution A, for 30 minutes at laboratory room temperature. This seemed to give images of adequate contrast, with background fog just beginning to be noticeable on fresh film.

### VIII Data Analysis

After chemical processing of the film was completed the film was respliced and each frame was numbered.

The film was read with a Benson-Lehner model N-2 film reader capable of indicating 4 digits with the least digit representing 0.005 mm (0.0002 in.) in the film image. The film images, however, varied in density and sharpness from frame to frame due to variation in Xenon flash intensity, duration, and jitter in flash initiation among the four Xenon flash tubes, as well as from oil splash in the bearing chamber and on the bearing chamber window.

Readings were taken by aligning a cross-hair onto the lowest edge of the notch for R1, the bottom of the beam end for R2, the top of the beam end for R3, and the top of the notch for R4. The computer program listed in Appendix I was used to calculate differences  $R2-R1$ ,  $R3-R1$ ,  $R4-R1$ ,  $R3-R2$ ,  $R4-R3$ , and  $R4-R2$ . From  $R4-R1$  and  $R3-R2$  a consistency check was available to pull out or correct obviously defective readings as the notch dimension and beam height should always be of constant value. After subtraction of undeflected (zero) readings, the other four differences give four separate indications of the beam deflection in that film frame.

The computer program also calculated average values of notch size for the photo set and normalized the deflection indications on the average notch size to compensate for image size variation with focus setting. It then scales the deflections to the lineal measured notch dimension. The deflection indications are then multiplied by the spring constant determined in the force transducer calibration, and are listed and plotted by a Calcomp plotter.

Figure 5 is representative of photographs obtained.

It was possible to determine cage to shaft speed ratio with some accuracy over 10 successive photographs of multiple shaft revolutions from the following considerations.

The derotating prism is synchronized to rotate at half the separator speed thus producing a stationary image of the separator to be photographed. Protractors which are mounted on the stationary outer race and on the rotating inner race are visible in the photographs. Four Xenon flash tubes with a flash duration of 50 microseconds permit clear instantaneous photographs of the stationary separator and stop the motion of the protractor images. Typically 100 to 200 photographs were taken at a cine frame rate of 16 per second for each case investigated.

In these photographs the angle turned through by the separator (cage) can be determined from the difference in angle on the stationary outer race protractor between two consecutive frames. Thus,

$$2\Delta\theta_p = \Delta\theta_c = \Delta\theta_o = \left(\frac{W_c}{W_s}\right) W_s \Delta t \quad (1)$$

where:

$\Delta\theta_p$  = true prism angle turned through

$\Delta\theta_c$  = true cage angle turned through

$\Delta\theta_o$  = angle difference  $+360^\circ \times$  number of revolutions between photographs

$\frac{W_c}{W_s}$  = separator to shaft speed ratio in the operating bearing

$W_s$  = shaft speed

$\Delta t$  = time between photographs

The protractors are engraved with angle increasing in the direction of shaft rotation. The shaft turns through a greater angle than does the separator; consequently, the cage photographs centered on the transducer in the cage show the inner race angles decreasing. The



true angle that the shaft has turned through in the 1/16 second between successive frames may be determined from the protractor angles photographed by

$$\Delta\theta_s = \Delta\theta_o - \Delta\theta_{st} = \left(\frac{W_c}{W_s}\right)W_s \Delta t - W_s \Delta t \quad (2)$$

where:

$\Delta\theta_s$  = angle difference on inner race protractor between photographs

$(\theta_{s_{i+1}} - \theta_{s_i})$  with  $i$  being the frame number

$\Delta\theta_{st}$  = true angle turned through by the shaft in time  $\Delta t$

From equation 2, then  $\Delta\theta_{st} = \Delta\theta_o - \Delta\theta_s$ , and  $W_c \Delta t = \Delta\theta_o$ ,

$W_s \Delta t = \Delta\theta_{st}$  so:

$$\frac{W_c}{W_s} = \frac{\Delta\theta_o}{\Delta\theta_o - \Delta\theta_s} \quad (3)$$

where  $\Delta\theta_s$  is a negative number.

Care must be taken in calculating angle differences  $\Delta\theta_o$  and  $\Delta\theta_s$  between photographs and in using equation (3). Multiple revolutions of shaft and separator occur without this being apparent in the photographs. At 16 frames per second with a nominal value of 0.441 for  $W_c/W_s$  the ranges of angle differences given in Table 4 may be anticipated.

To obtain the true angle of rotation of the cage between successive frames, it is necessary to:

1. Subtract the angle read from the reference point of the separator in the photograph from that read in the i-1 frame.
2. Determine the number of full rotations between frames using Table 4.
3. Add the number of full rotations to the difference found in step 1.

These considerations led to the cage/shaft speed ratios that appear on the cage force figure captions and in the cage/shaft speed ratio versus load figures.

#### IX Results and Discussion

This investigation was undertaken to experimentally evaluate ball to cage contact forces. It was subsequently noted that information on cage to inner race land contact force, cage to inner race land operating clearance, and cage to shaft speed ratios could also be extracted from the data obtained.

##### A. Ball to Cage Contact Forces

The principal results of this investigation are the ball to cage contact forces shown in Figures 6-8. These show the ball force on the cage as a function of ball location in the bearing. Ball location is measured clockwise from the centerline of the radial load at 0°

(360°). Table 2 summarizes the shaft speeds, loads, spring constants, figure identification system, and loads used in the investigation.

Different spring constants were necessary as the investigation progressed from 1000 to 4000 rpm and to higher speeds. Larger forces were

encountered and cantilever deflections approaching the ball to cage pocket clearance were observed.

Data was obtained at 1000 rpm with a spring constant of 1.49 N/mm (8.51 lb/in). These forces were small and of similar nature to those at higher speeds. The 1000 rpm results are not presented as they are too small to be visible on the scales used to present the higher speed results. Centrifugal force at 12000 rpm deflected the 17.2 N/mm (98.2 lb/in) beam out to contact the cage so that friction limited the motion of the cantilever.

All the data at 12000 rpm was taken with the 61.8 N/mm (353 lb/in) spring constant cantilever. Some lower speed cases were also run with the larger spring constant cantilevers.

Positive forces in the figures are those exerted by balls tending to accelerate the cage. Negative forces are those exerted by balls tending to retard or decelerate the cage. In general the stiffer cantilever beam deflecting elements indicate greater forces, with more scatter in the film readings.

The force indicated by a cantilever deflection is created by a ball advancing into the cantilever located on the cage. A ball's advance relative to the cage, which moves with average ball speed, is determined by ball kinematics such as ball location on the raceway path, deflections, etc. The motion of the ball relative to the average ball will deflect the cantilever until the ball begins to recede from the cantilever due to ball kinematics, provided limiting traction forces are not exceeded. Thus the cantilever is deflected as much as necessary to accommodate the ball advance relative to the cage. For a given ball advance, the stiffer cantilever's deflection indicates larger force. The stiffer cantilever deflecting elements will also have smaller deflections. Errors in measuring their deflection will produce

larger variation in the force measurements. All of the variation in the figures may not be due to errors in cantilever deflection. It is possible that there is some variation in the balls' motion as they traverse various portions of raceway surfaces with possible cage motions of oscillation, rocking and impacting on balls and inner race land surfaces.

Figures 9 and 10 summarize the variation of magnitude and location of cage forces with speed for radially loaded bearings. Figure 11 summarizes the variation of magnitude of cage forces with speed for thrust loaded bearings. As might be expected the equally loaded balls in thrust loaded cases do not show much variation in cage force with ball location within the bearing.

The approximately 1 lb. negative force in pure thrust loaded cases indicates the balls are decelerating (retarding) the cage uniformly. This is consistent with the cage being driven by the higher speed shaft surface on which the cage is guided.

Centrifugal force moves the tip of the cantilever beam out by a noticeable amount in photographs taken at 12000 rpm. It is felt that the radial centrifugal deflections do not affect the deflection characteristics of the beam in the tangential direction. It was reasoned that the portion of the beam that is bent by the ball is only that part extending from a fixed end in one rail of the cage to the center of the ball pocket where contact with the ball takes place. The larger portion of the beam extends from the center of the ball pocket and through the other rail of the cage. It is acting as a straight pointer to magnify the deflection at the center of the cage pocket. Over the part of the beam stressed in bending the radial deflection is small compared to beam dimensions.

#### B. Cage to Inner Race Land Contact Force

From the data of Figures 6, 7, and 8 it was possible to derive the force between the cage and its guiding contact with the inner race land. This was obtained by taking horizontal and vertical components of each force point as plotted in Figures 6, 7, and 8. Adding vertical and horizontal forces in an 18 degree sector, and dividing by the number of forces in the sector gave the average force one of the 20 balls would exert on the cage. The sum of the 20 ball forces should equal the resultant force that the inner race must exert on the cage. The angular location of the resultant force was obtained by taking the arc tangent of the ratio of horizontal to vertical force components. Figure 12 summarizes the magnitude and direction of the cage to inner race land force due to ball contact forces for various speeds and loads. It should be noted that this did not include the 3.5N (0.78 lb) weight of the cage.

#### C. Cage to Inner Race Land Operating Clearance

Figure 13 shows the separation between the cage and the inner race as a function of location from the zero degree index on the stationary outer race protractor. What appears in Figure 13 to be cage to inner race contact may actually be a close approach or small clearance that was shadowed by the optical angle and projection of the inner race image onto the cage image in the film plane. It appears that cage motion is somewhat erratic in the 12000 rpm speed case. The thrust loaded condition indicated an almost constant cage to inner race clearance. A clearance was visible in every one of the photographs read for the thrust loaded case.

The location of the cage to shaft contact indicated in Fig. 13a seems to agree with that of Fig. 12g. Figure 13c likewise agrees with

Fig. 12b. Figure 13b, however, indicates cage to shaft contact somewhere between 45 and 190 degrees, possibly centered at 120 degrees much of the time, while the corresponding point in Fig. 12b was found to be located at 40 degrees. It would seem that there are uncertainties in the cage force measurements and their locations that are not always averaged away by the simple device of calculating an average force per ball and adding the 20 ball to cage forces vectorially to arrive at a cage to shaft resultant force.

#### D. Cage to Shaft Speed Ratios

Figure 14 shows the cage to shaft speed ratios calculated by the method described in Section VIII Data Analysis. It may be noted that data taken before January 12, 1977 (also identified by the spring constant of 4.7 N/mm) were taken with a PWA 506111 bearing while the balance of the data was taken with a PWA 506110 bearing. The different spring constants used may have influenced the cage motion through their effect on cage forces. It is also possible that internal bearing clearances changed due to changes in temperatures of bearing components. The bearings used were of split inner race construction with presumably some gothic arch to the inner race surfaces to prevent ball contact with radial oil passages between the races.

All data obtained fell between cage to shaft speed ratios of 0.465 and 0.433. There was a general trend for cage to shaft speed ratio to decrease with load. It would seem that the loads employed did not encourage skidding, and that the cage to shaft speed ratio variations observed were due to deflections of bearing components due to load and temperature.

### X Conclusion

Ball to cage contact forces were evaluated experimentally. They appear to be greatest in radially loaded bearings operating at high speed, and are of the order of 25 N (5 lb) at the maximum. Resultant cage to inner race land forces vary in a similar manner with values up to 20 N (4 lb). Resultant force as used here is the vector sum around the bearing of the average forces on each ball, and is equal to the vector sum of cage to shaft normal and tangential force components. Cage to shaft speed ratios indicated that the load conditions employed did not encourage skidding.

## XI References

1. Brown, P.F., "Bearings and Dampers for Advanced Jet Engines", Paper 700318 SAE National Air Transportation Meeting, New York, New York, April 20-23, 1970.
2. Gupta, P.K., Transient Ball Motion and Skid in Ball Bearings
3. Harris, T.A., "An Analytical Method to Predict Skidding in Thrust Loaded Angular Contact Ball Bearings", Journal of Lubrication Technology, Trans. ASME, Series F, Vol. 73, 1971, pp. 17-24.
4. Poplawski, J.V., "Slip and Cage Forces in A High Speed Roller Bearing", Journal of Lubrication Technology, Trans. ASME, Series F, Vol. 72, pp.
5. Walters, C.T., "The Dynamics of Ball Bearings", Journal of Lubrication Technology, Trans. ASME, Series F, Vol. 93, 1971, pp. 1-10.
6. Signer, H.R., "Experimental Ball Bearing Dynamics Study", NASA CR 1345 28, October 1973.



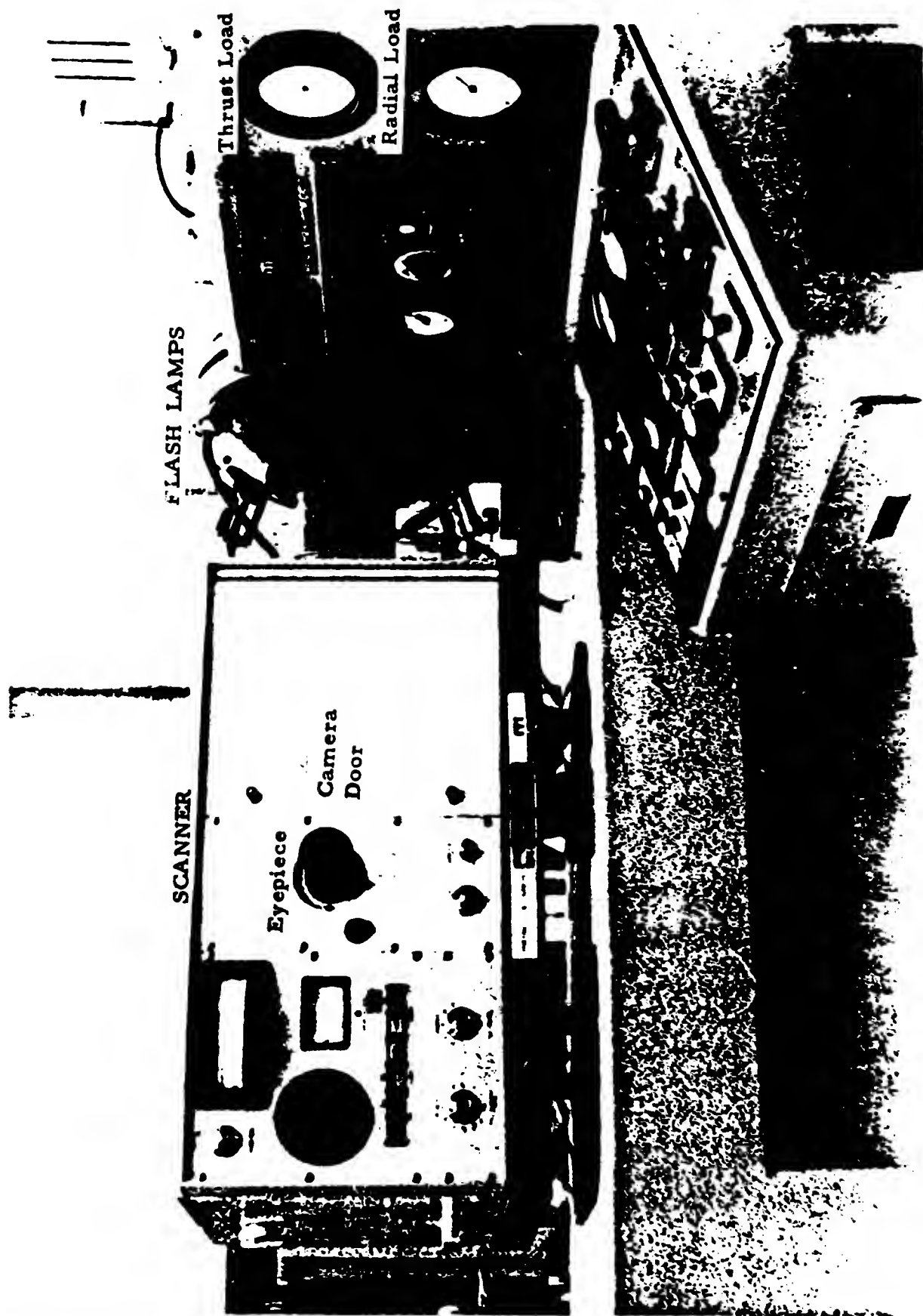


FIG. 1-A SEPARATOR  
STUDY MACHINE

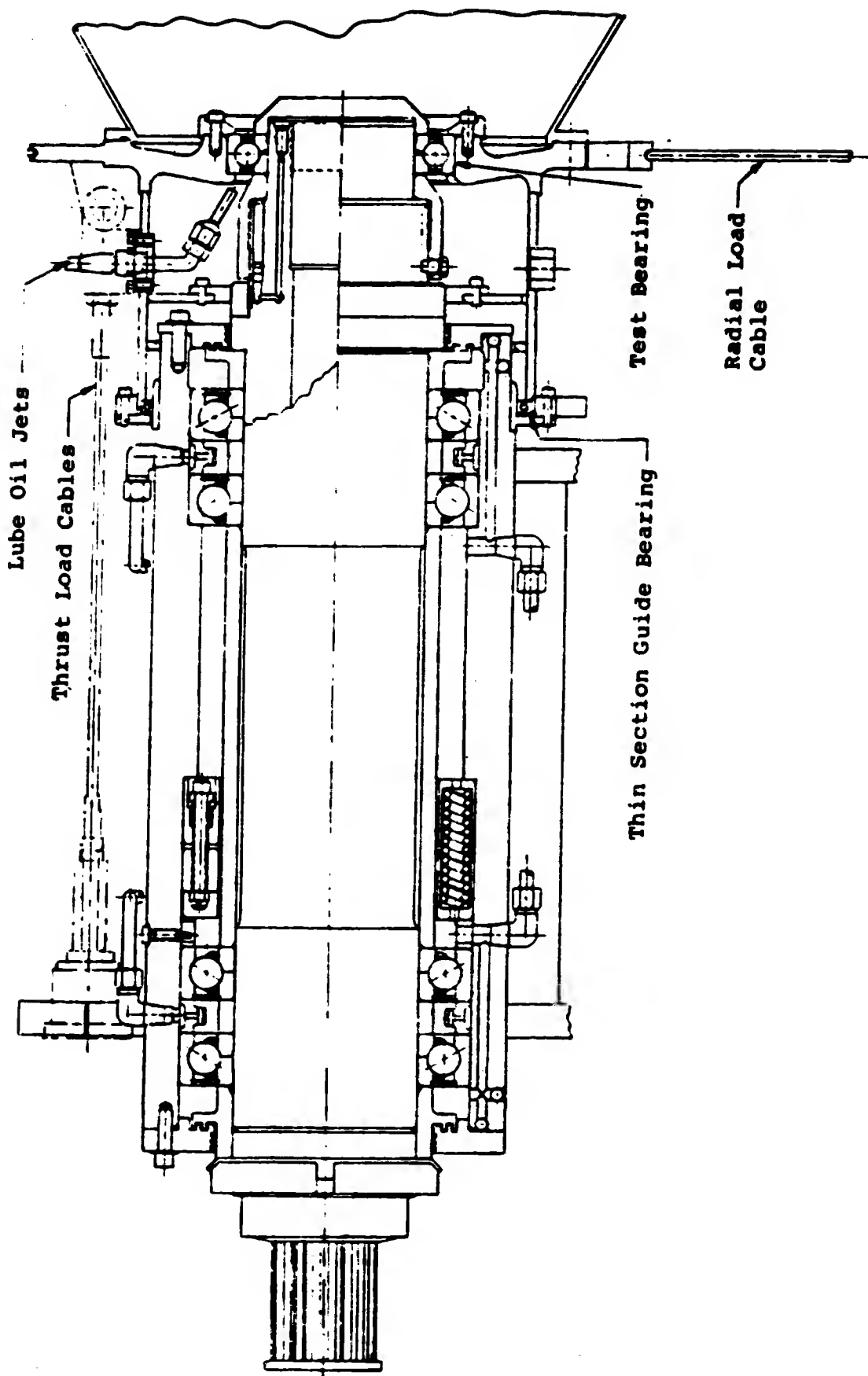


FIG. 1b SCHEMATIC OF SHAFT ASSEMBLY

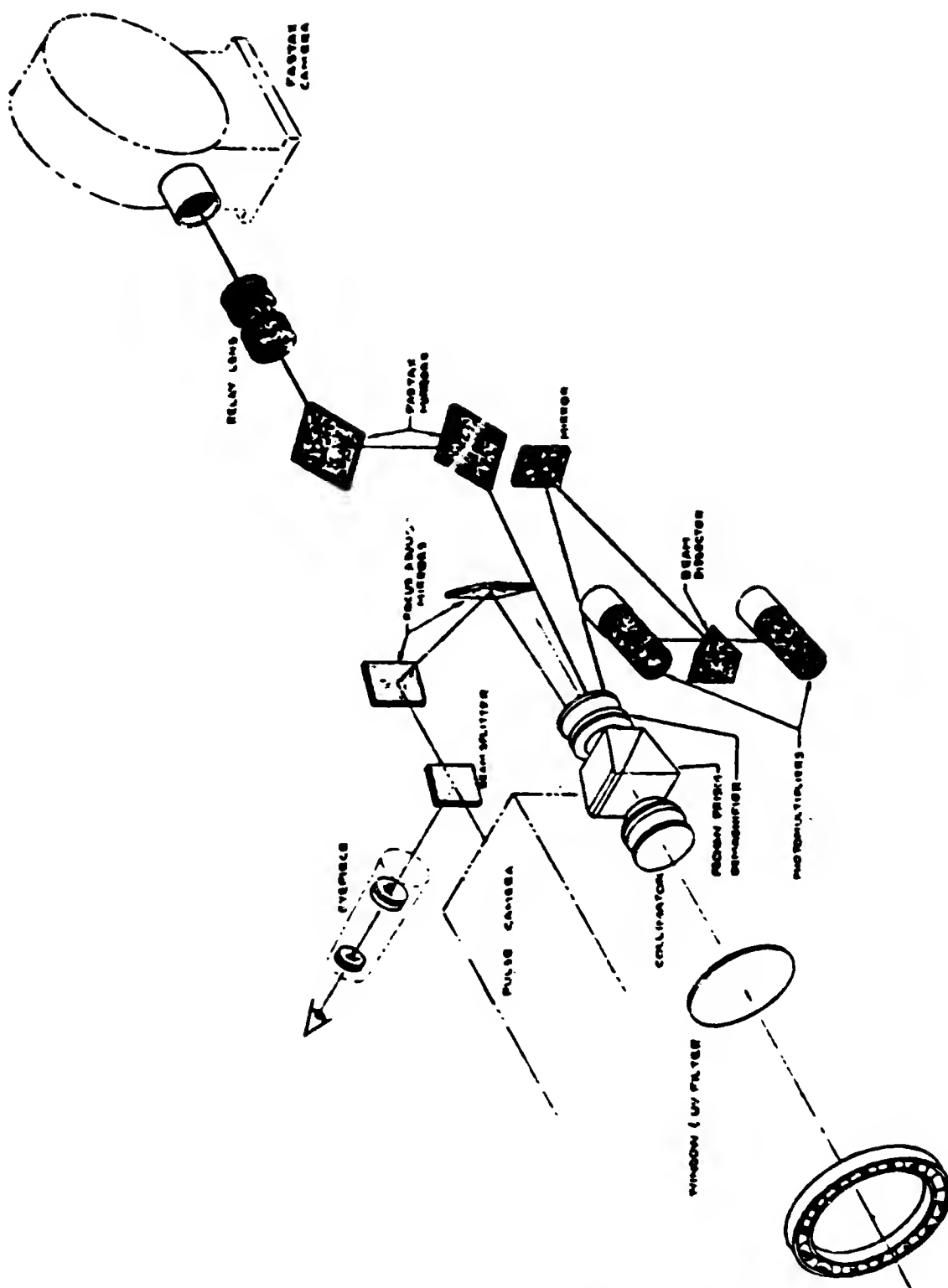


FIG. 1 c OPTICAL PATHS THROUGH THE BEARING SCANNER

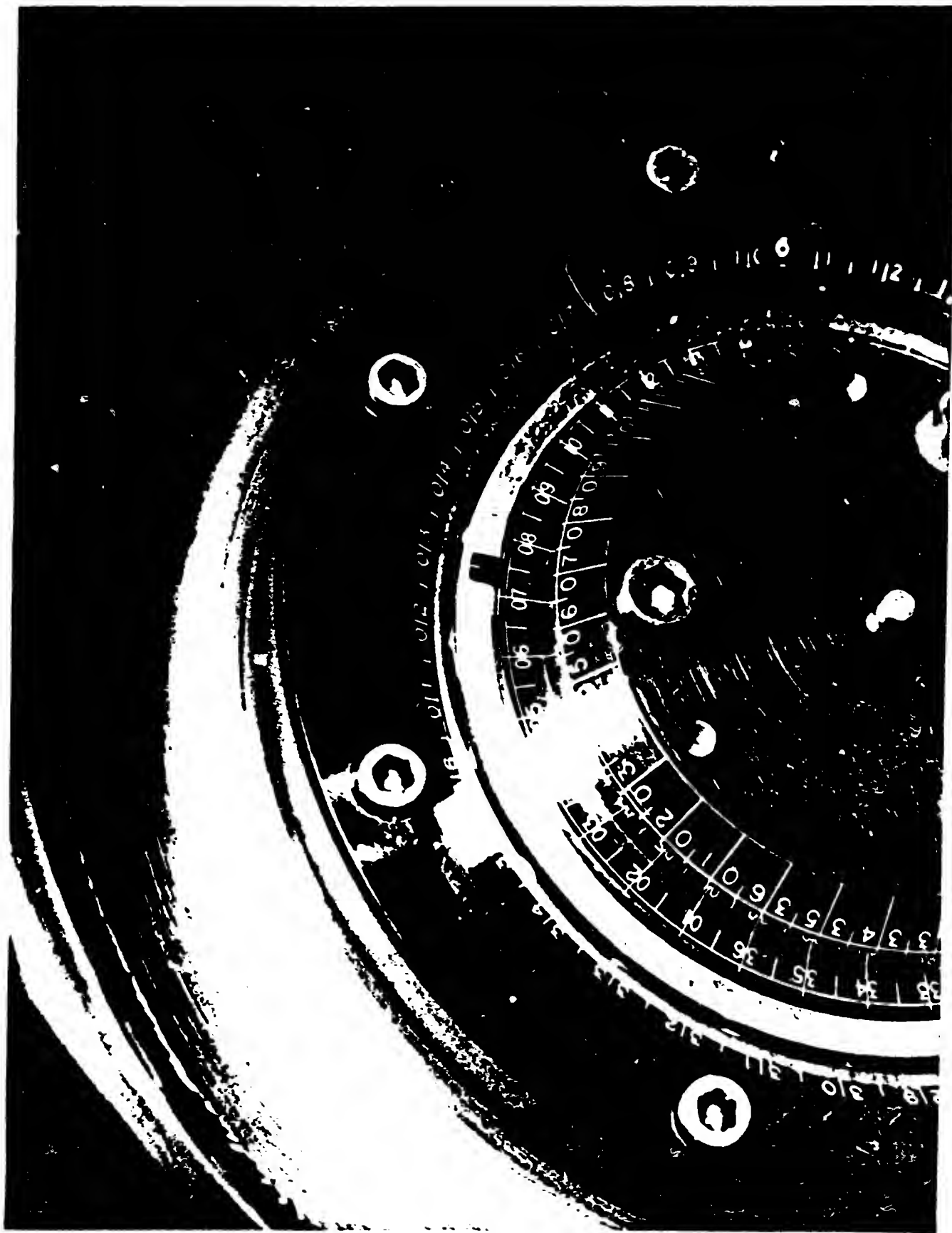


FIG. 2 TEST BEARING  
IN SEPARATOR STUDY  
MACHINE

RELIABILITY OF THE  
TESTING FACILITY IS POOR



FIG. 3 BALL CONTACT  
FORCE TRANSDUCER

7090113NYPAN1-07/14/

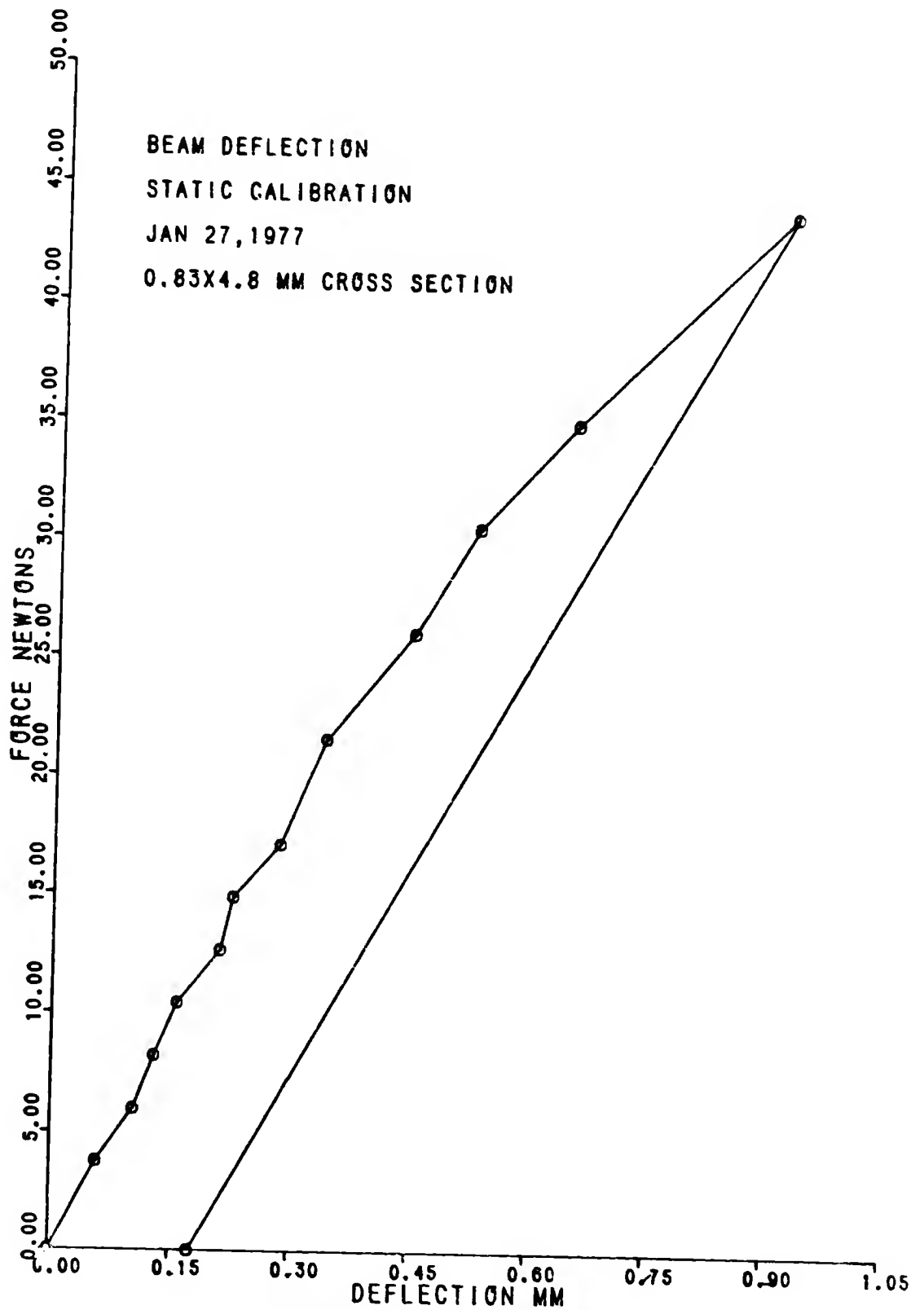


FIG. 4 SAMPLE FORCE  
TRANSDUCER CALIBRATION  
(61.8 N/mm BEAM)

REPRODUCIBILITY OF THE  
ORIGINAL PAGE IS POOR

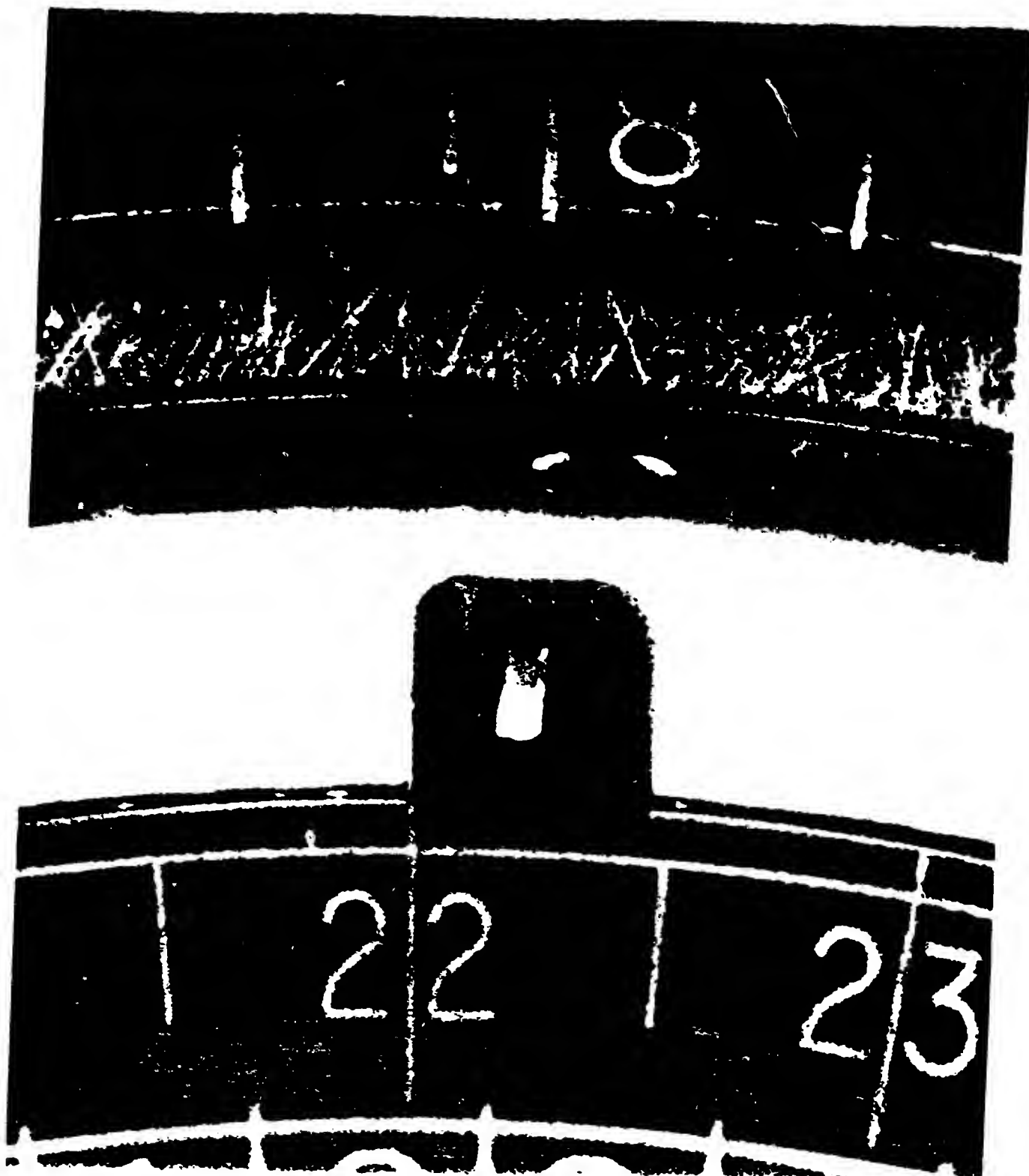


FIG. 5 EXAMPLE OF  
PHOTOGRAPHS TAKEN

REPRODUCIBILITY OF THE  
ORIGINAL PAGE IS POOR

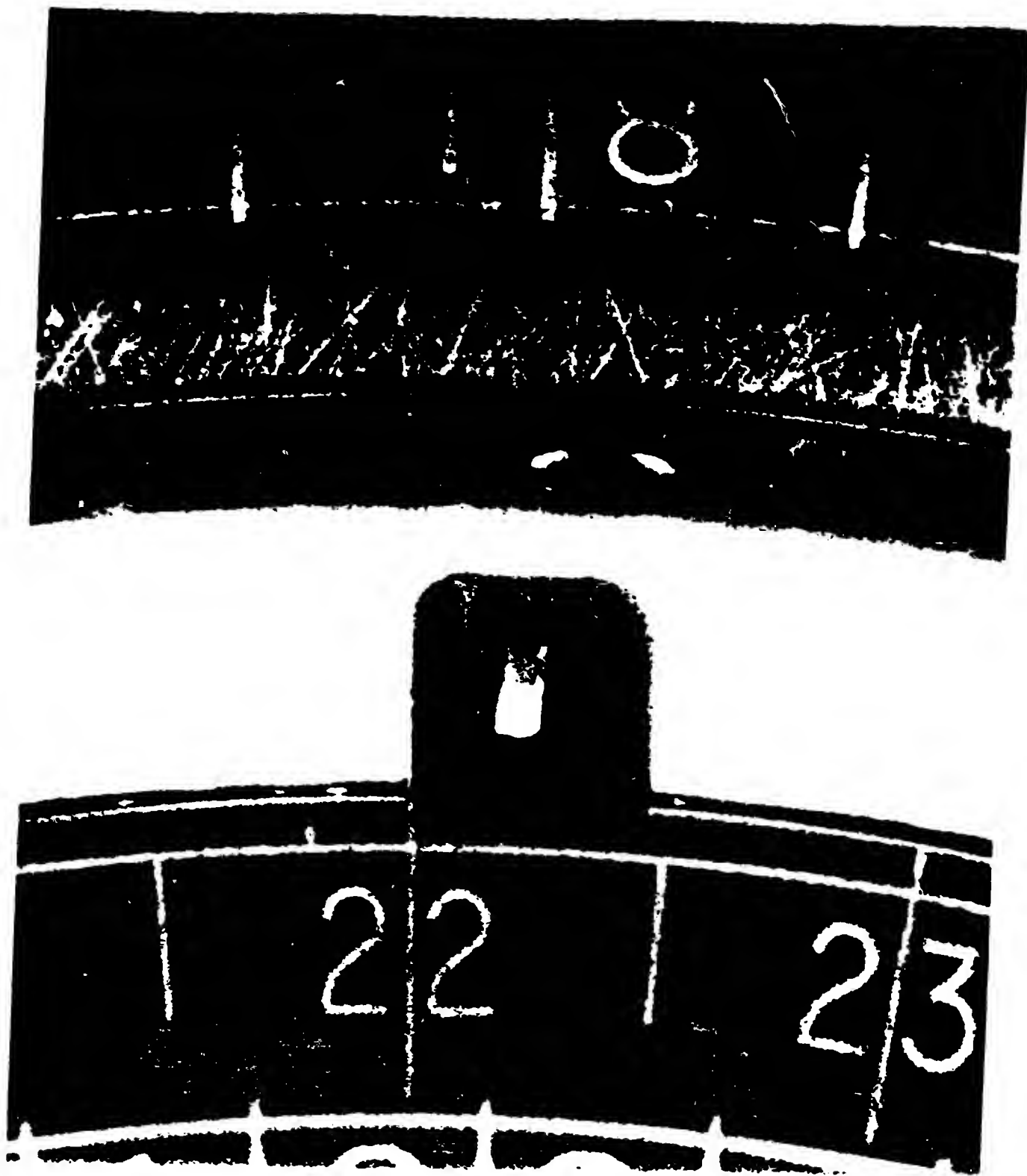


FIG. 5 EXAMPLE OF  
PHOTOGRAPHS TAKEN



706501-19N-1-AN5-1-06715777

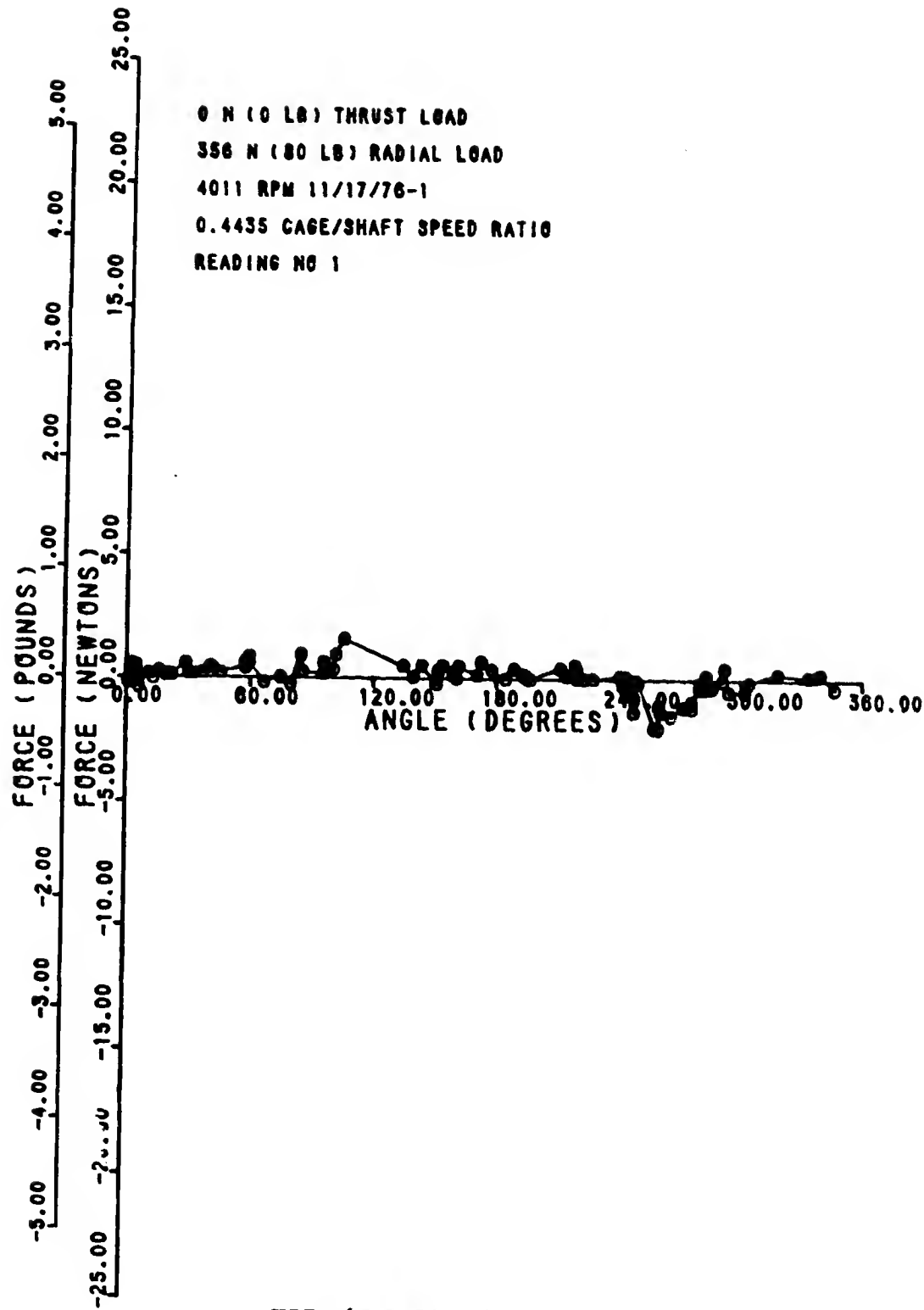


FIG. 6a-4.73 N/mm

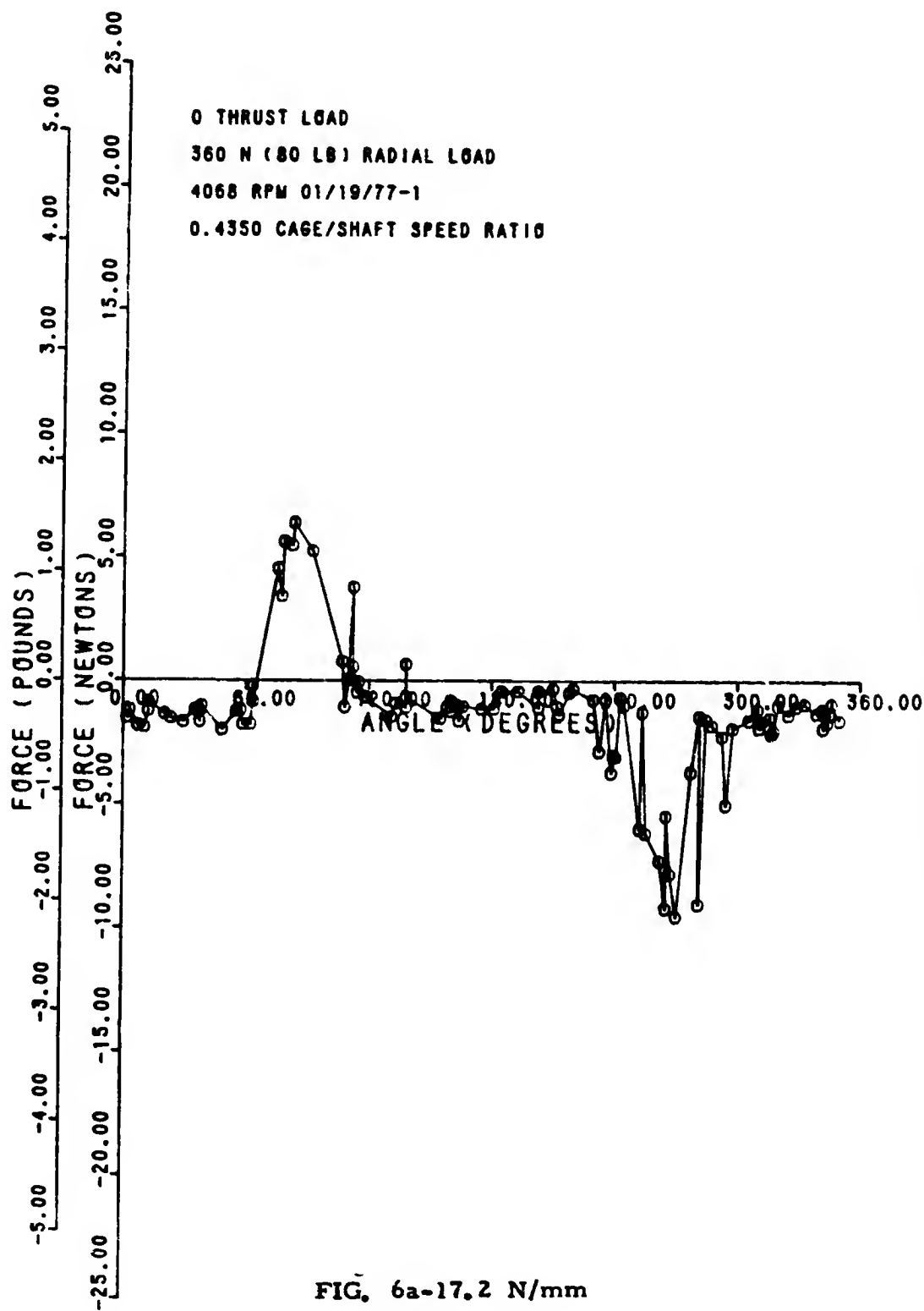


FIG. 6a-17.2 N/mm

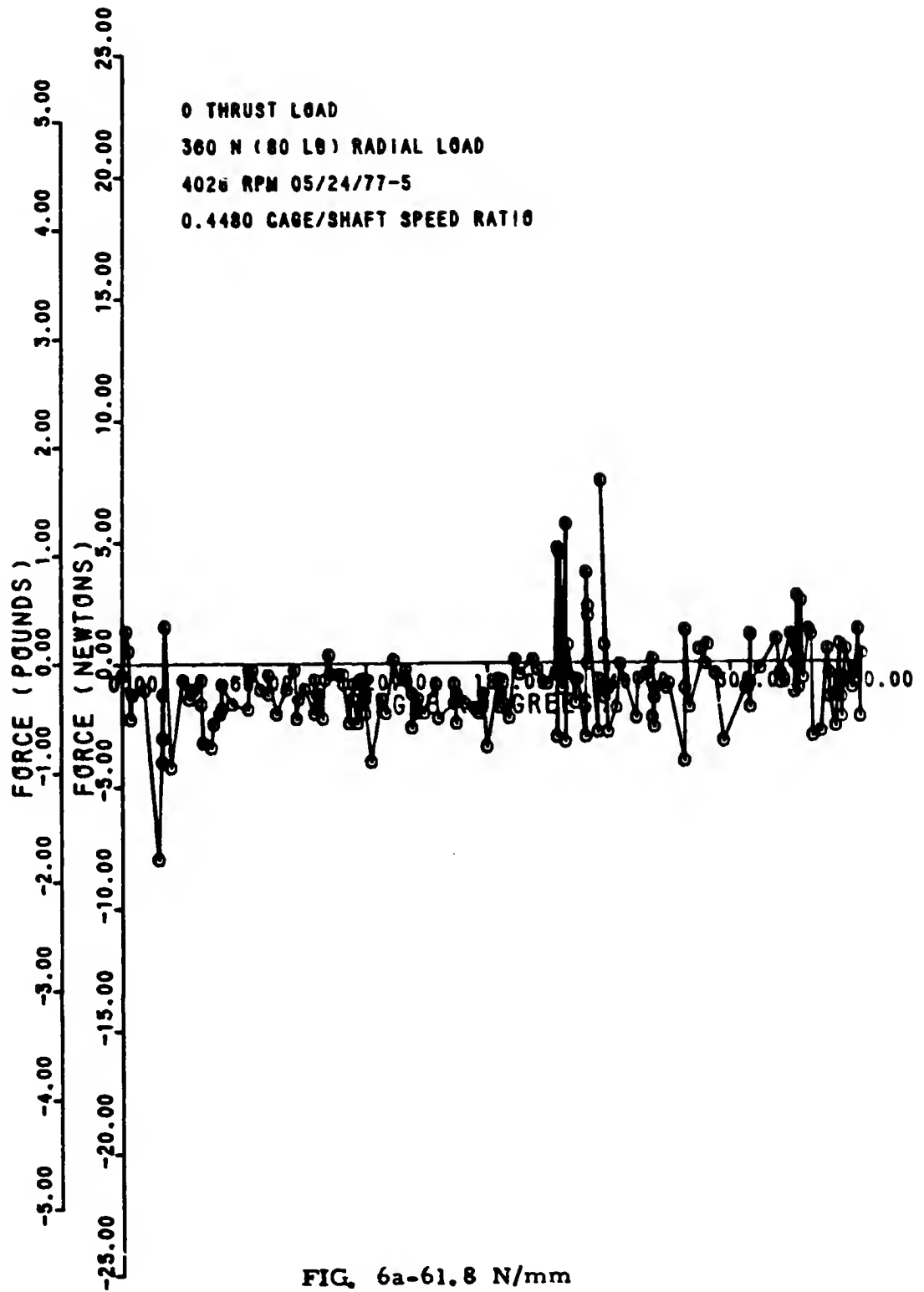


FIG. 6a-61.8 N/mm

70090113NYF AN5

06/15/77

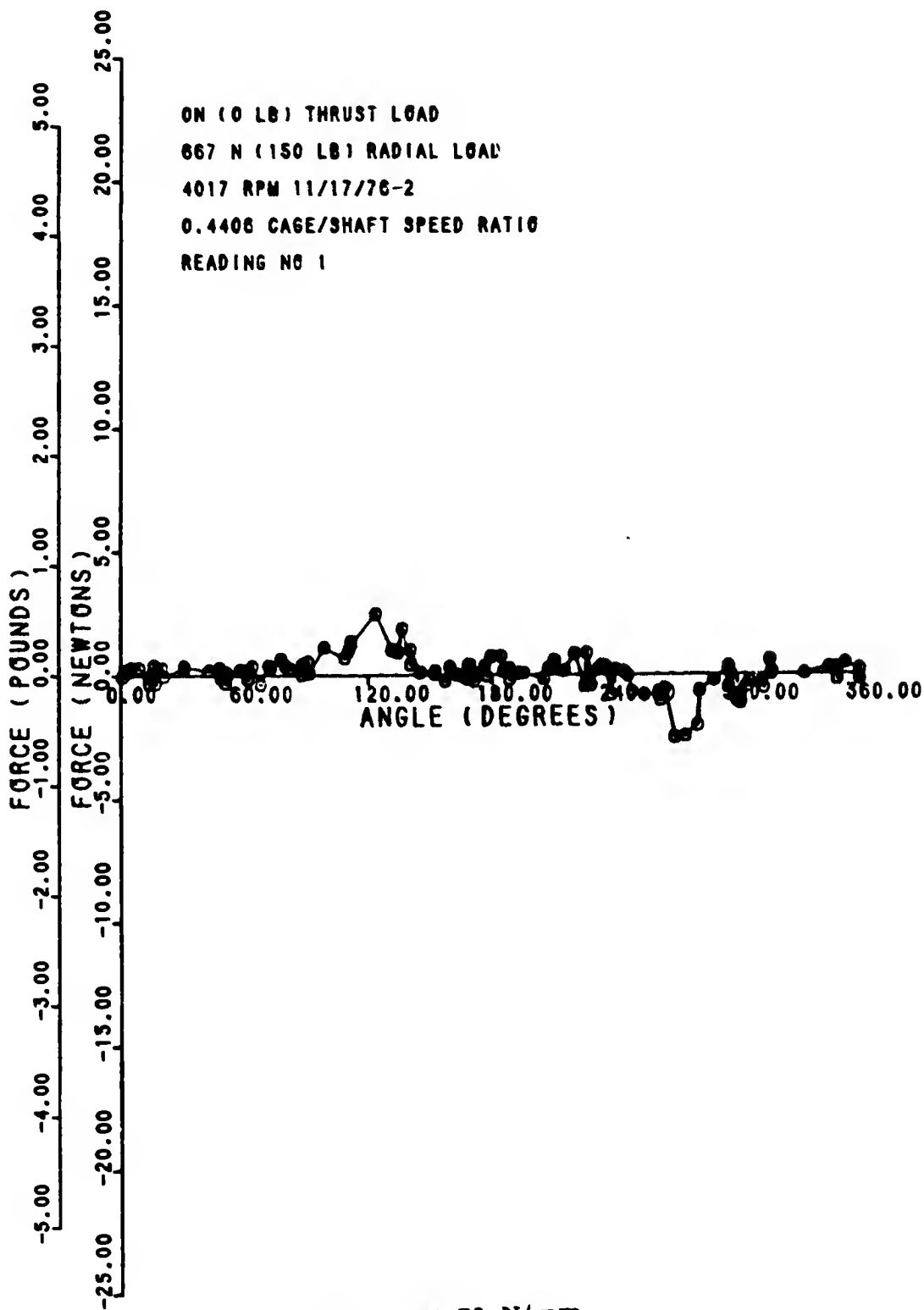


FIG. 6b-4.73 N/mm

700901:19NY: PANT  
05/06/77  
RDG # 2

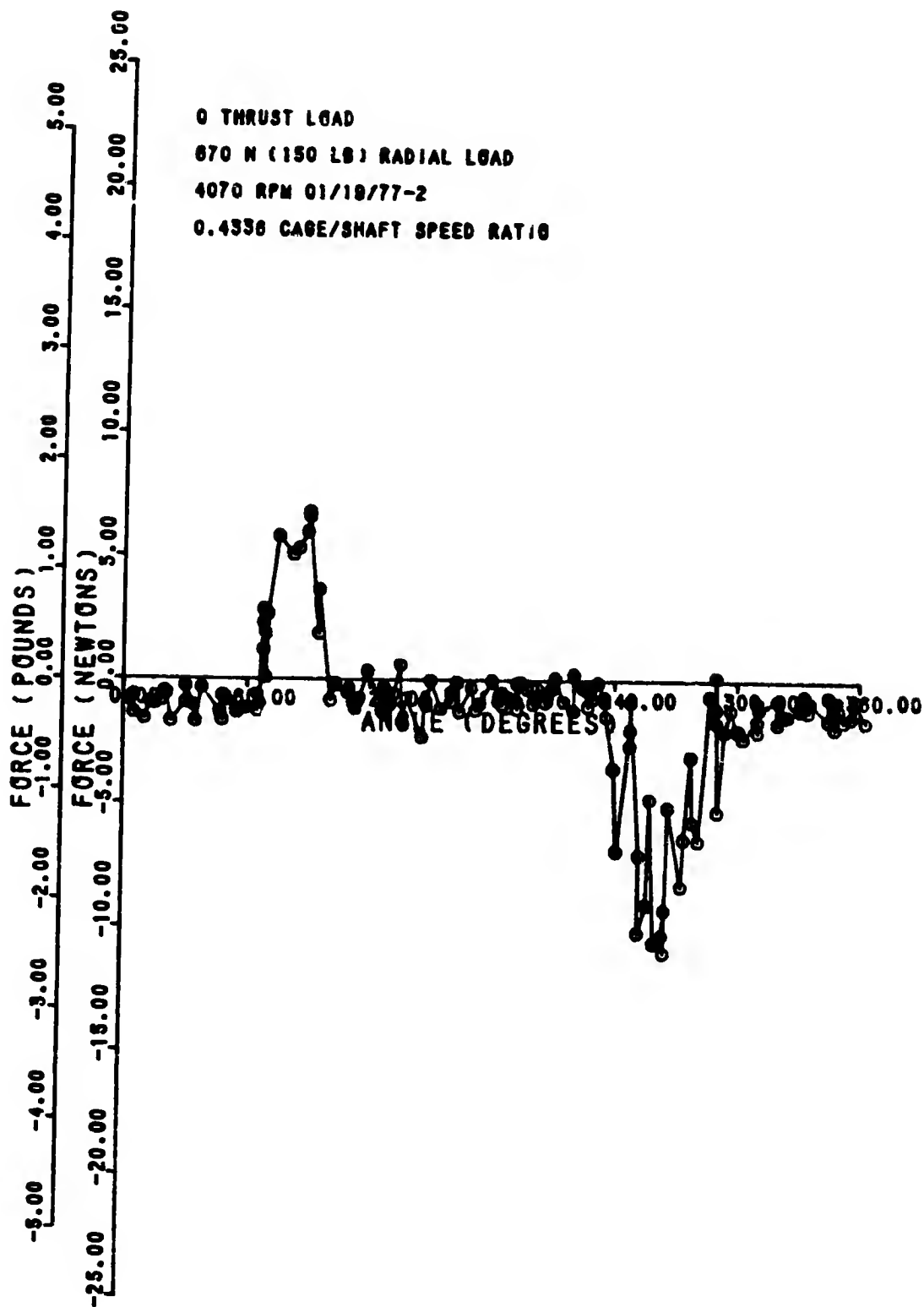


FIG. 6b-17.2 N/mm

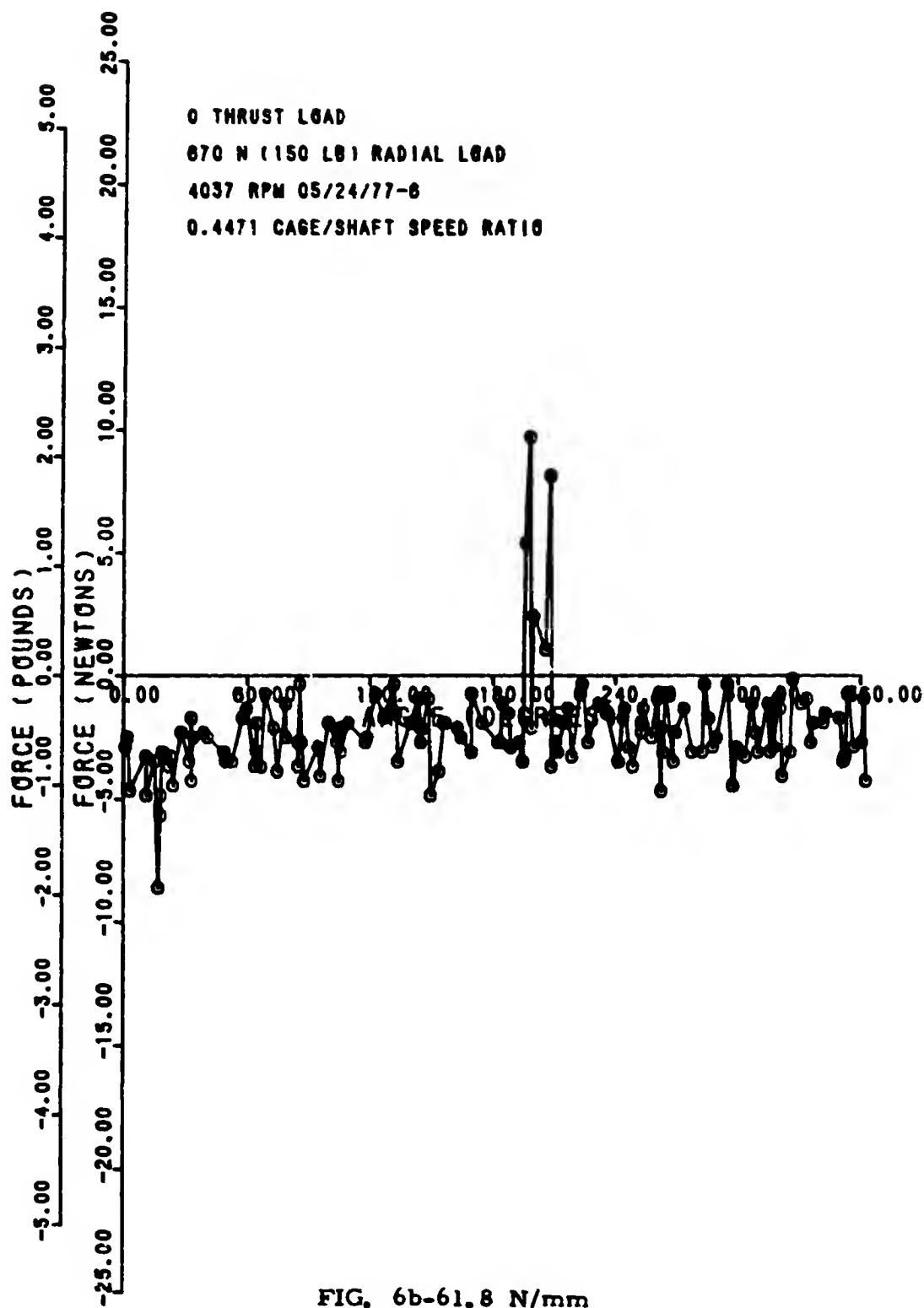


FIG. 6b-61.8 N/mm

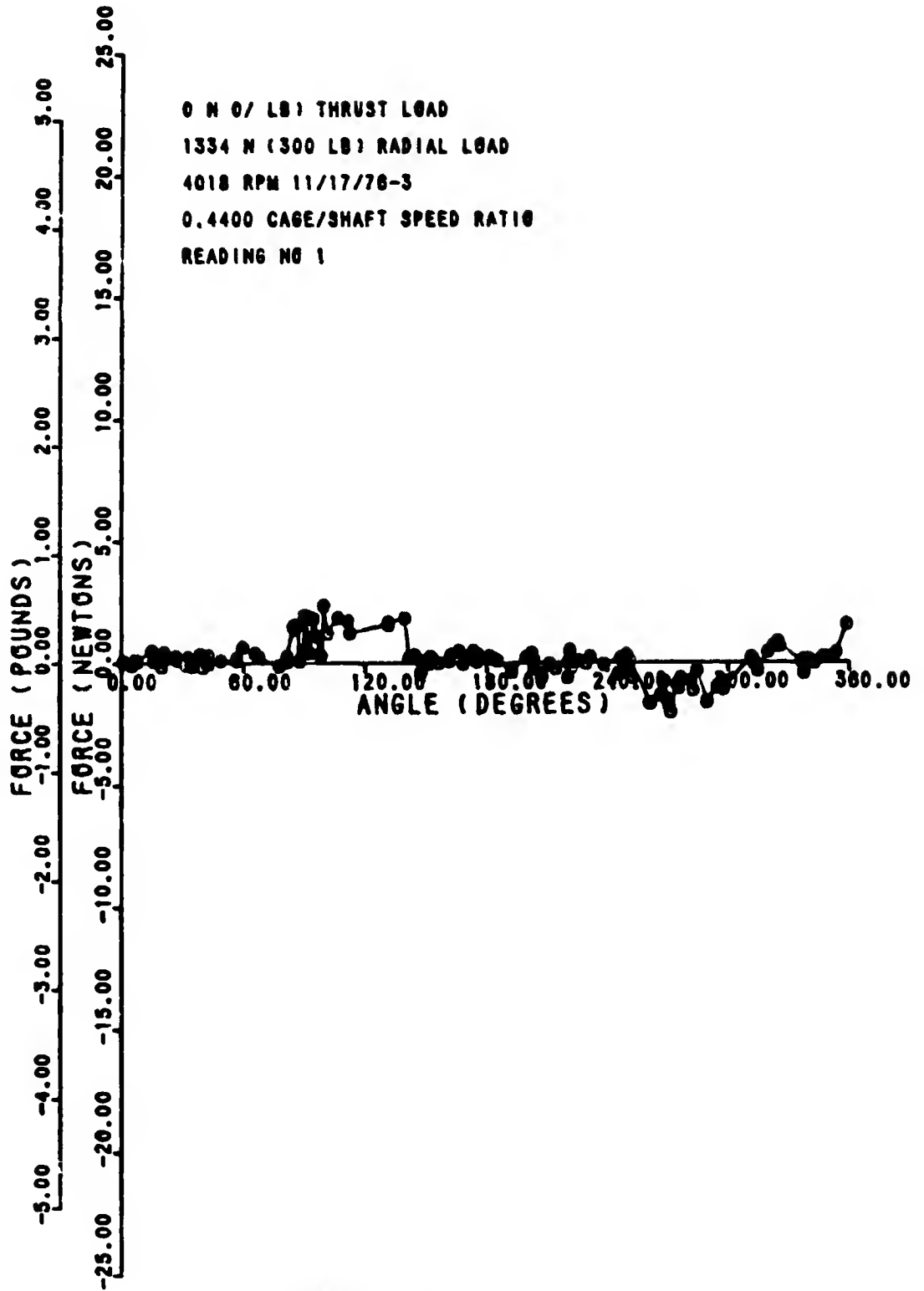


FIG. 6c-4.73 N/mm

7003011SNYP ANT

04/30/77

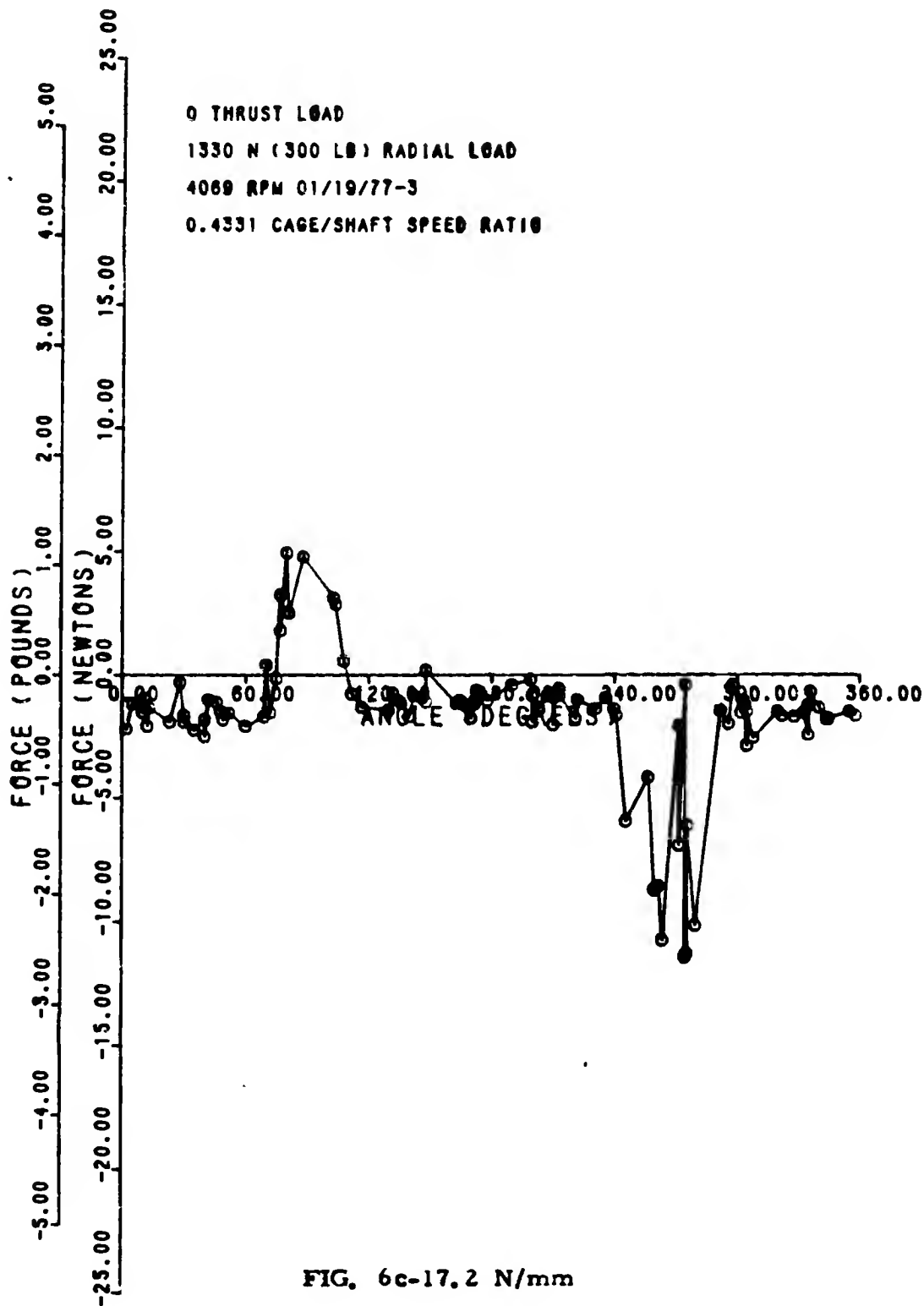


FIG. 6c-17.2 N/mm



70090115NYF AN16 06/02/77

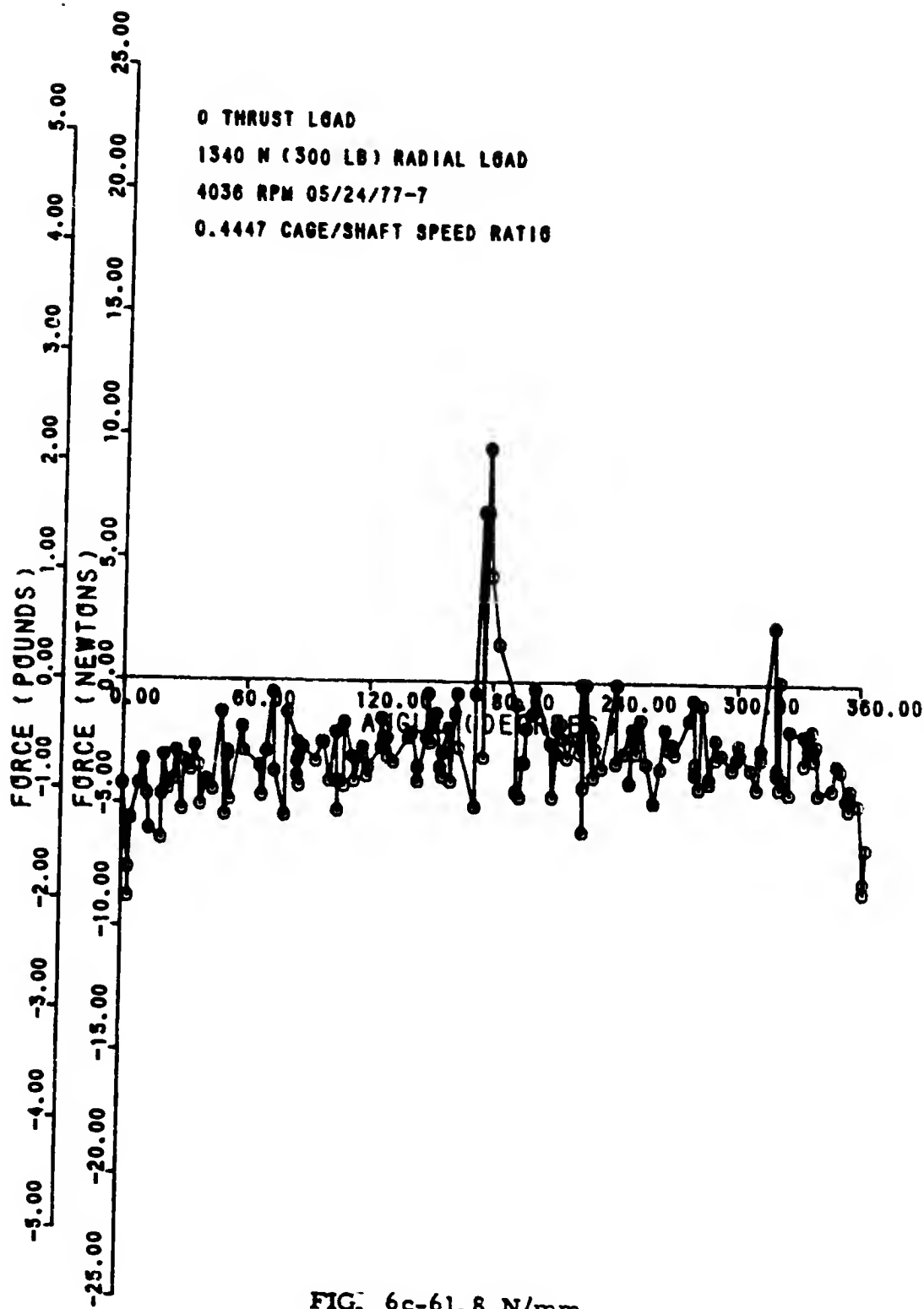


FIG. 6c-61.8 N/mm

70090T T9NYPAN3 03/11/77

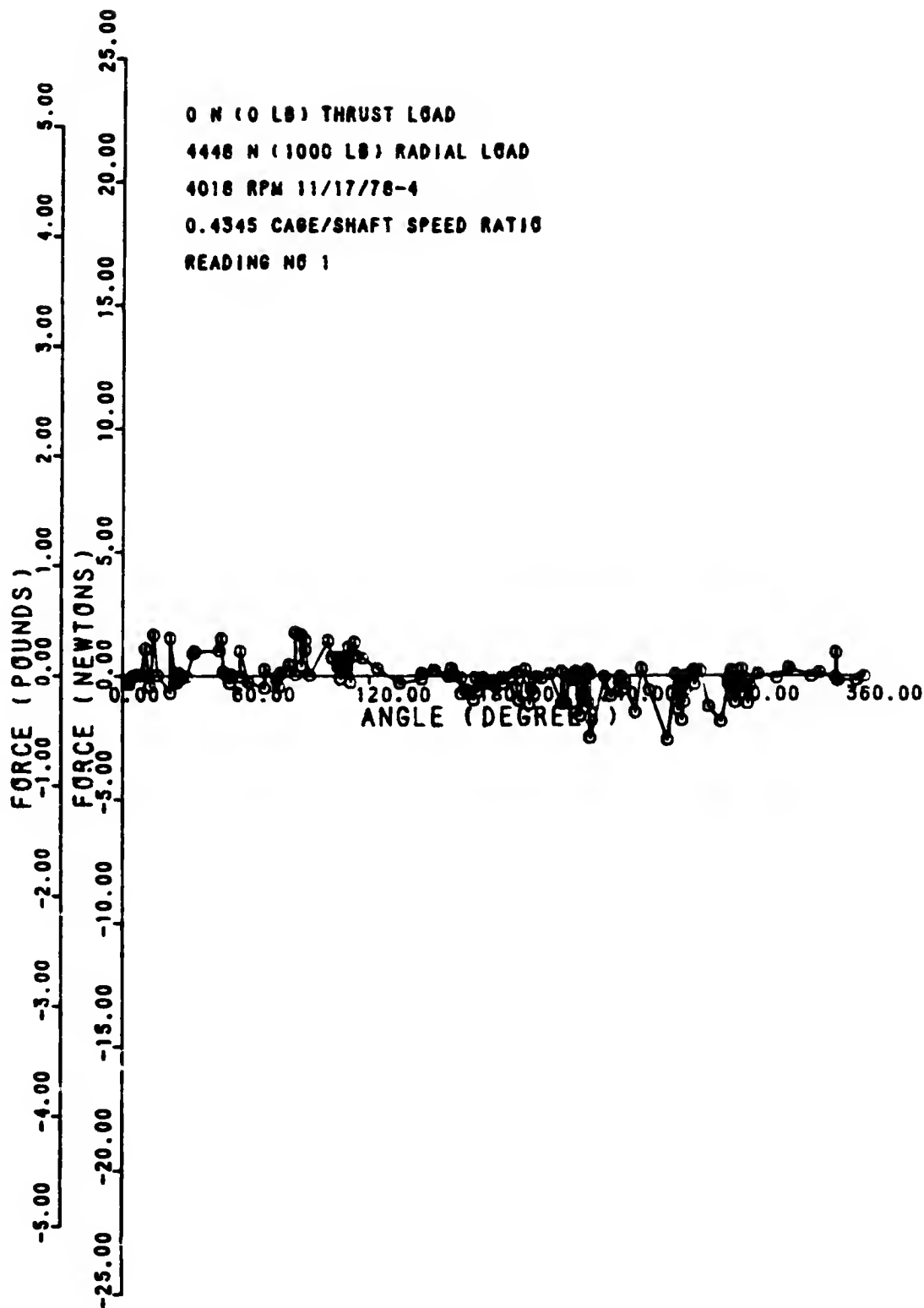


FIG. 6d-4.73 N/mm

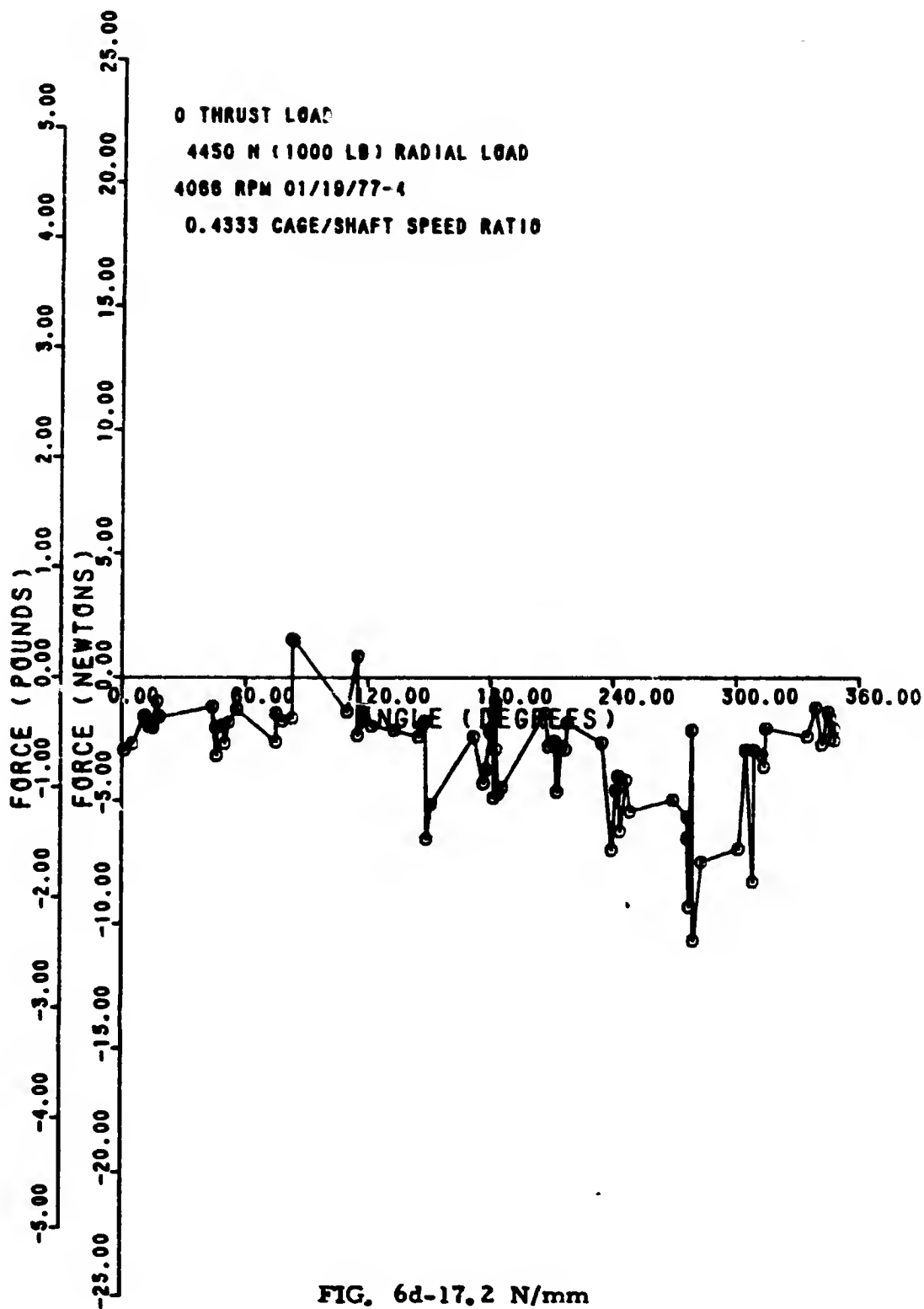
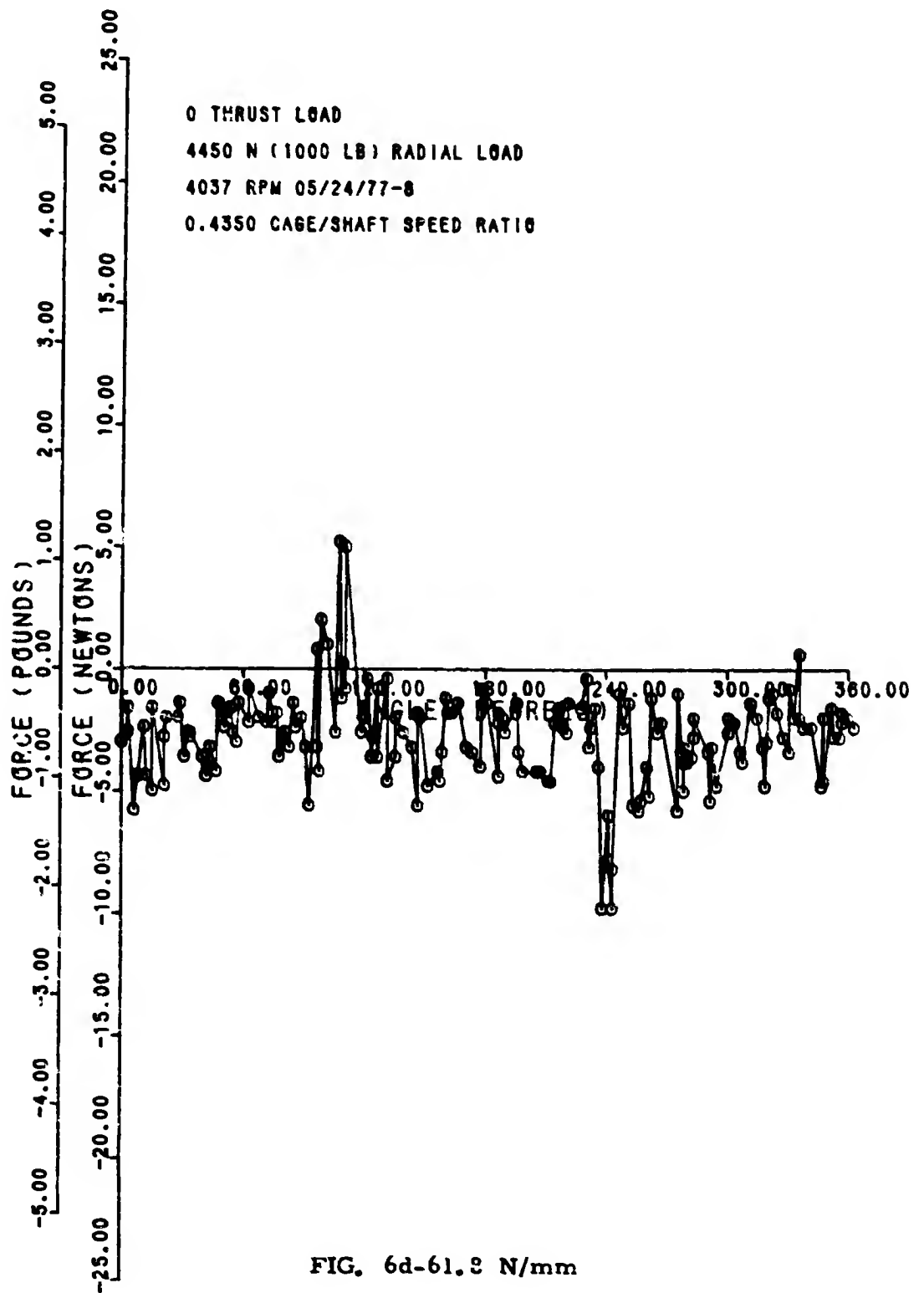


FIG. 6d-17.2 N/mm

700904 TSNIP, IN8 - - 06/07/77



70090119NYPAN4



05/03/77

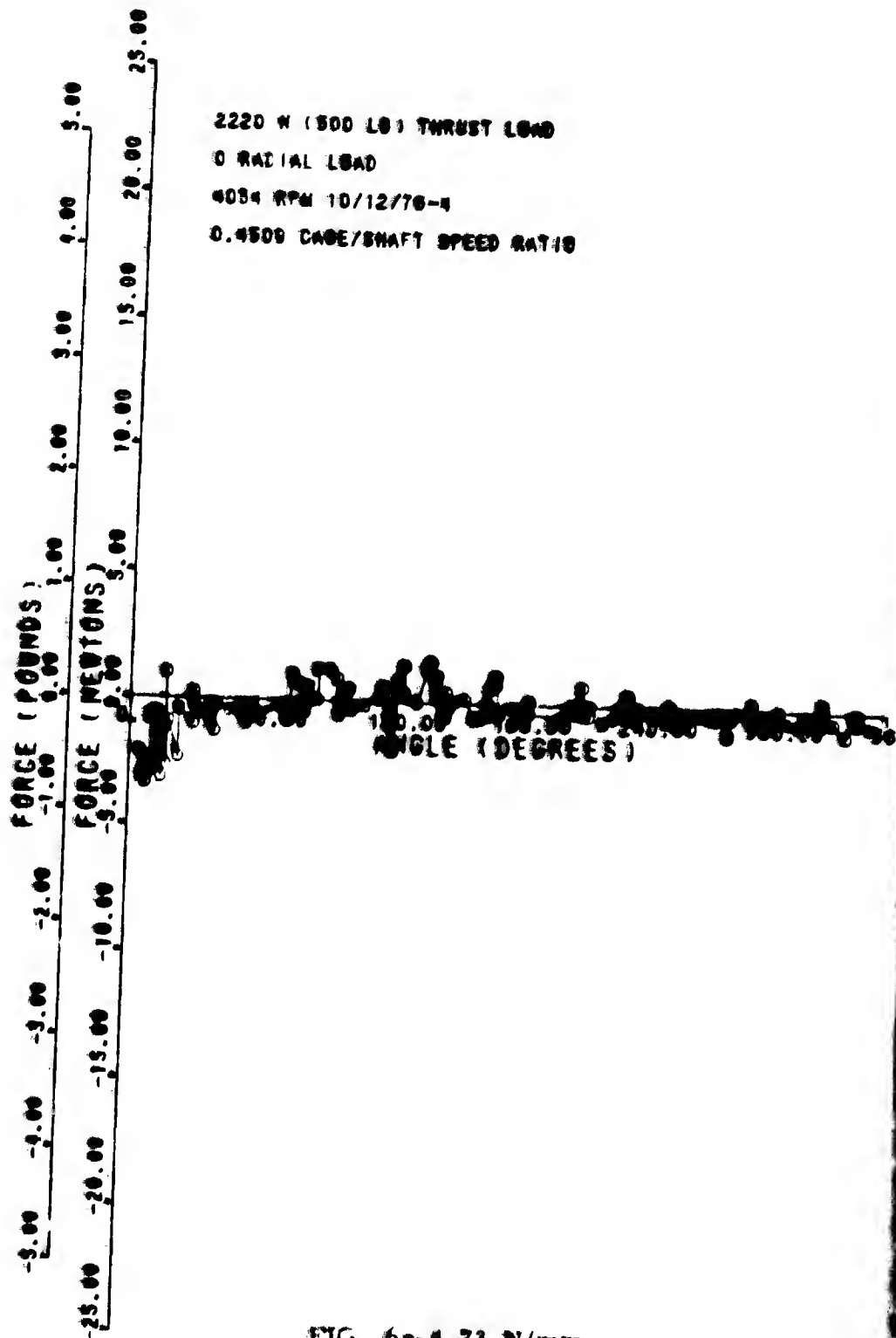


FIG. 6e-4. 73 N/mm

700901 J 9NYPAN2 - 02/28/77

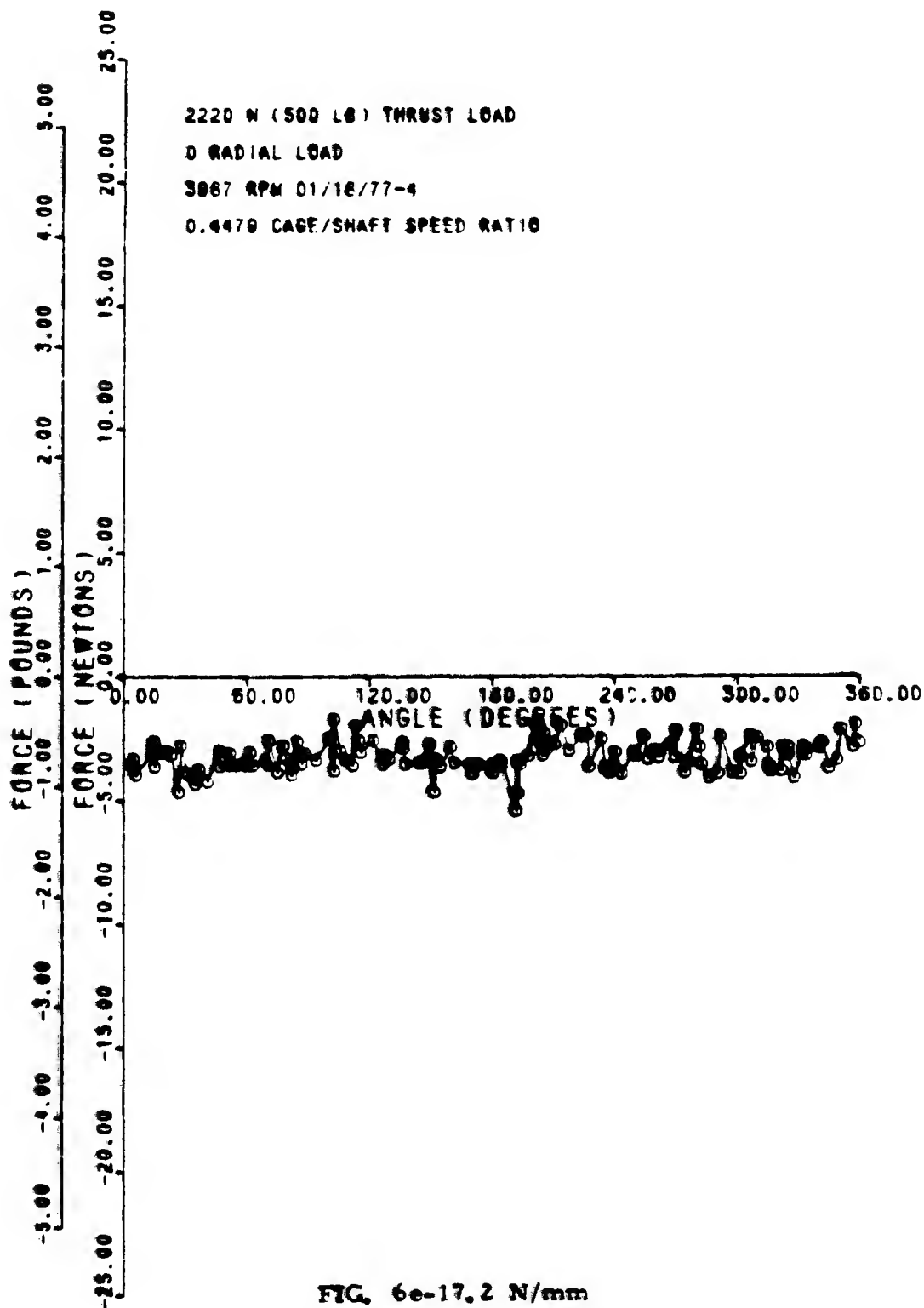


FIG. 6e-17.2 N/mm

70090419NYP AN:8 06/17/77

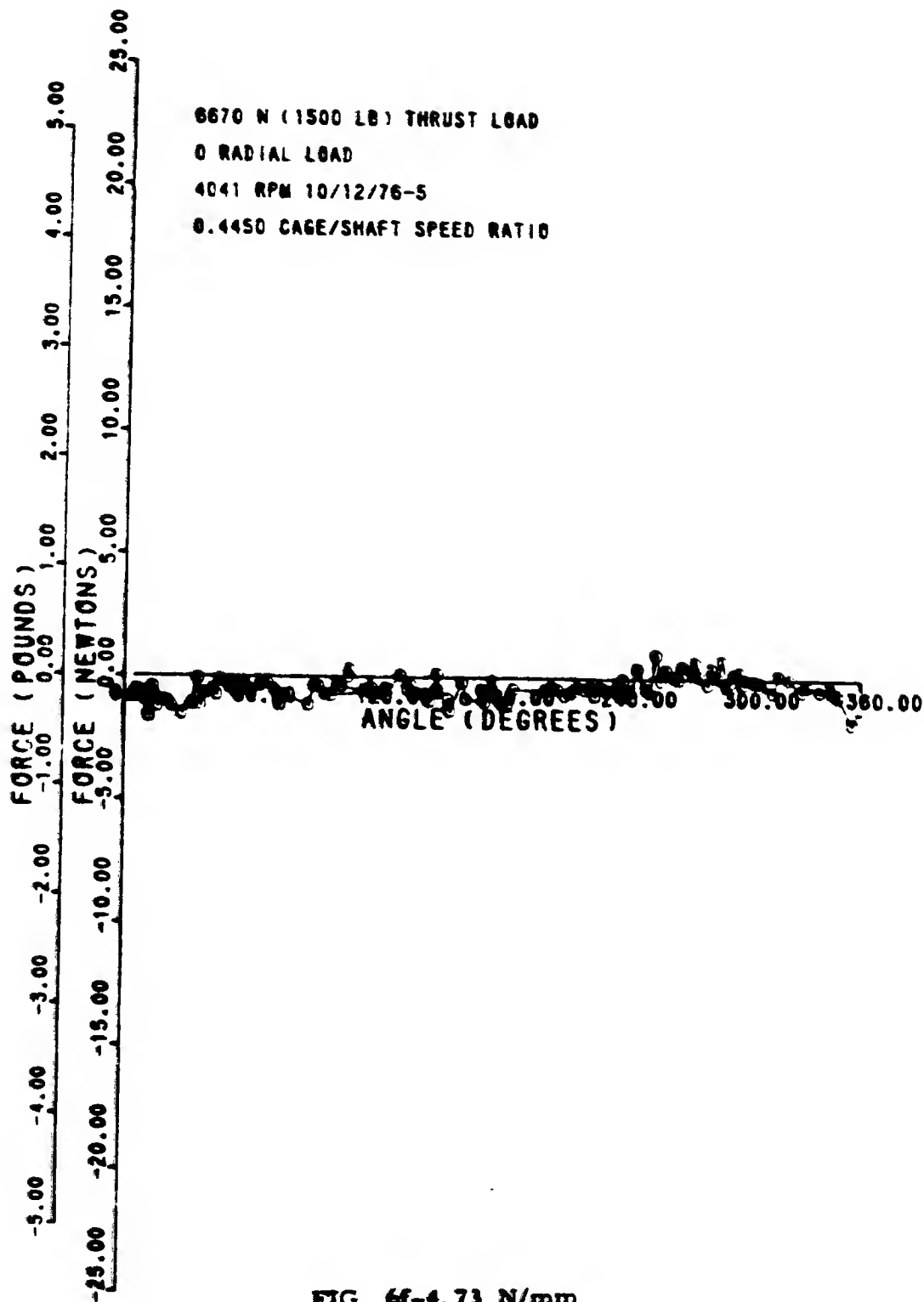


FIG. 6f-4.73 N/mm

700901T9NYP ANI I

02/26/77

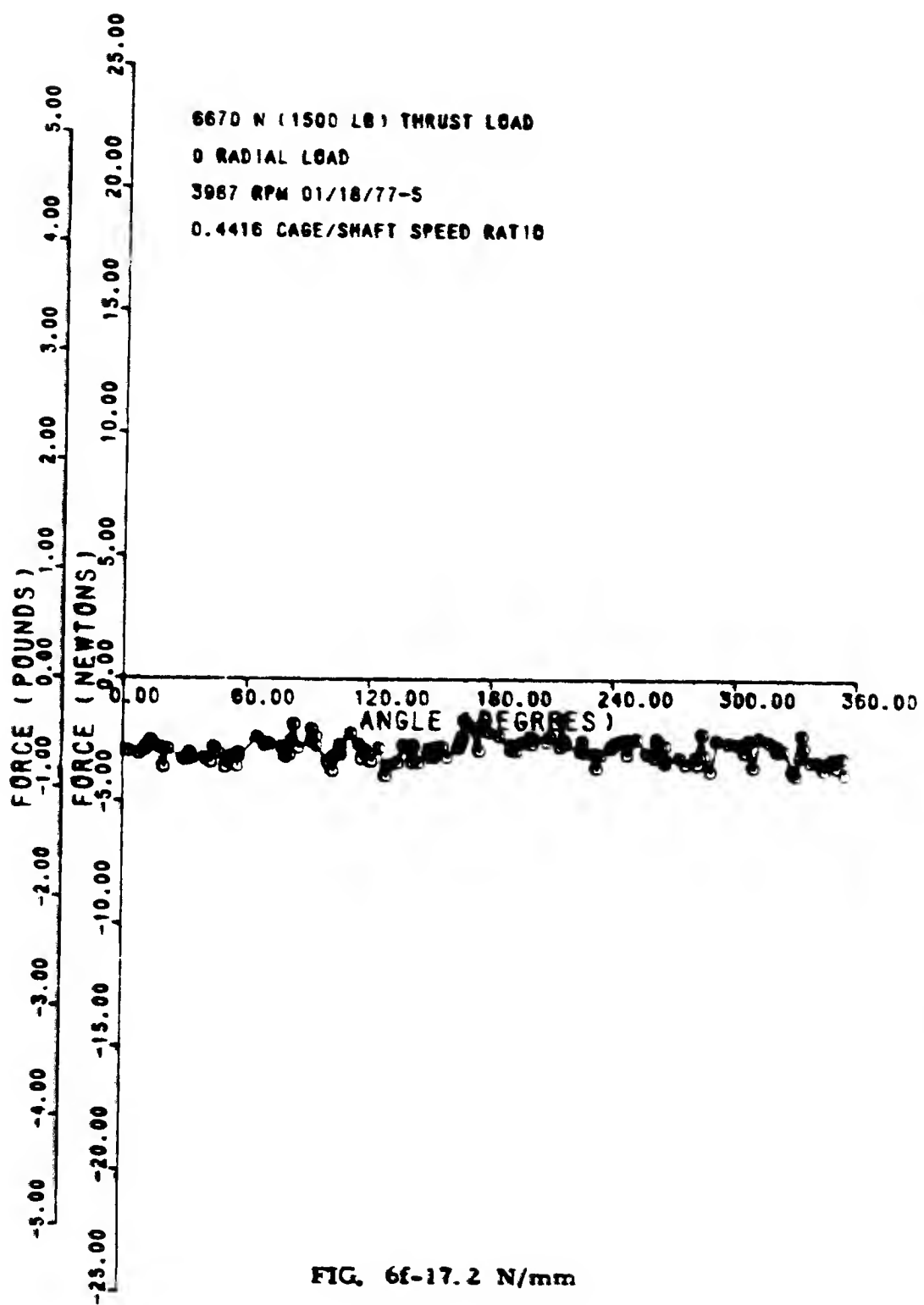


FIG. 6f-17.2 N/mm



700901'SNYF AN10 06/16/77

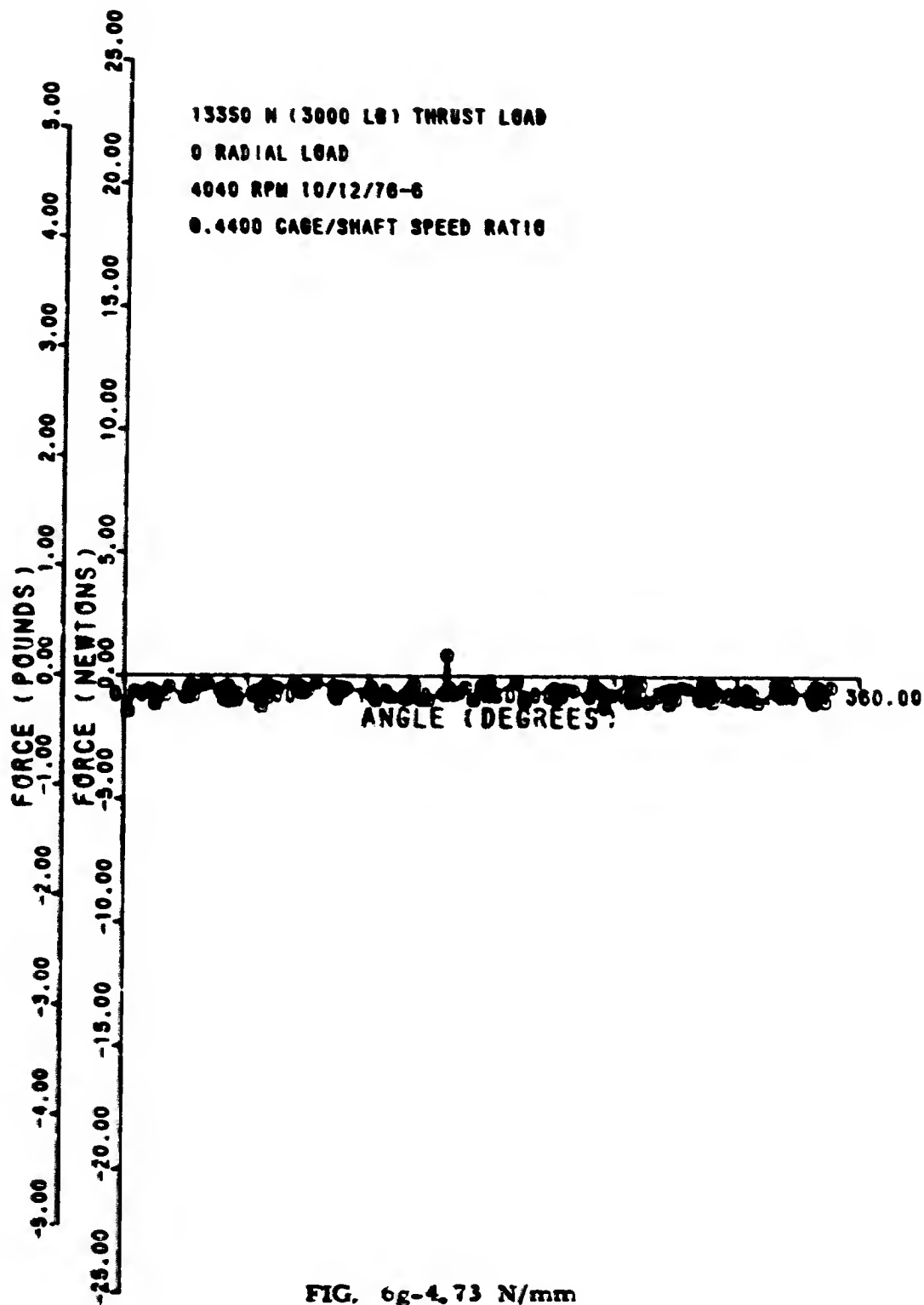


FIG. 6g-4.73 N/mm

7003011SNYPAN8 06/17/77

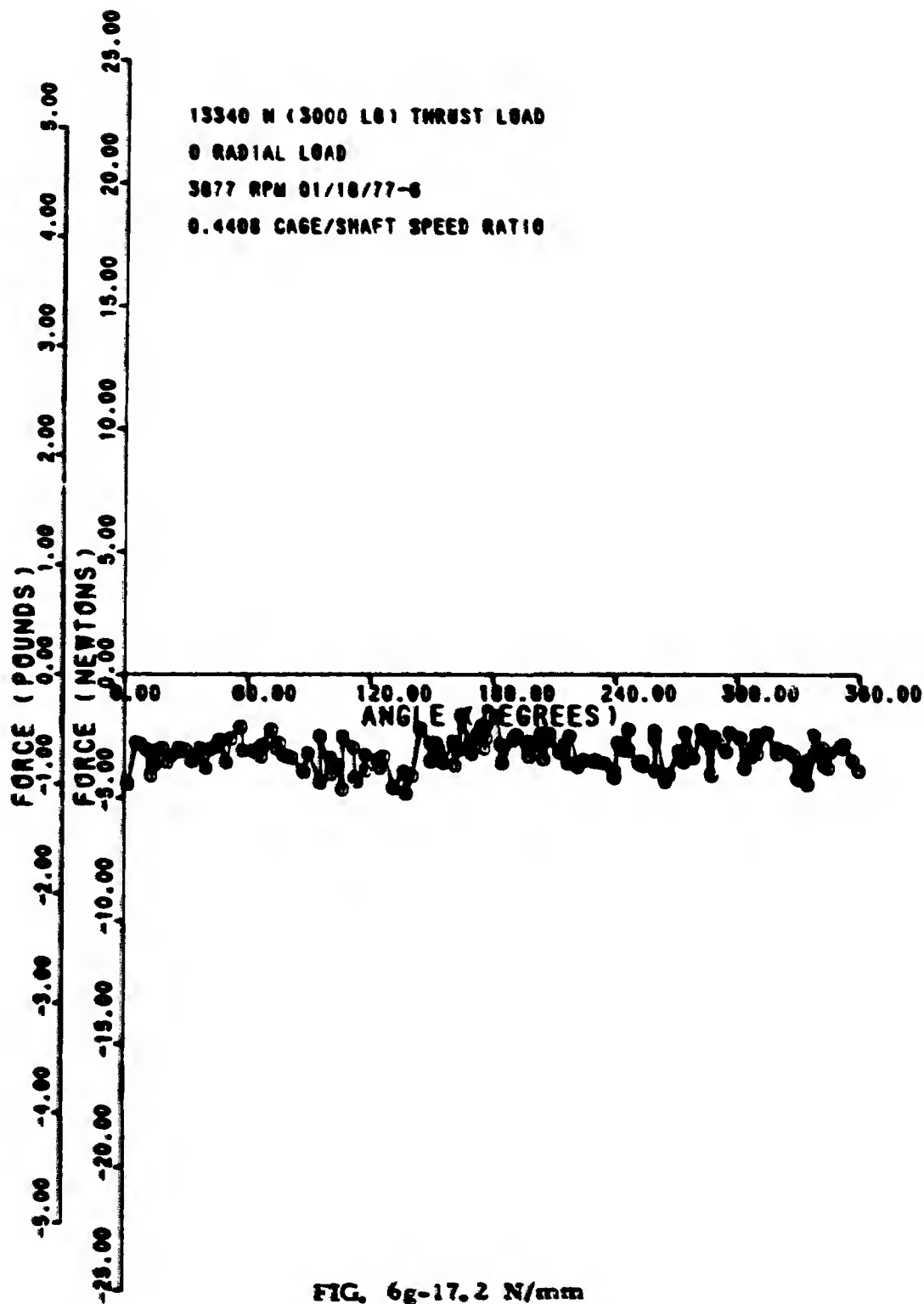


FIG. 6g-17.2 N/mm

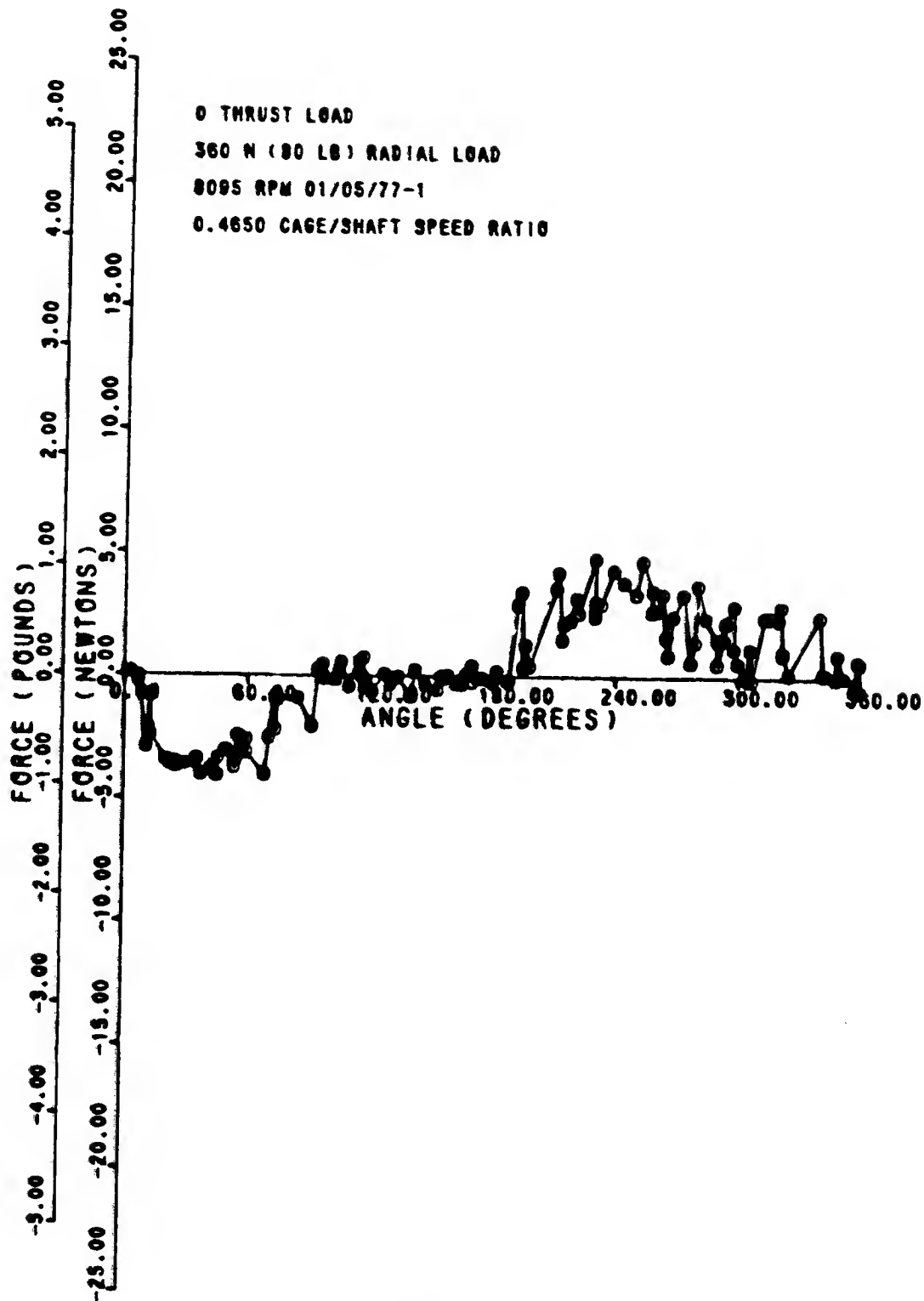


FIG. 7a-4.73 N/mm

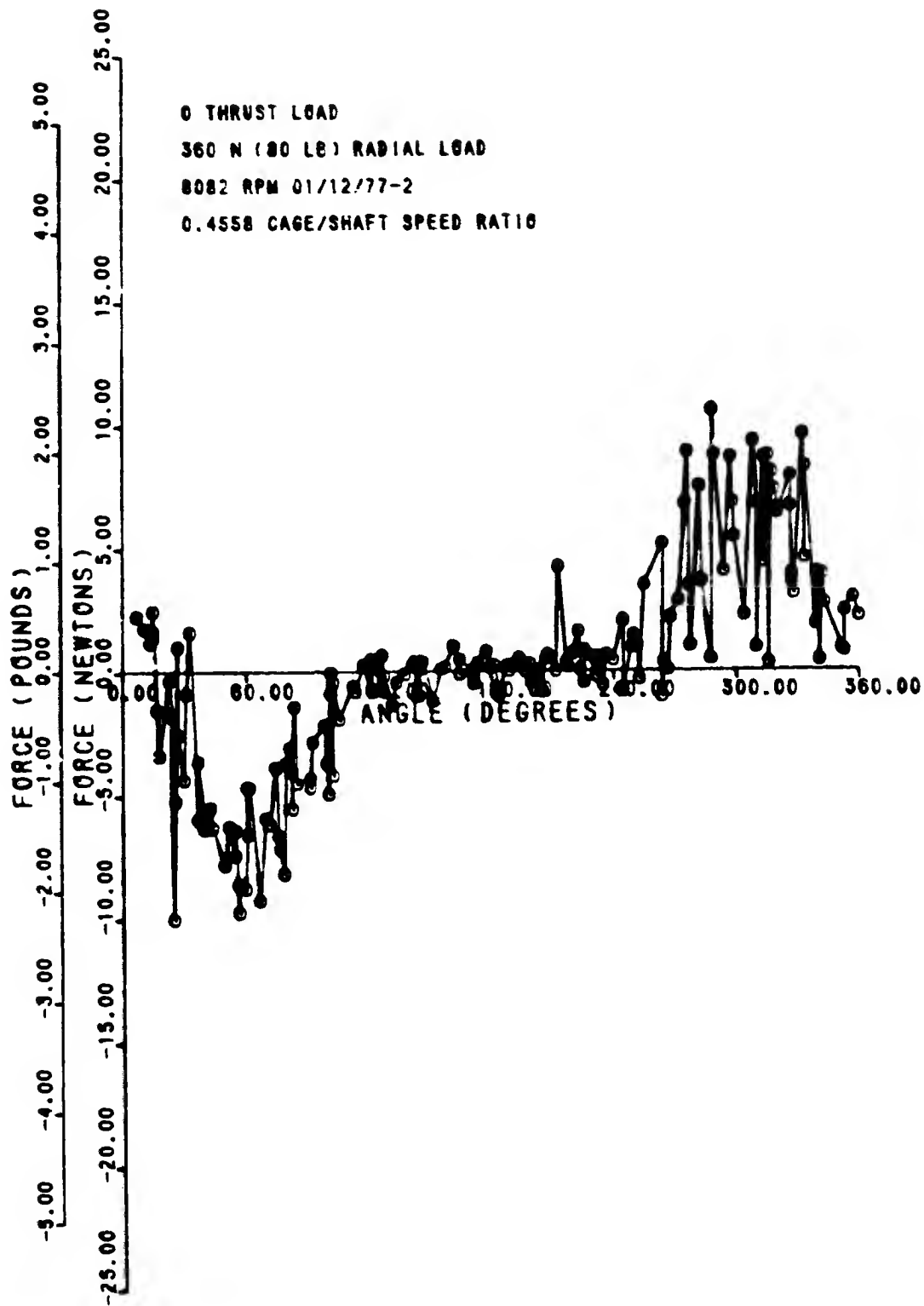


FIG. 7a-17.2 N/mm

7:00 90:1 9WYF ANI 06/14/77

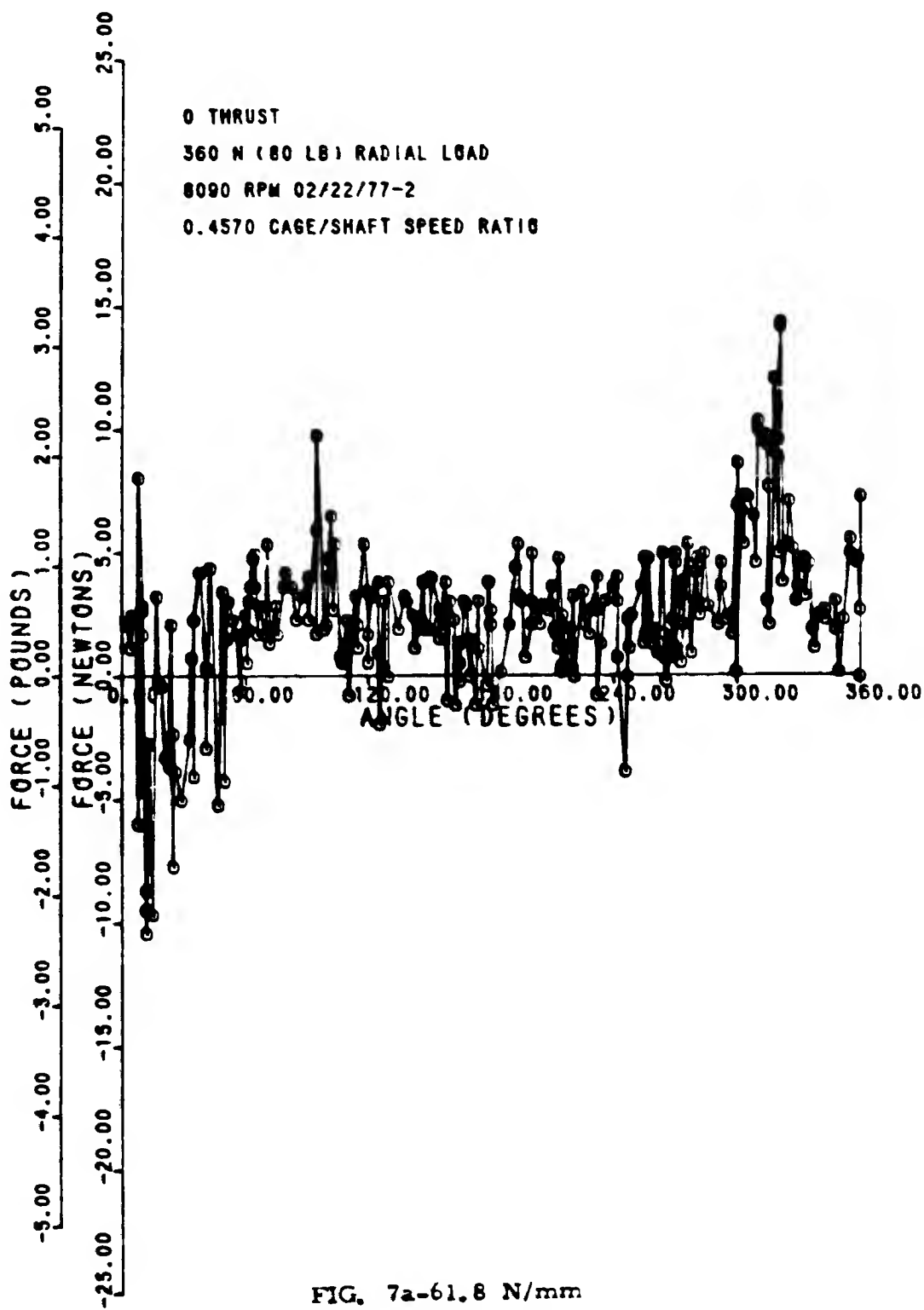


FIG. 7a-61.8 N/mm

70090113NYF ANI 06/15/77

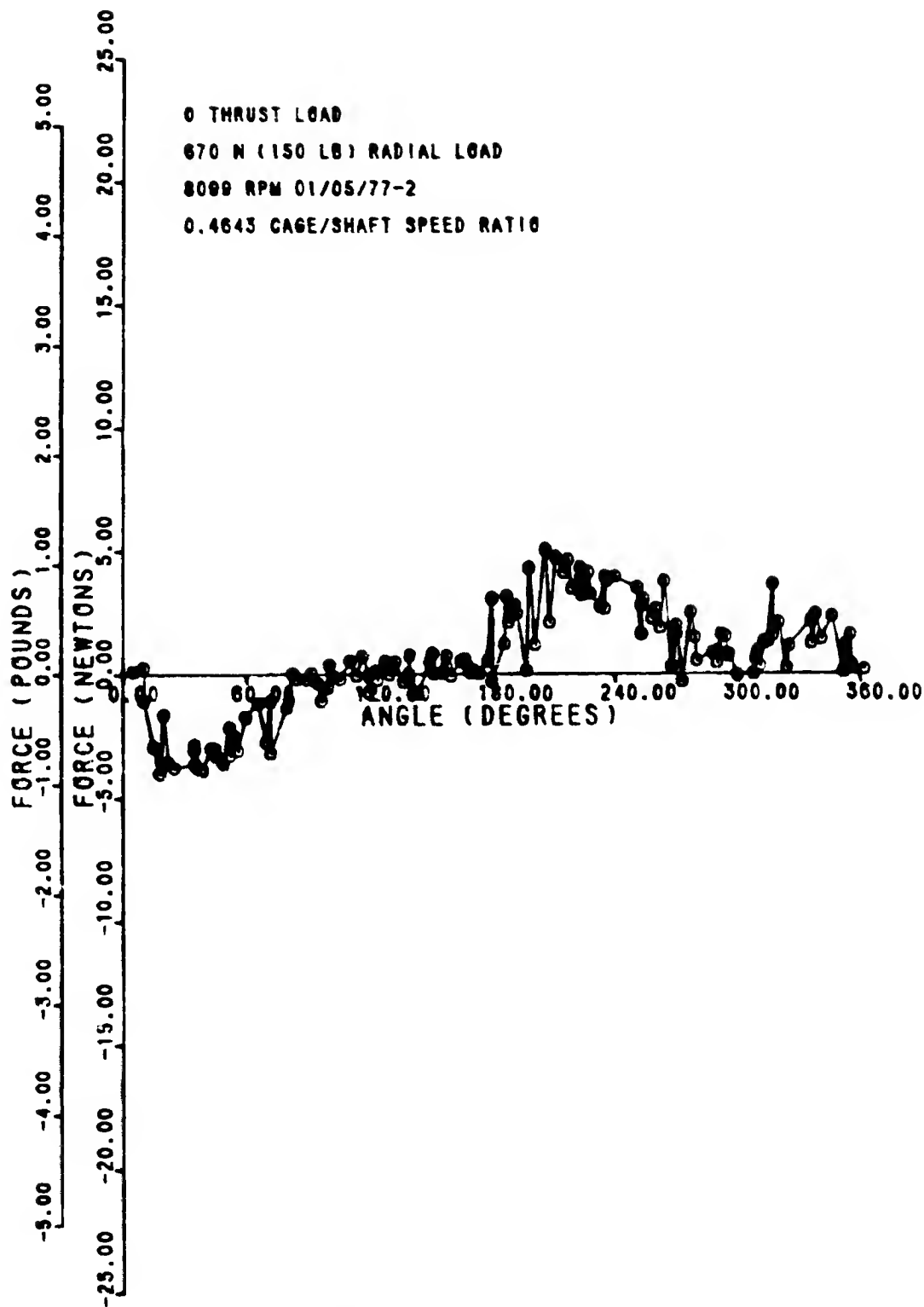


FIG. 7b-4.73 N/mm

7009011 YNYP AN11 02/22/77

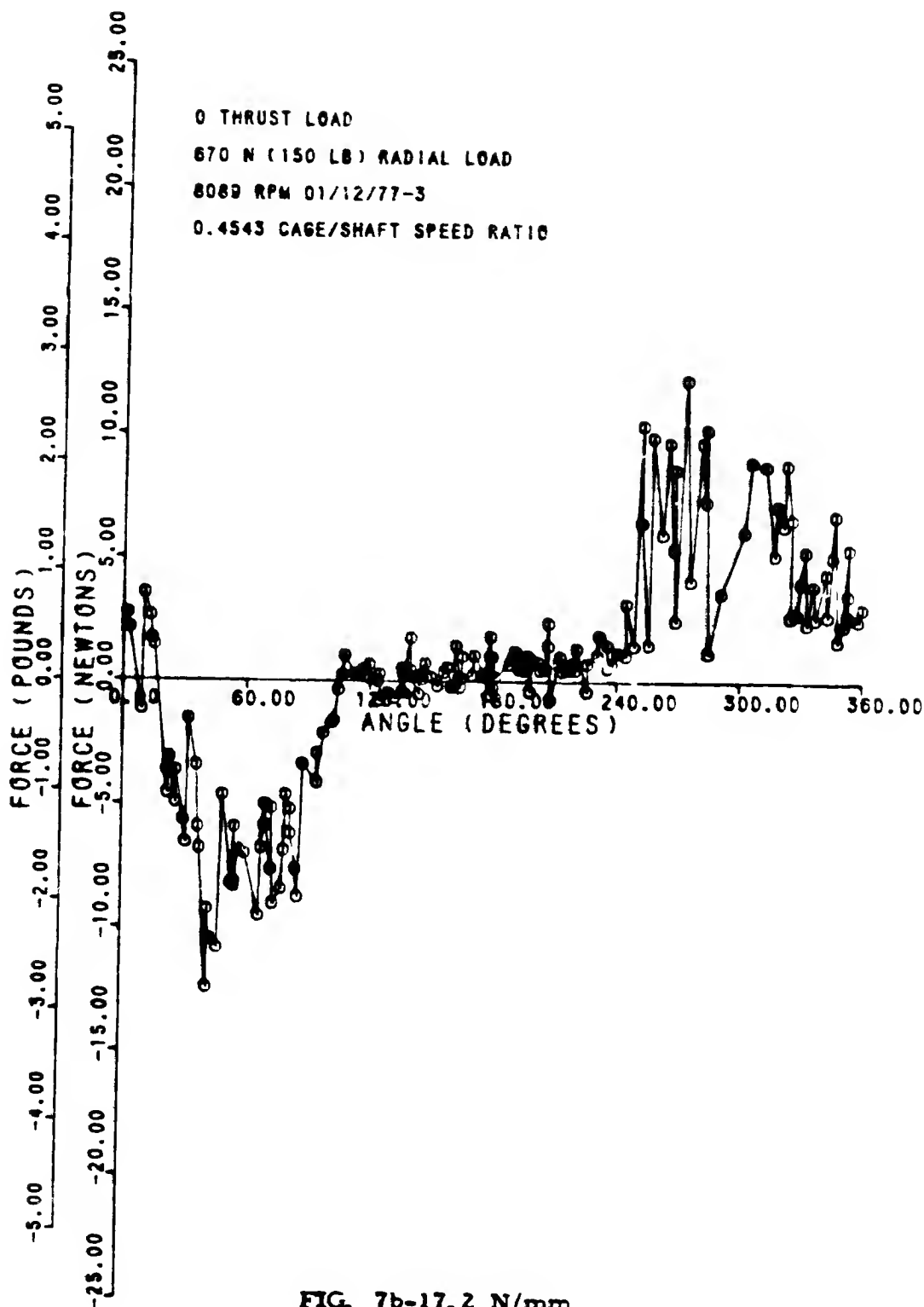


FIG. 7b-17.2 N/mm

7009011SNYPAN14

06/11/77

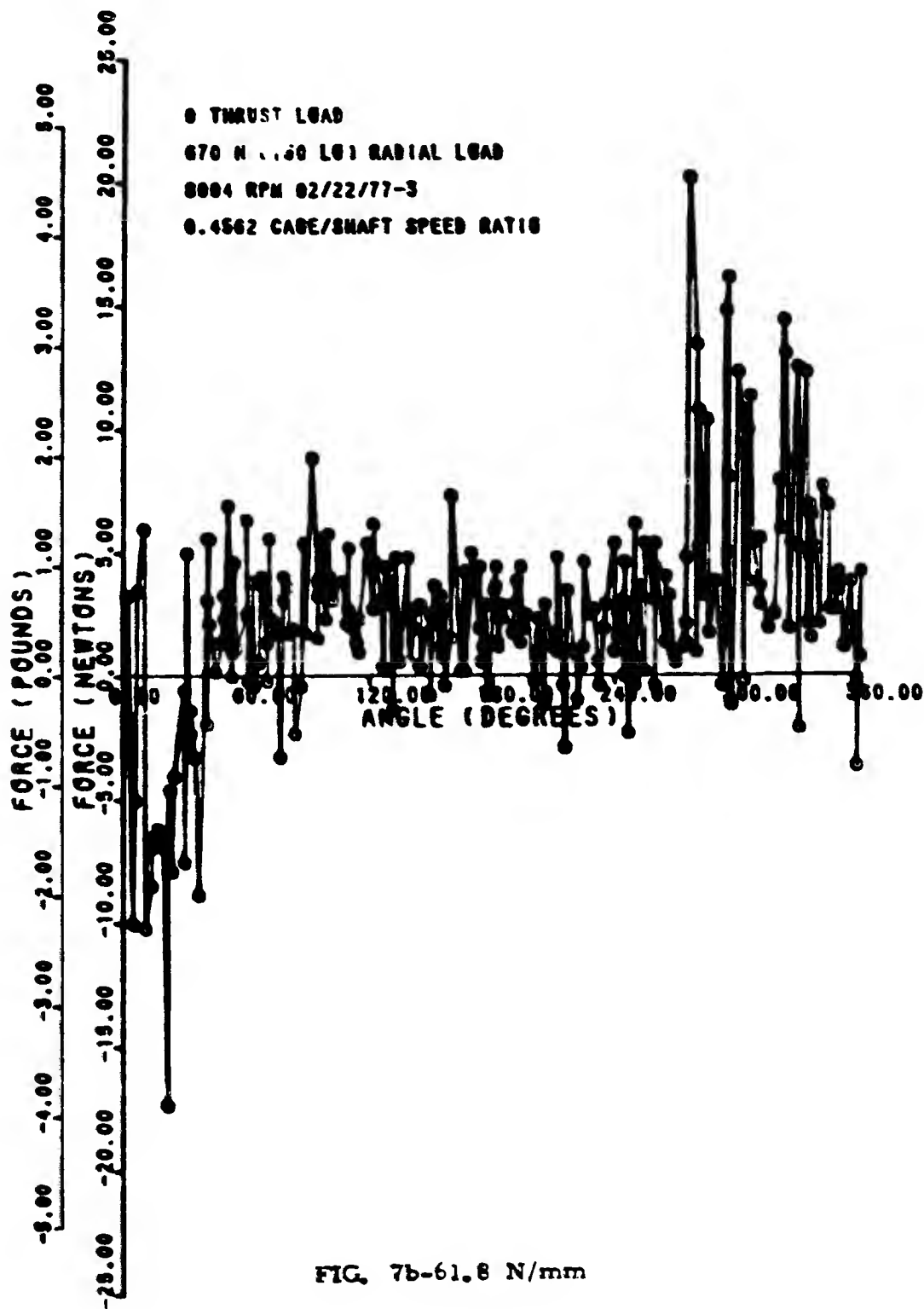


FIG. 7b-61.8 N/mm



70090119NYP AN 7 06/15/77

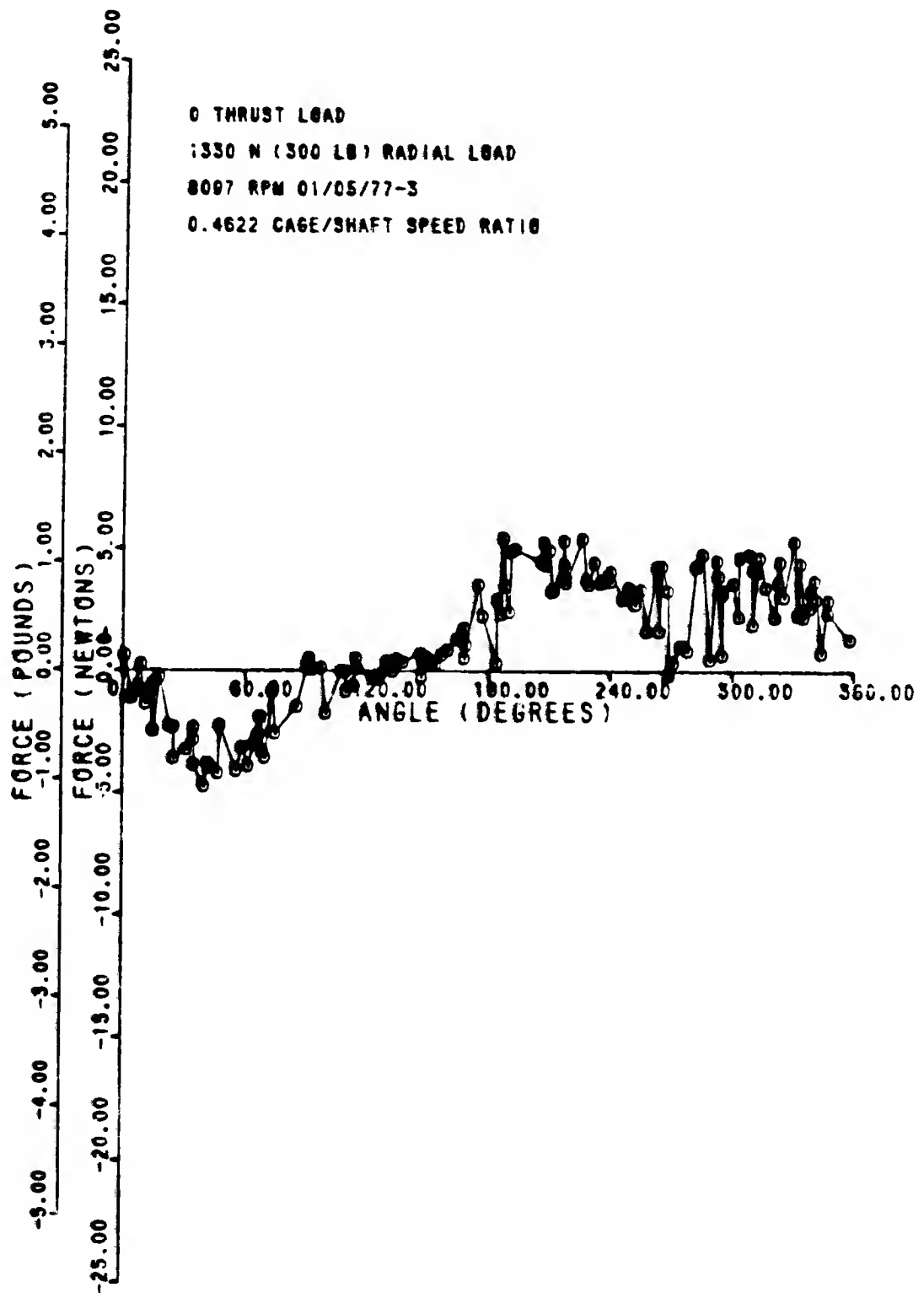


FIG. 7c-4.73 N/mm

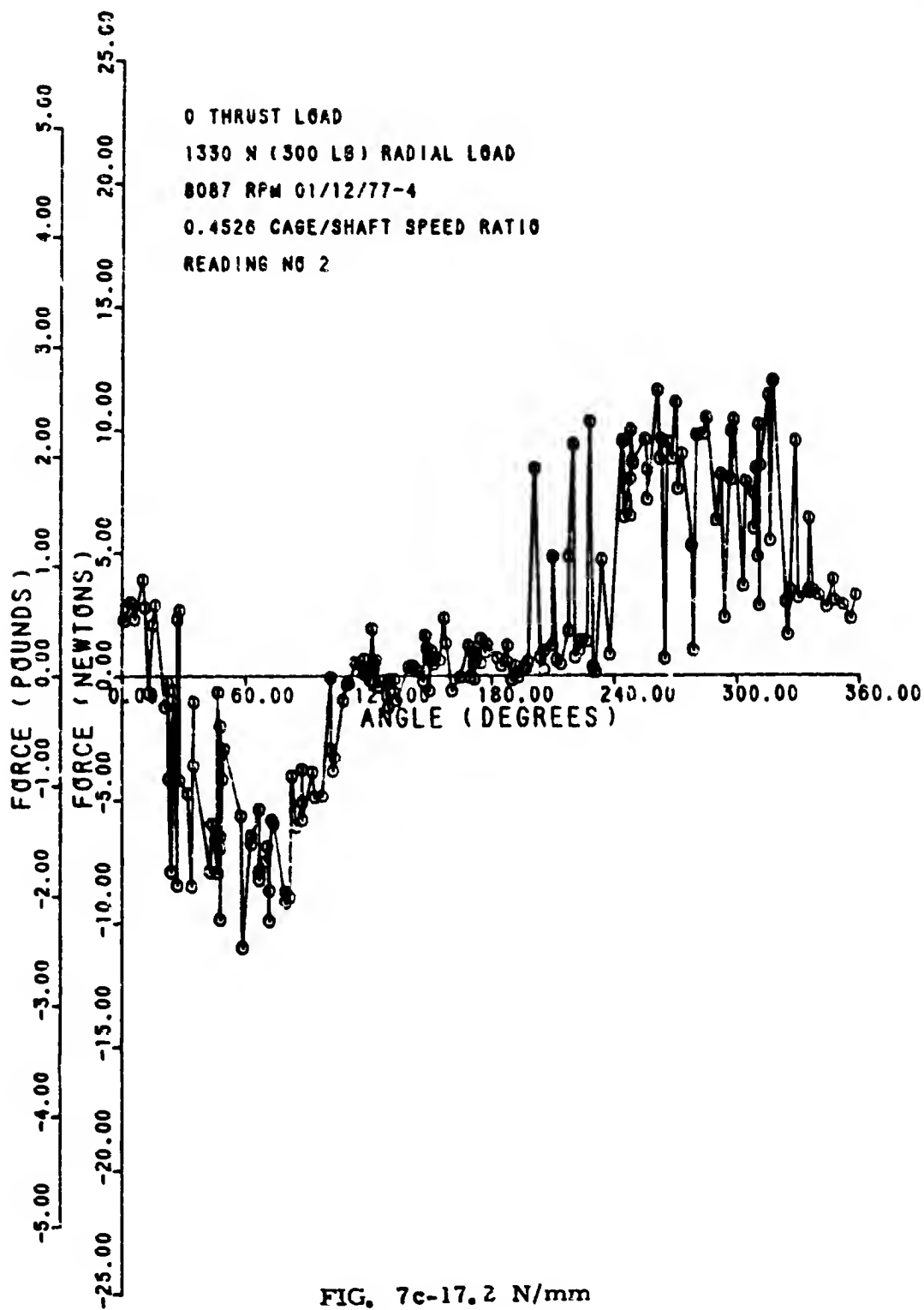


FIG. 7c-17.2 N/mm

70050119NYPAN 16

06/15/77

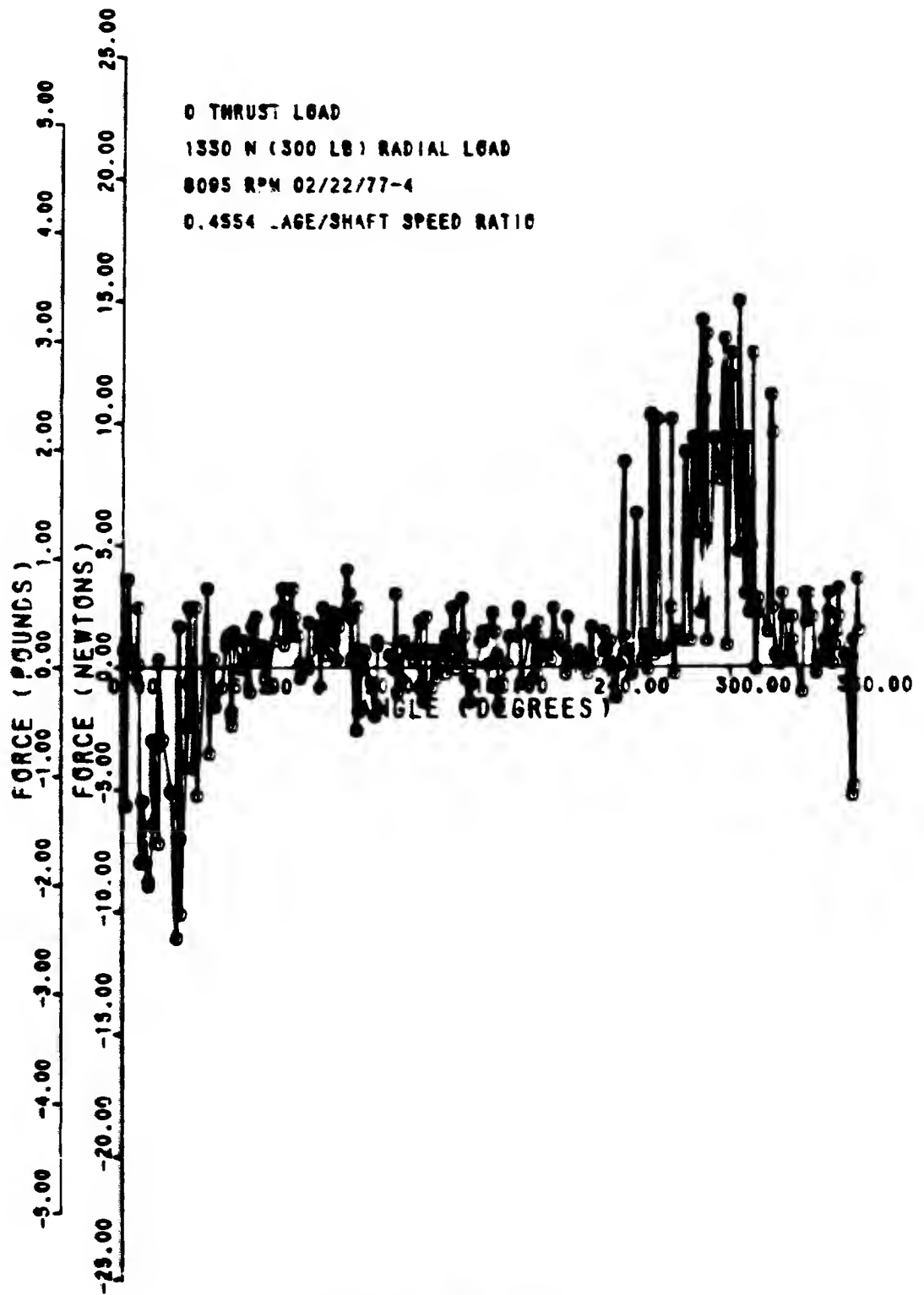


FIG. 7c-61.8 N/mm

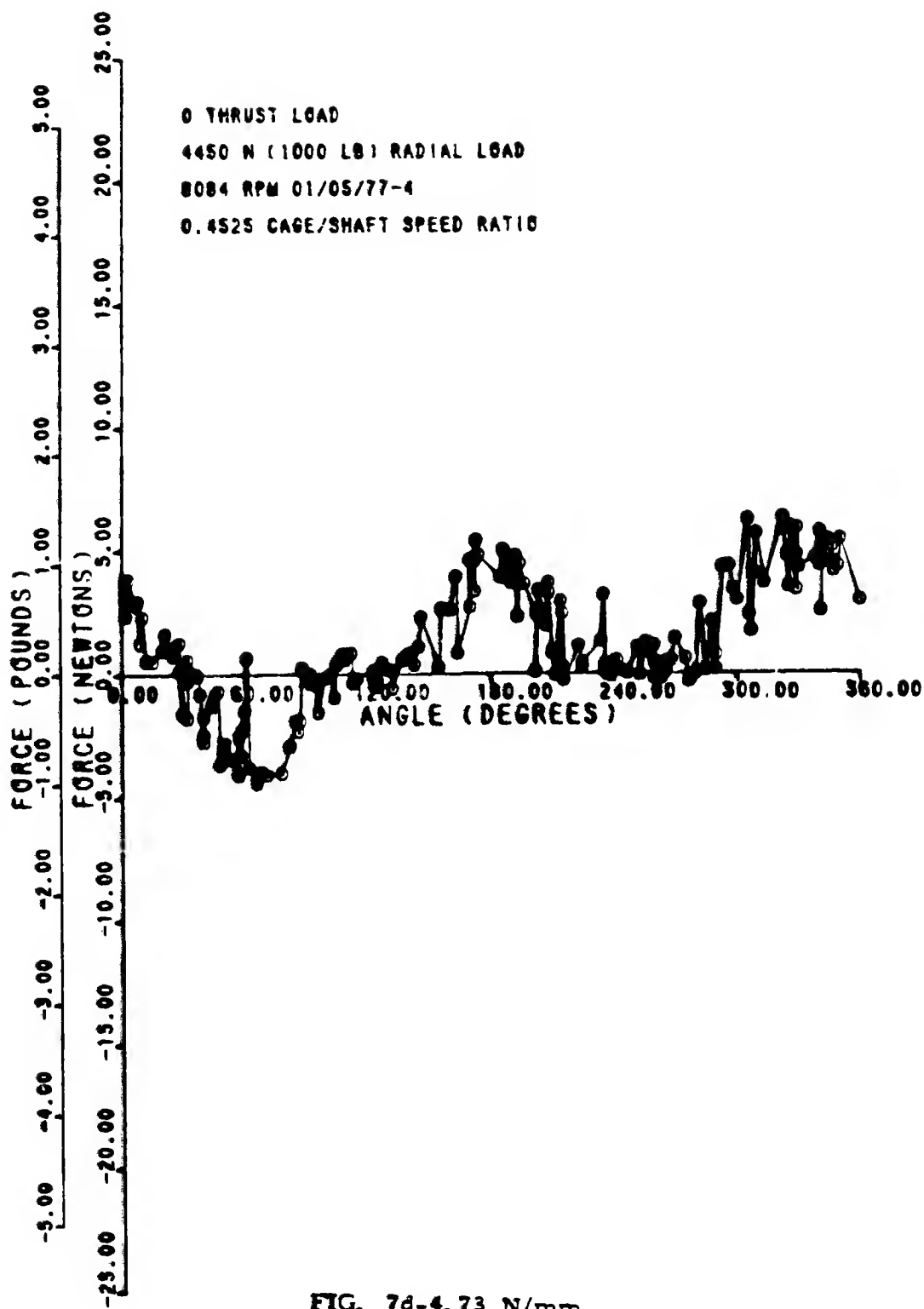


FIG. 7d-4.73 N/mm

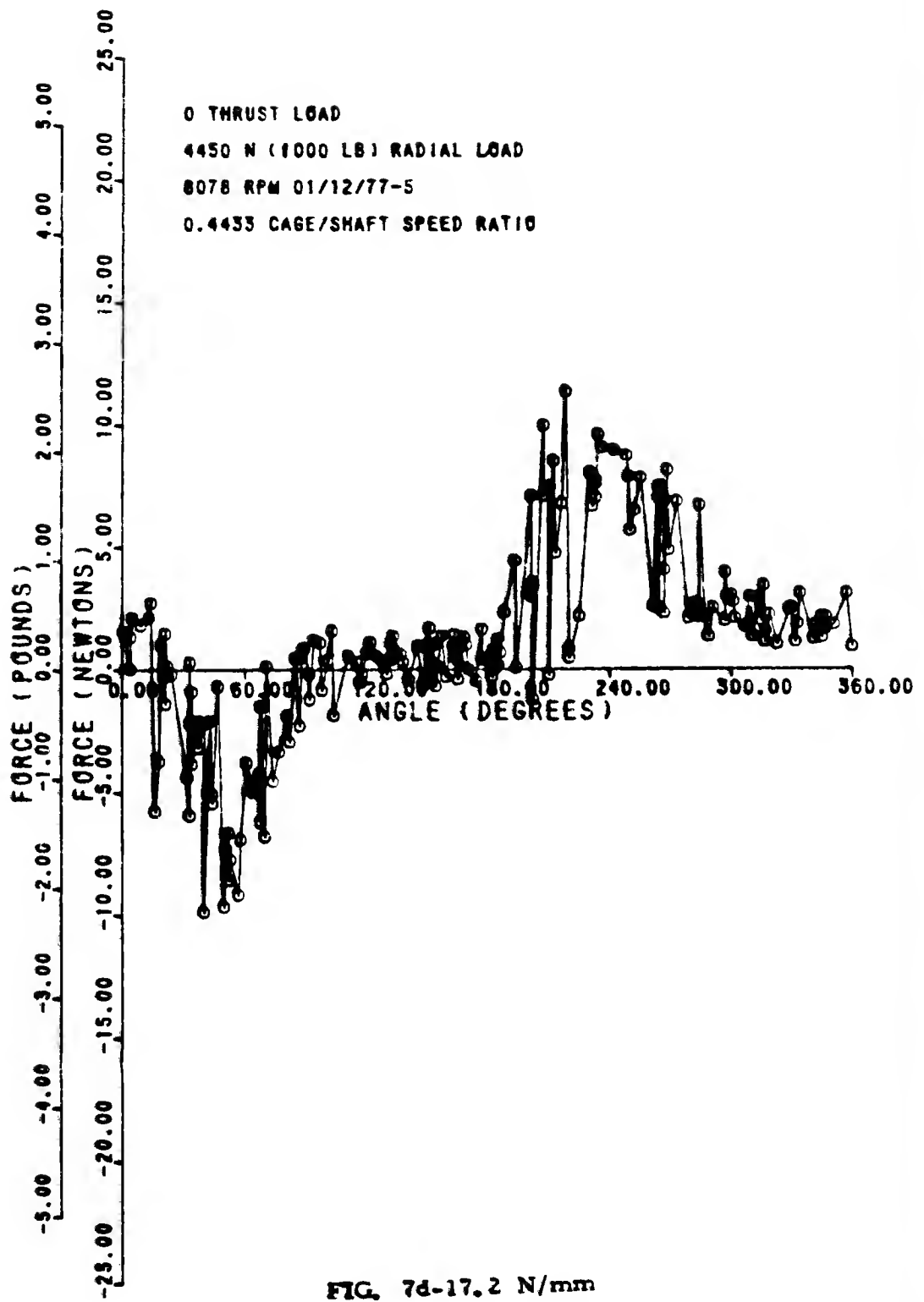


FIG. 7d-17.2 N/mm

70090119WYPAN6

06/11/77

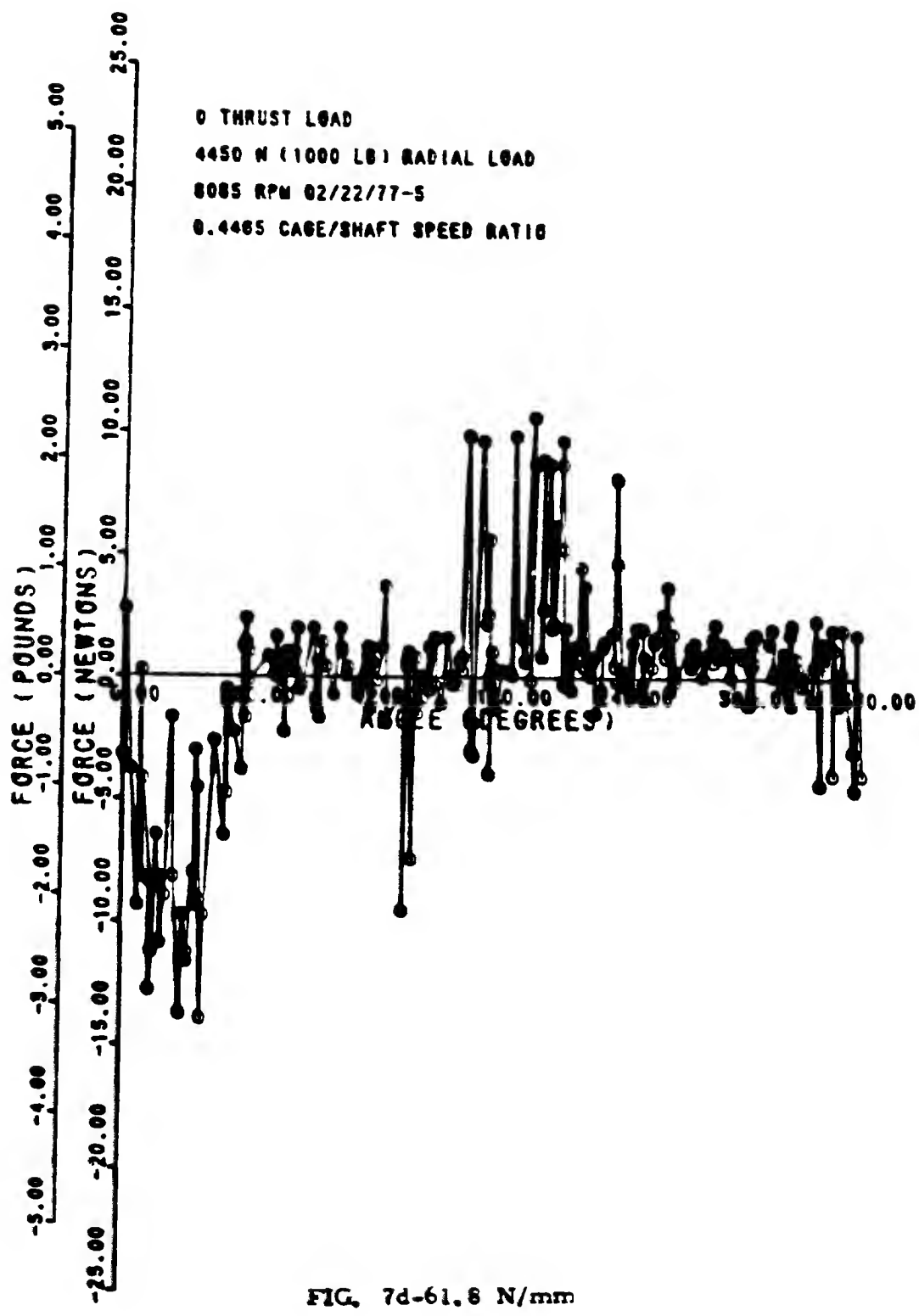


FIG. 7d-61.8 N/mm

700901-19NFFANG--06/16/77

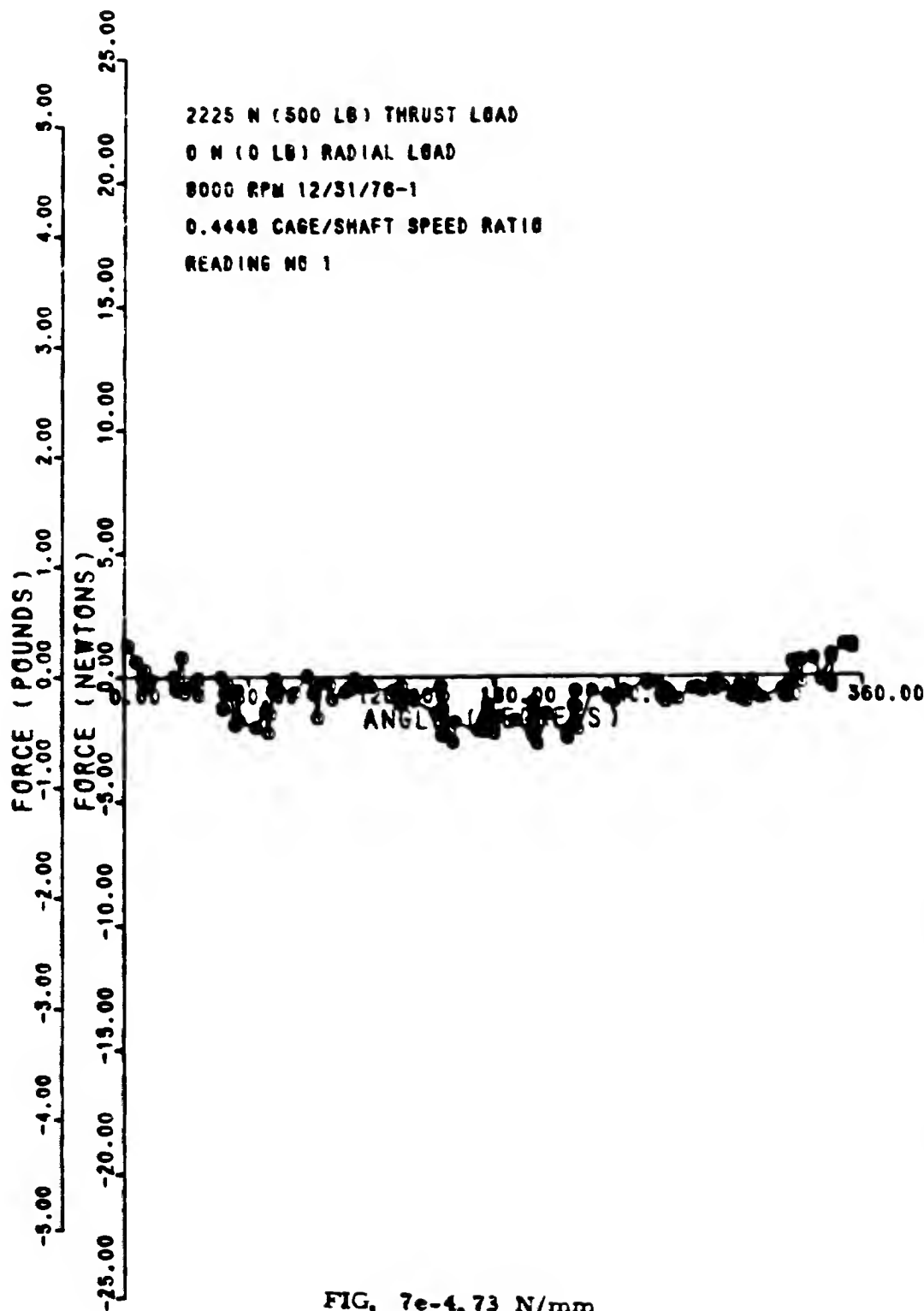


FIG. 7e-4. 73 N/mm

70090119NYPAN12 02/23/77

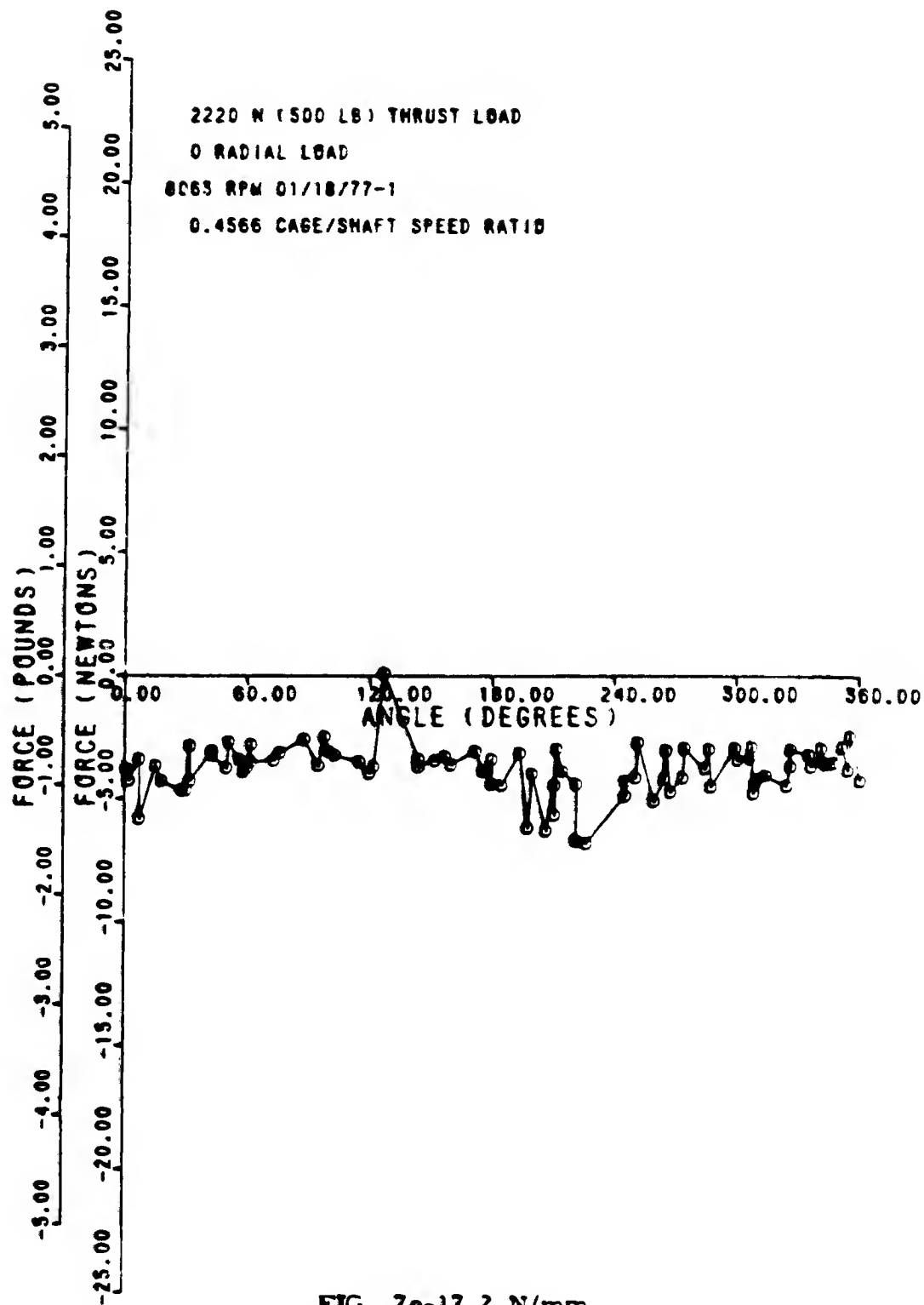
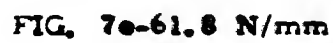


FIG. 7e-17.2 N/mm



03/17/77



70090119N 8 AN 8

06/15/77

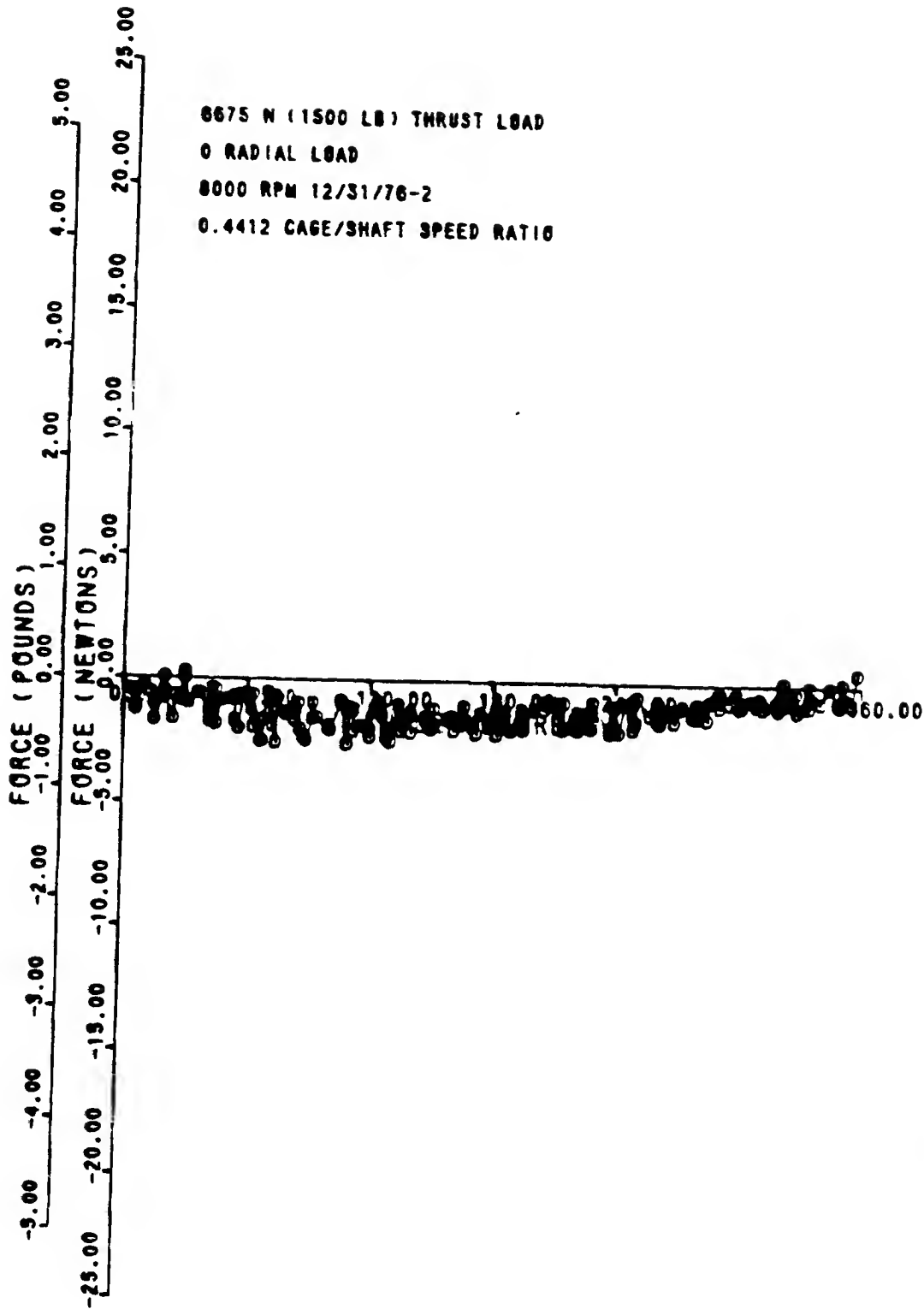


FIG. 78-4.73 N/mm

70090TT9NYPA NT ( 02/23/77

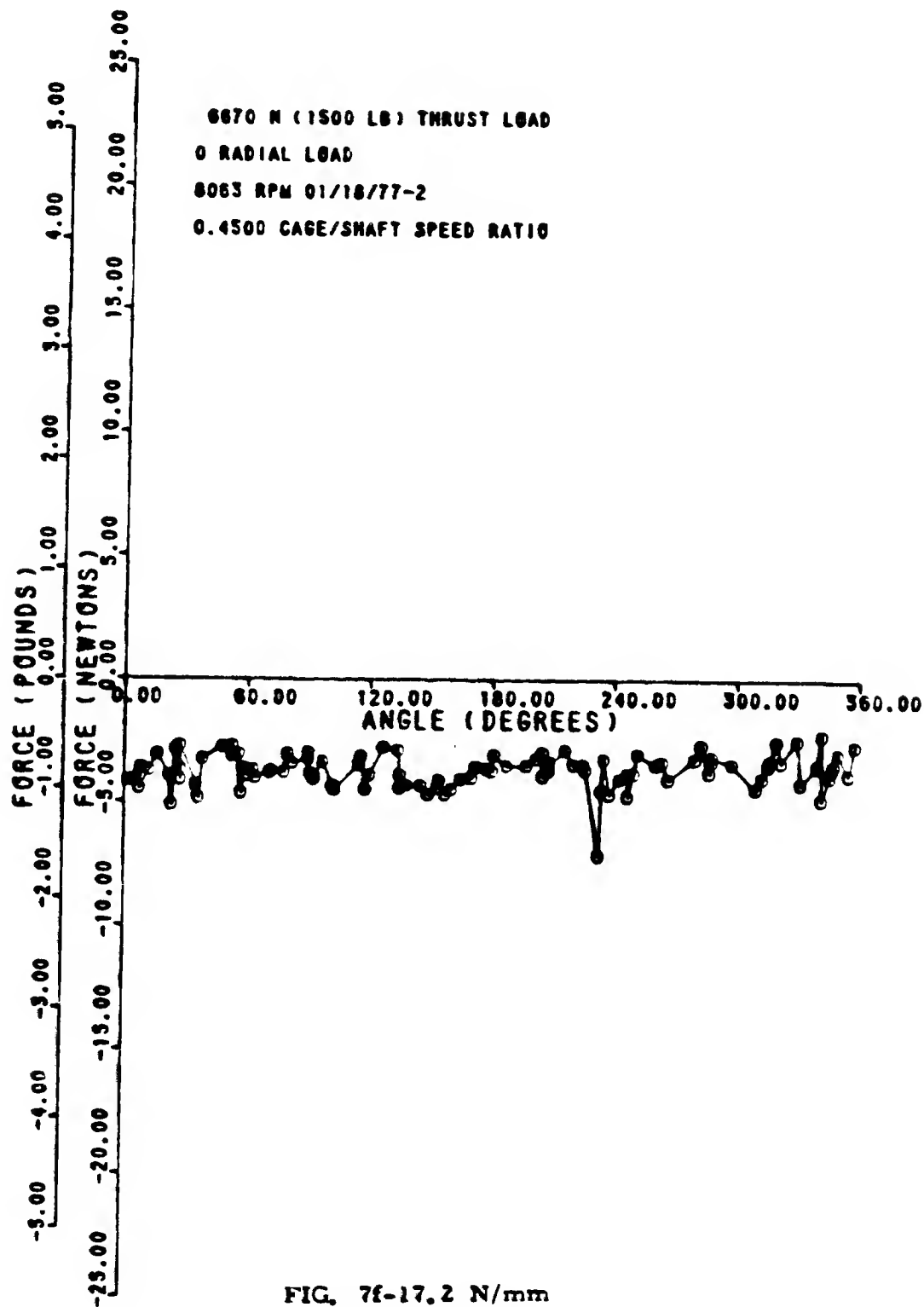


FIG. 7f-17.2 N/mm

70090119NYFAN2

03/19/77

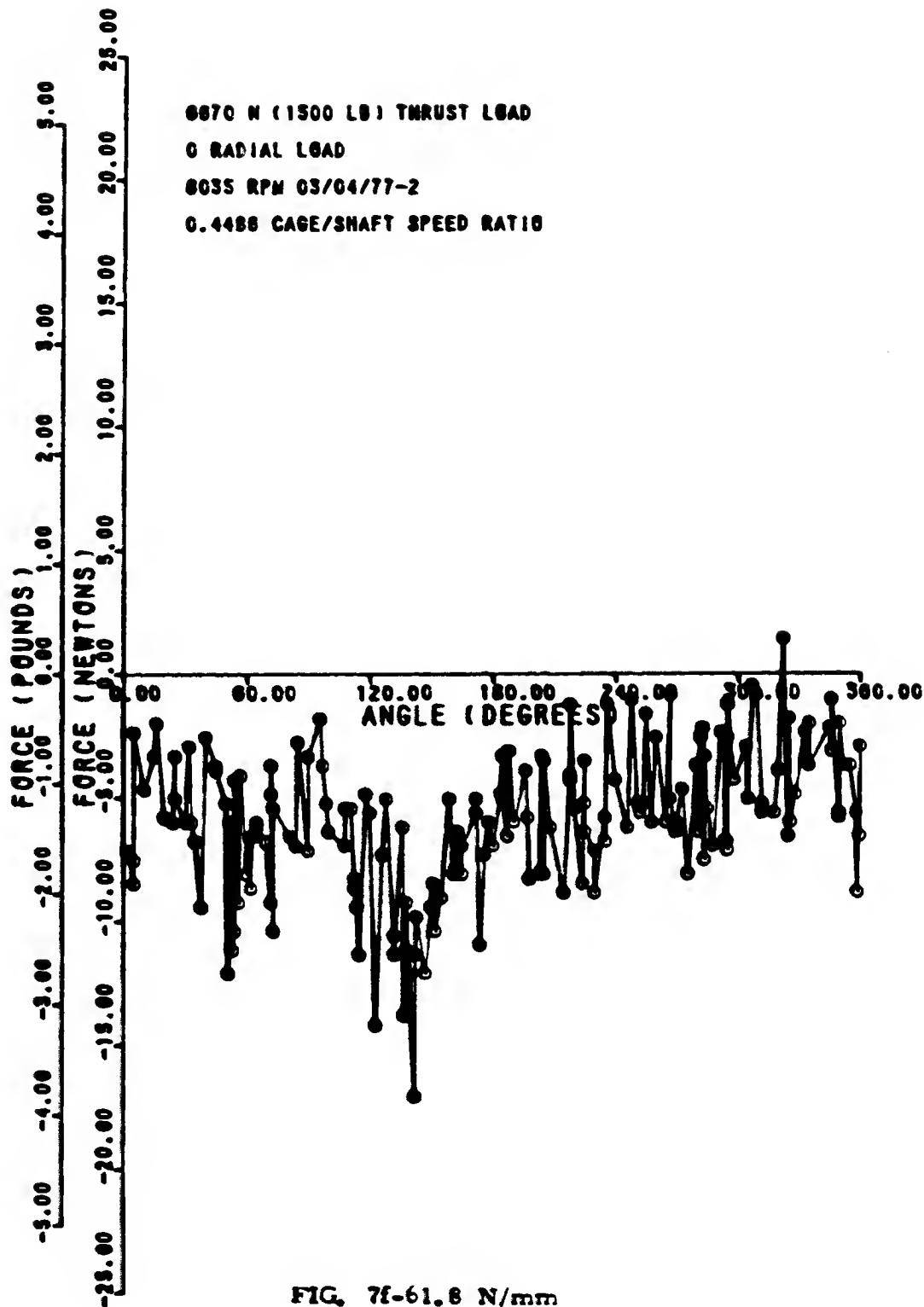


FIG. 7f-61.8 N/mm

70090119NYPAN 4 07/14/77

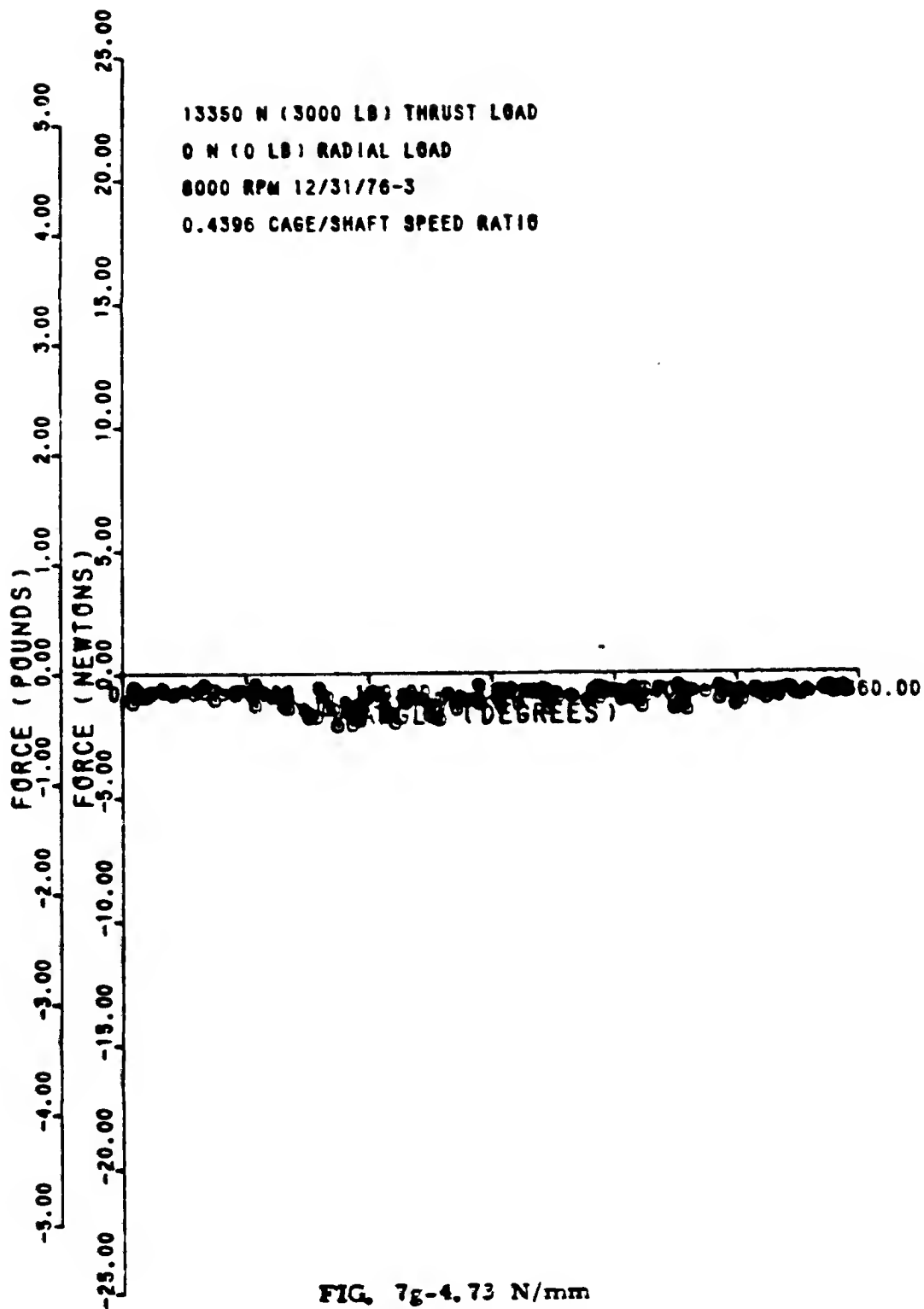


FIG. 7g-4.73 N/mm

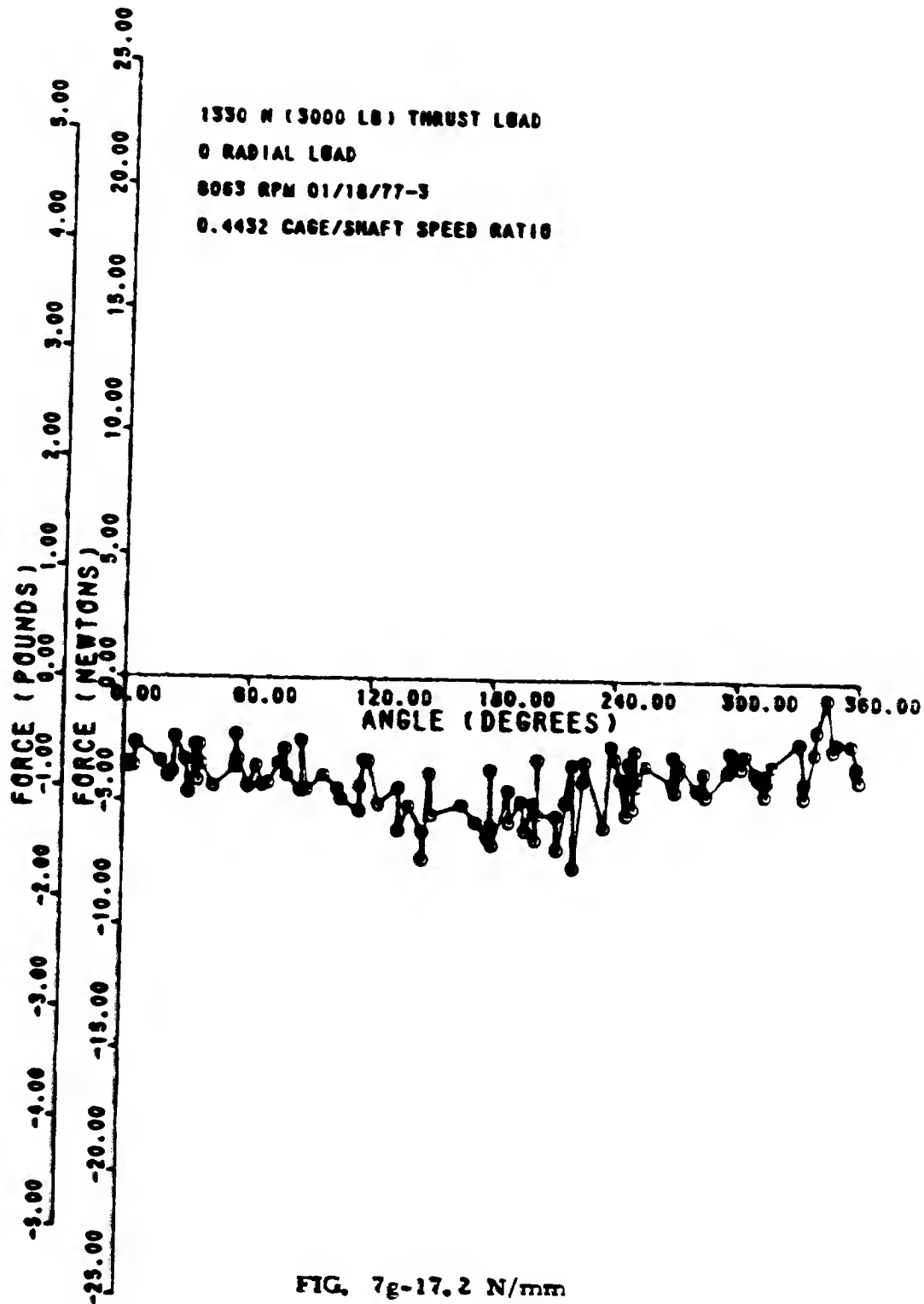


FIG. 7g-17.2 N/mm

70090119NYPAN5

03/12/77

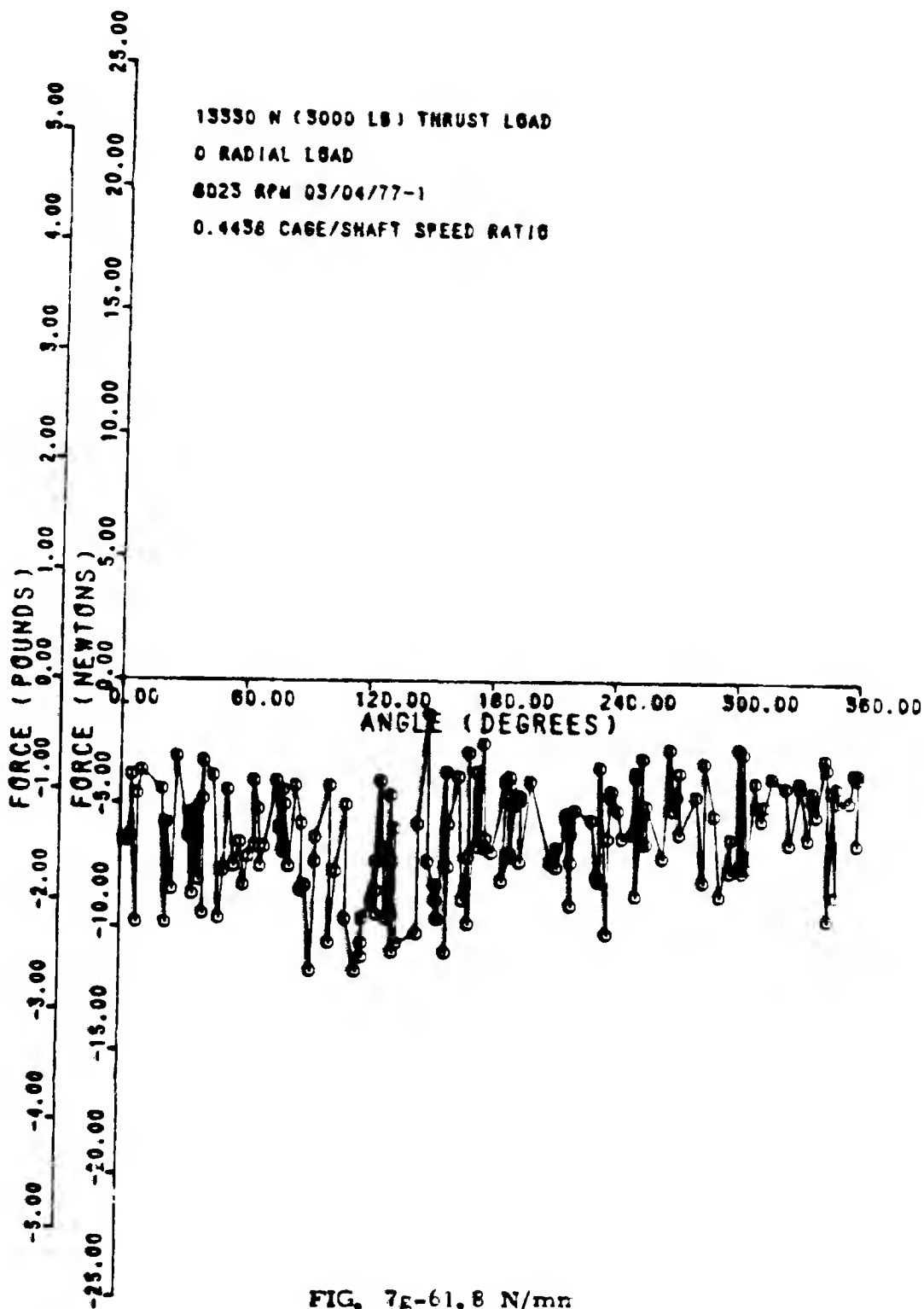


FIG. 7g-61.8 N/mm

7090419NYF AN7 06/13/77

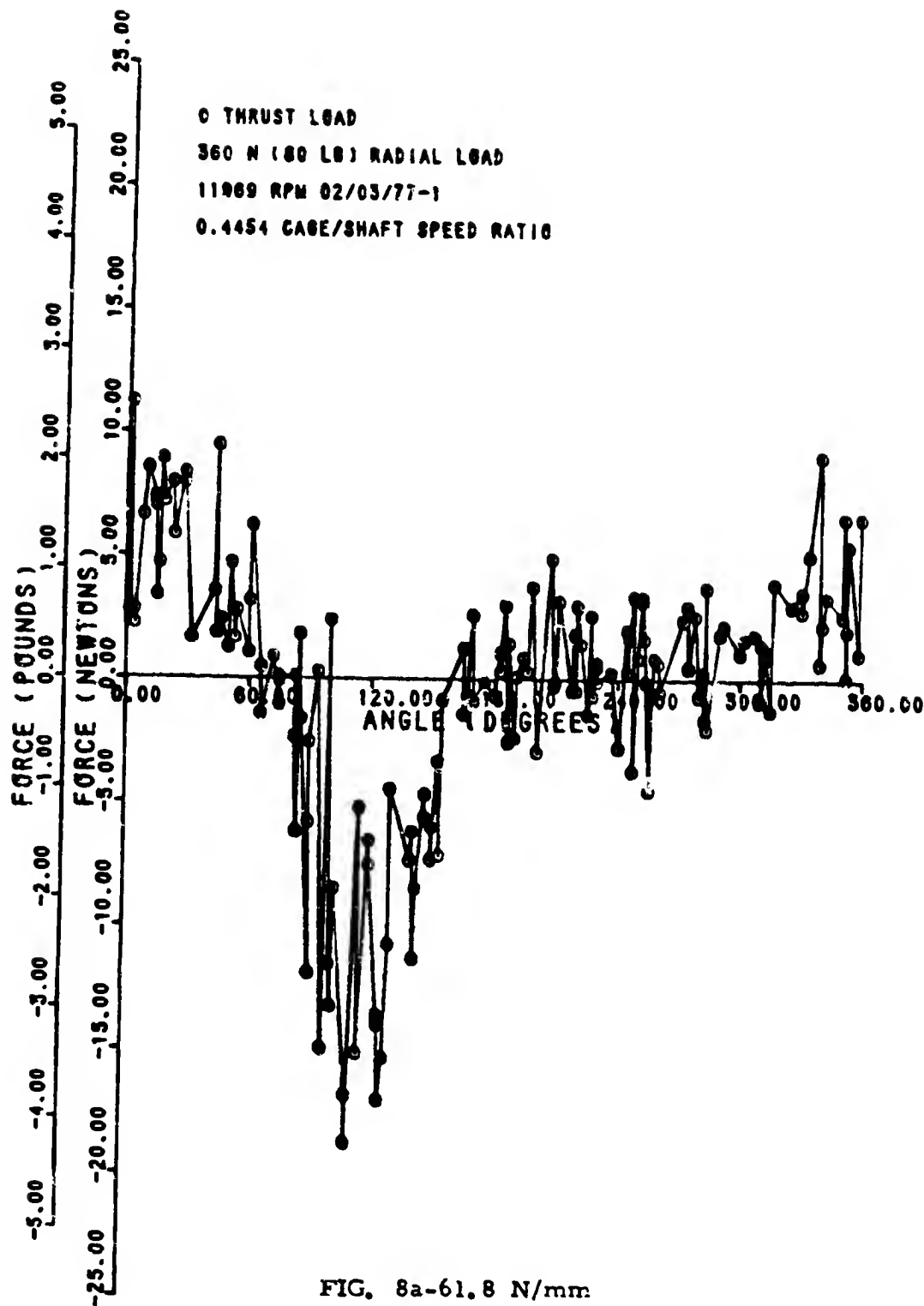


FIG. 8a-61.8 N/mm





7090119WYFAN5

06/17/77

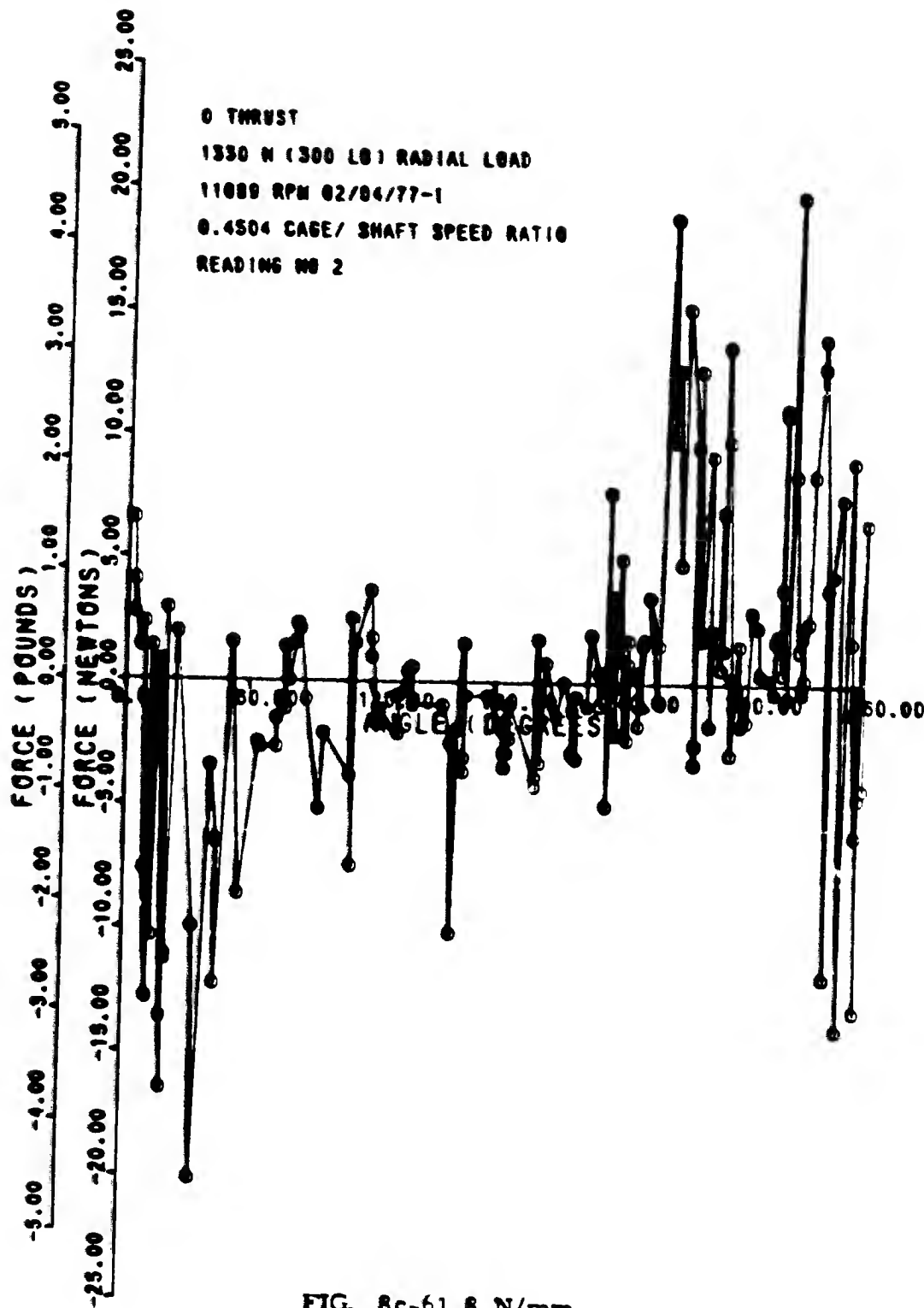
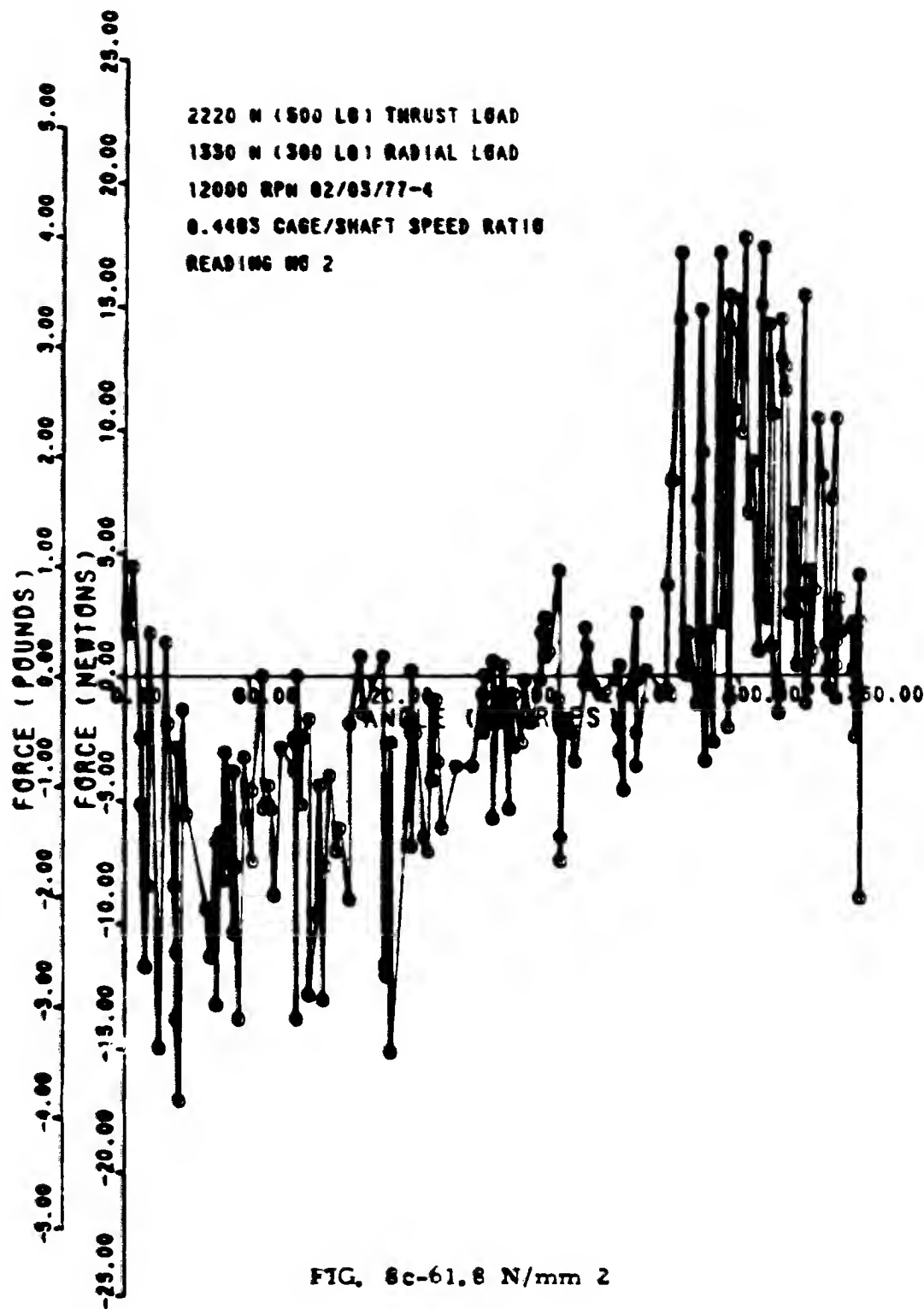


FIG. 8c-61.8 N/mm

700907T 9NY P A N 6  
06/14/77



70090119NYPAN4

03/11/77

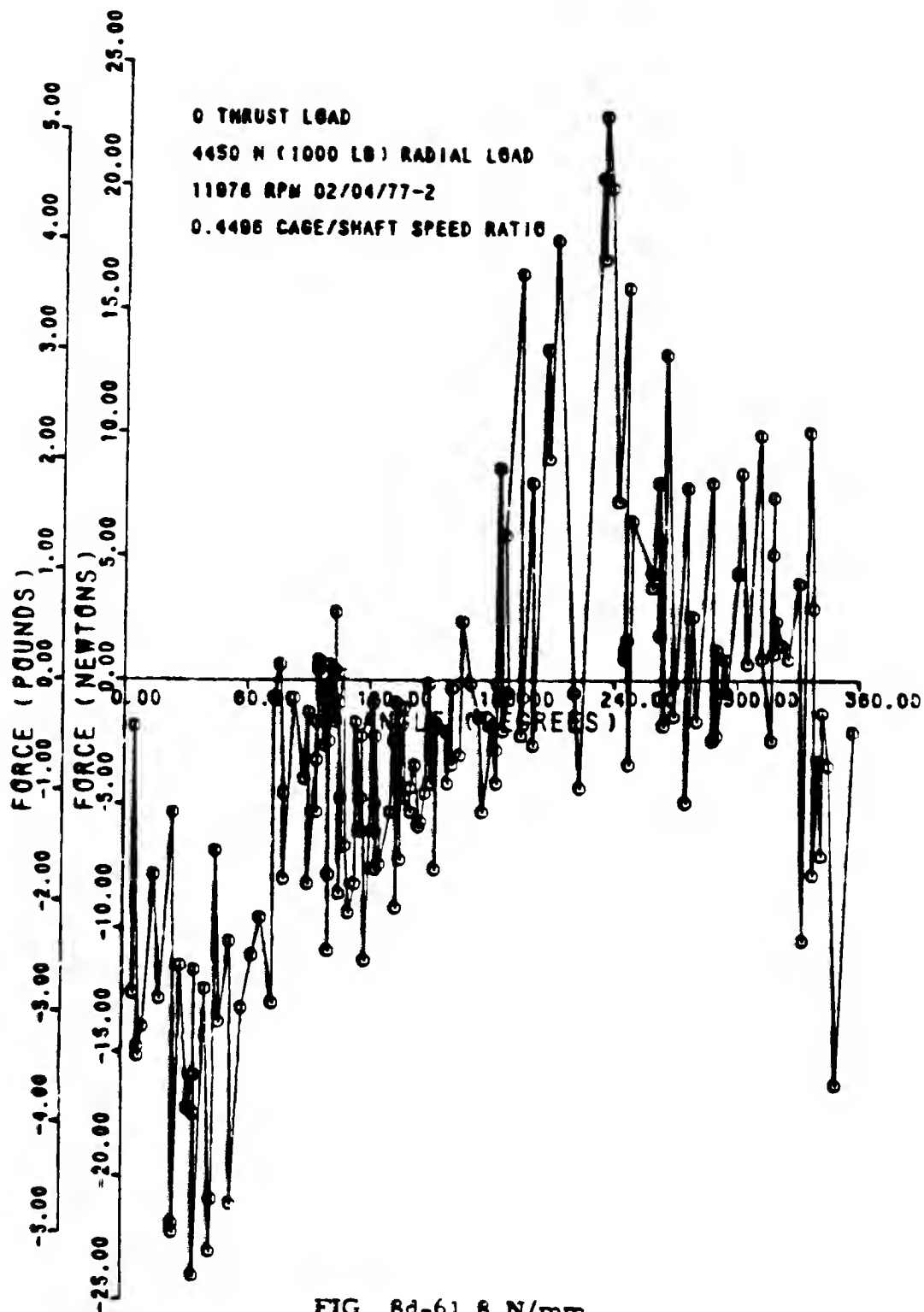


FIG. 8d-61.8 N/mm

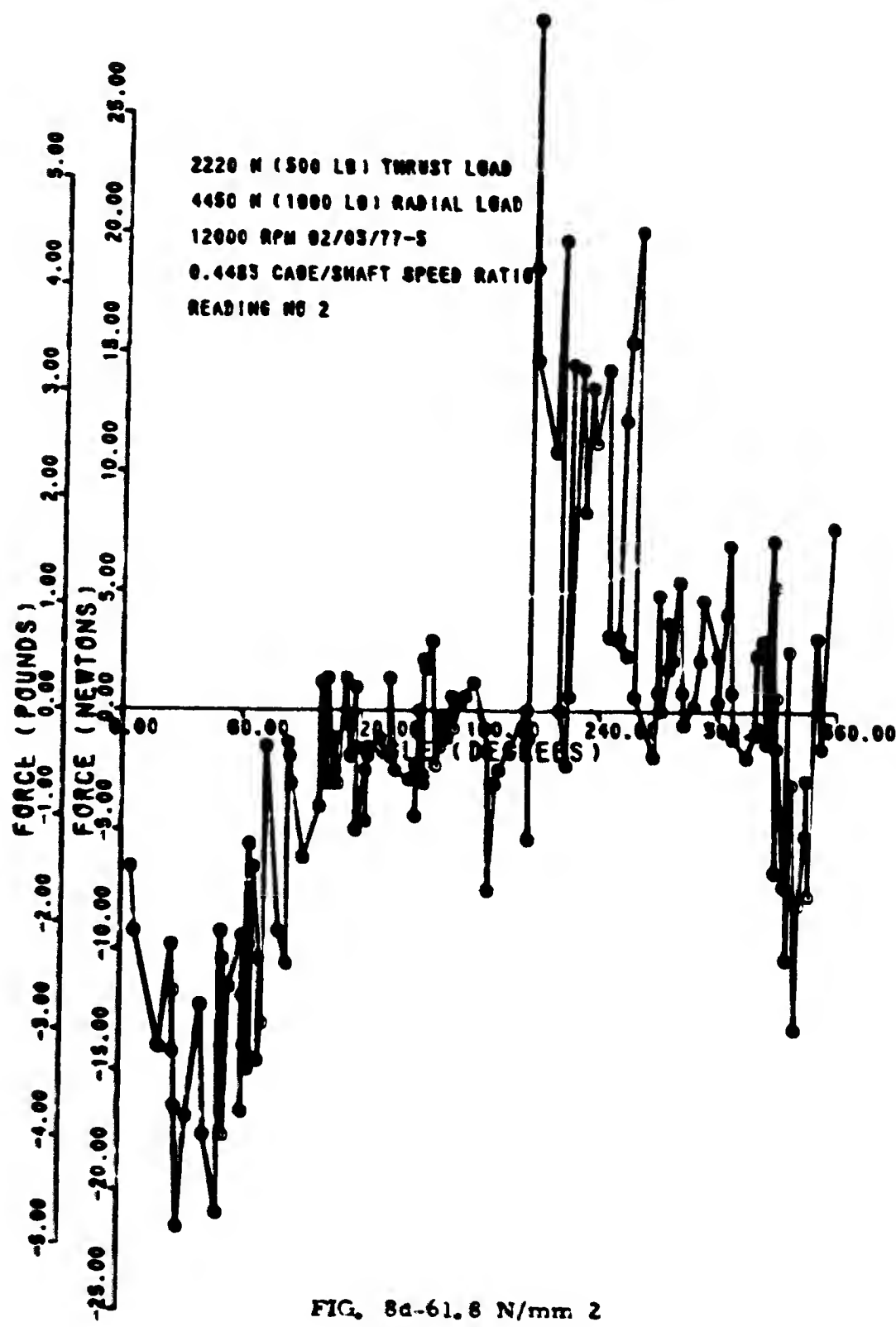


FIG. 8a-61.8 N/mm 2

70090119NYFAN6

02/25/77

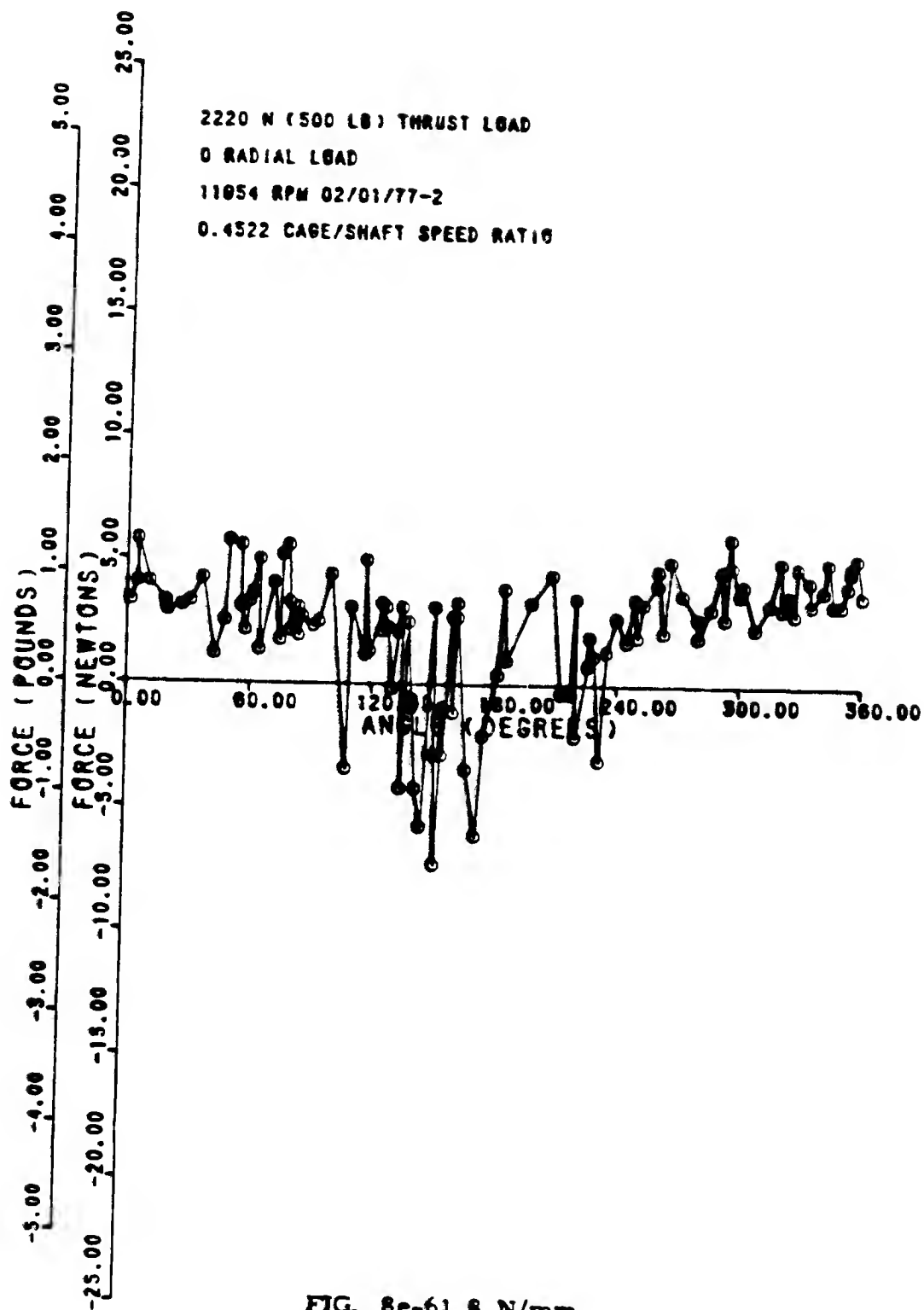


FIG. 8e-61.8 N/mm

70090TT5NYP-AN9-03/15/77

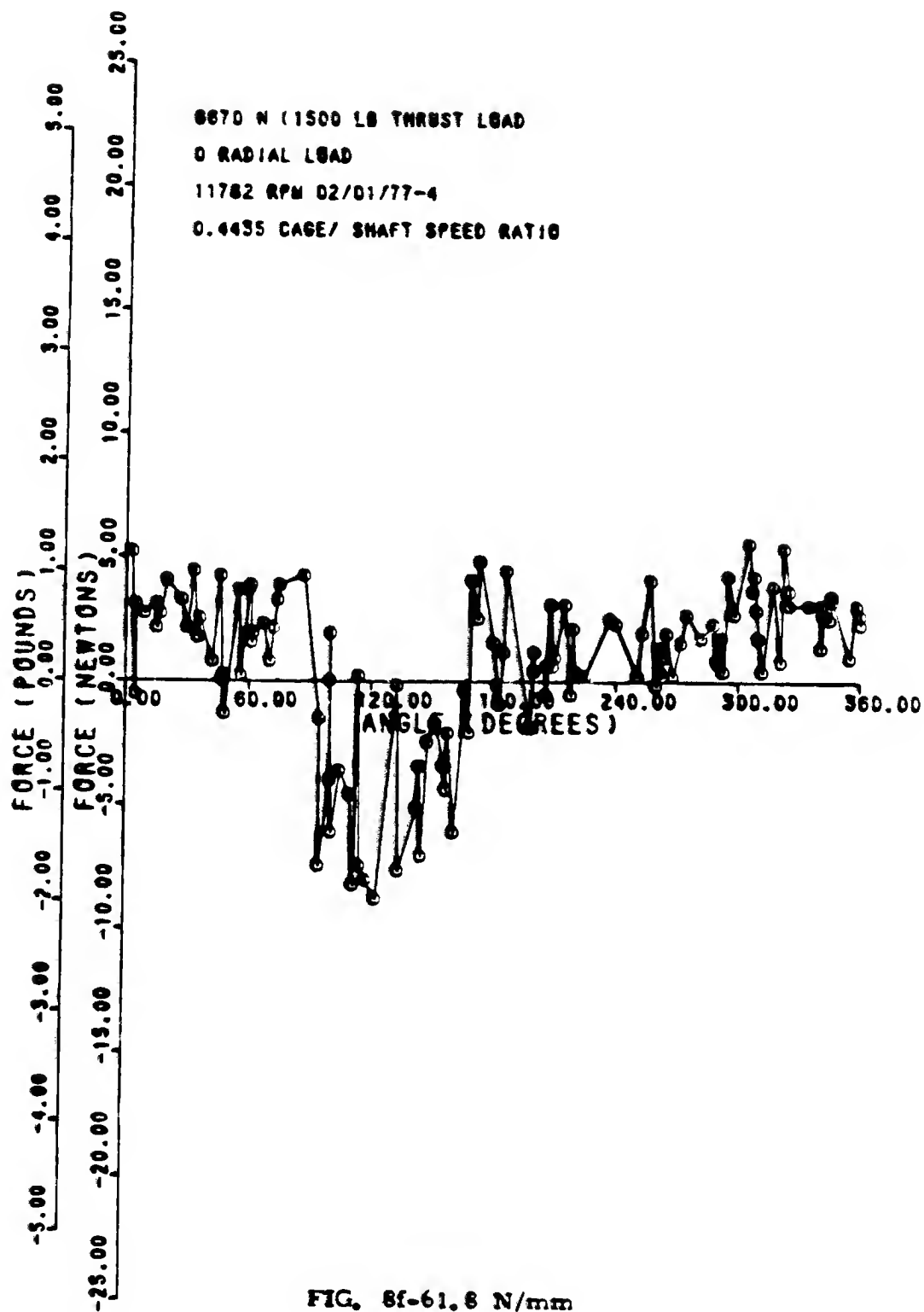


FIG. 8f-61.6 N/mm

70090705NYP AN I U 06/11/77

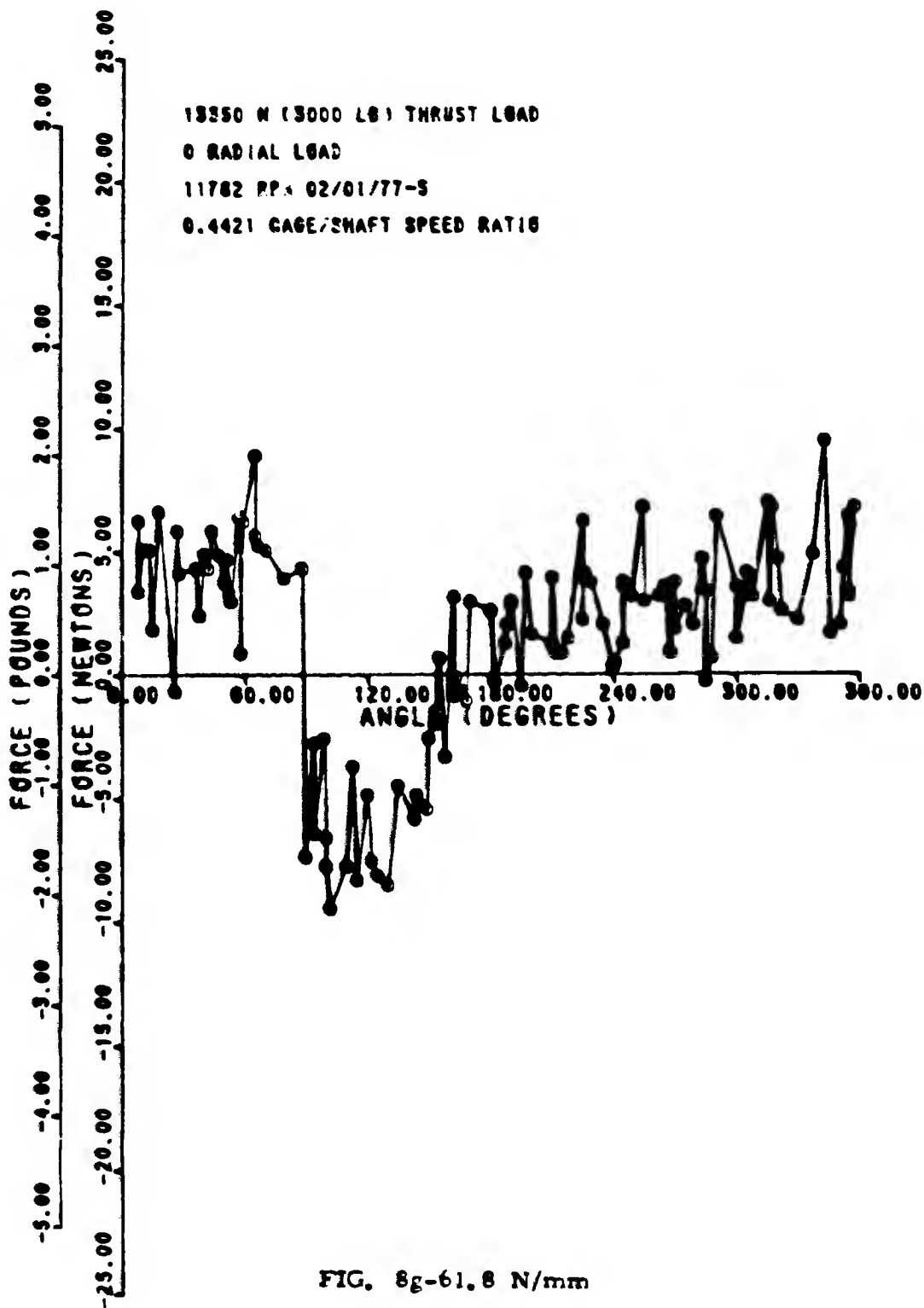
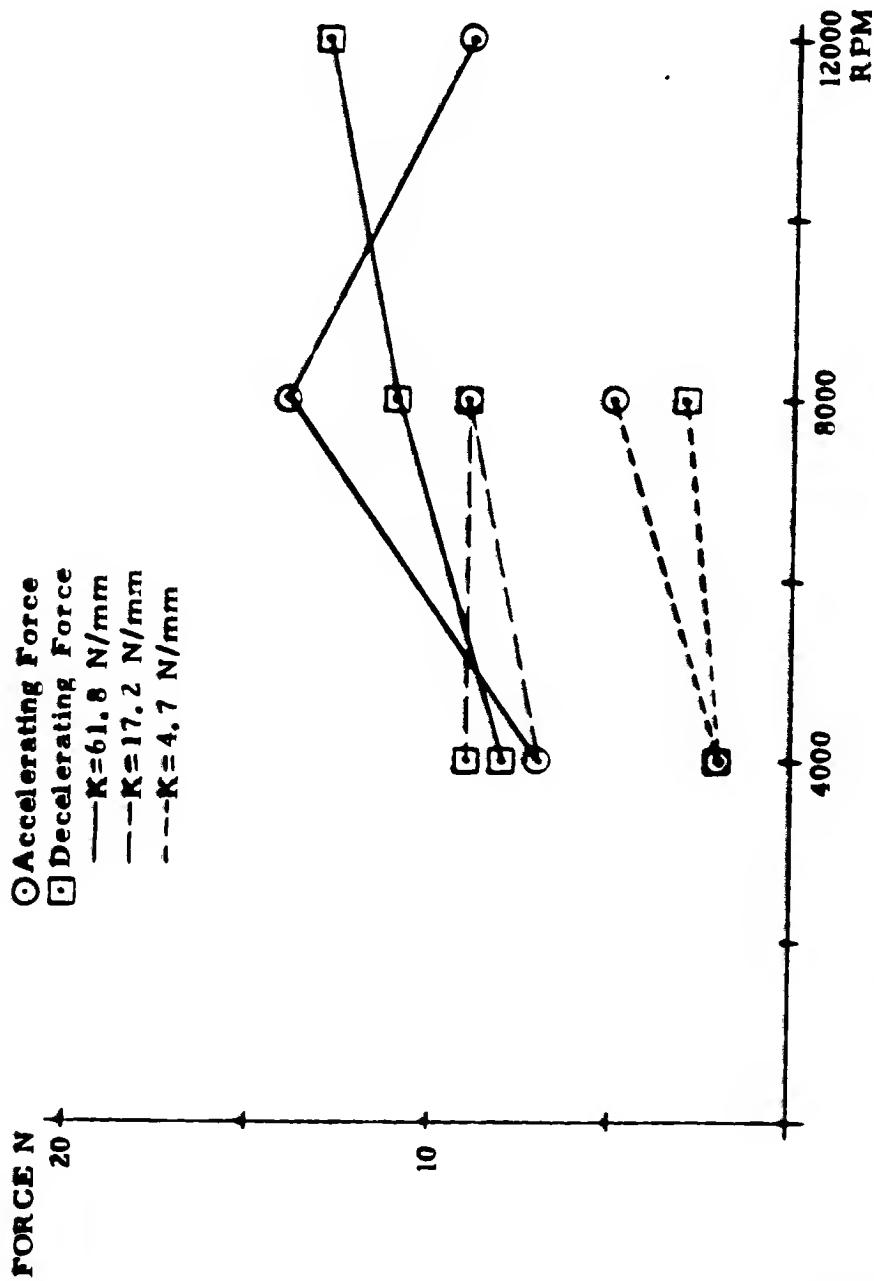


FIG. 8g-61.8 N/mm





**FIGURE 9a Cage Force Magnitude Versus Shaft Speed, 360 N Radial Load**

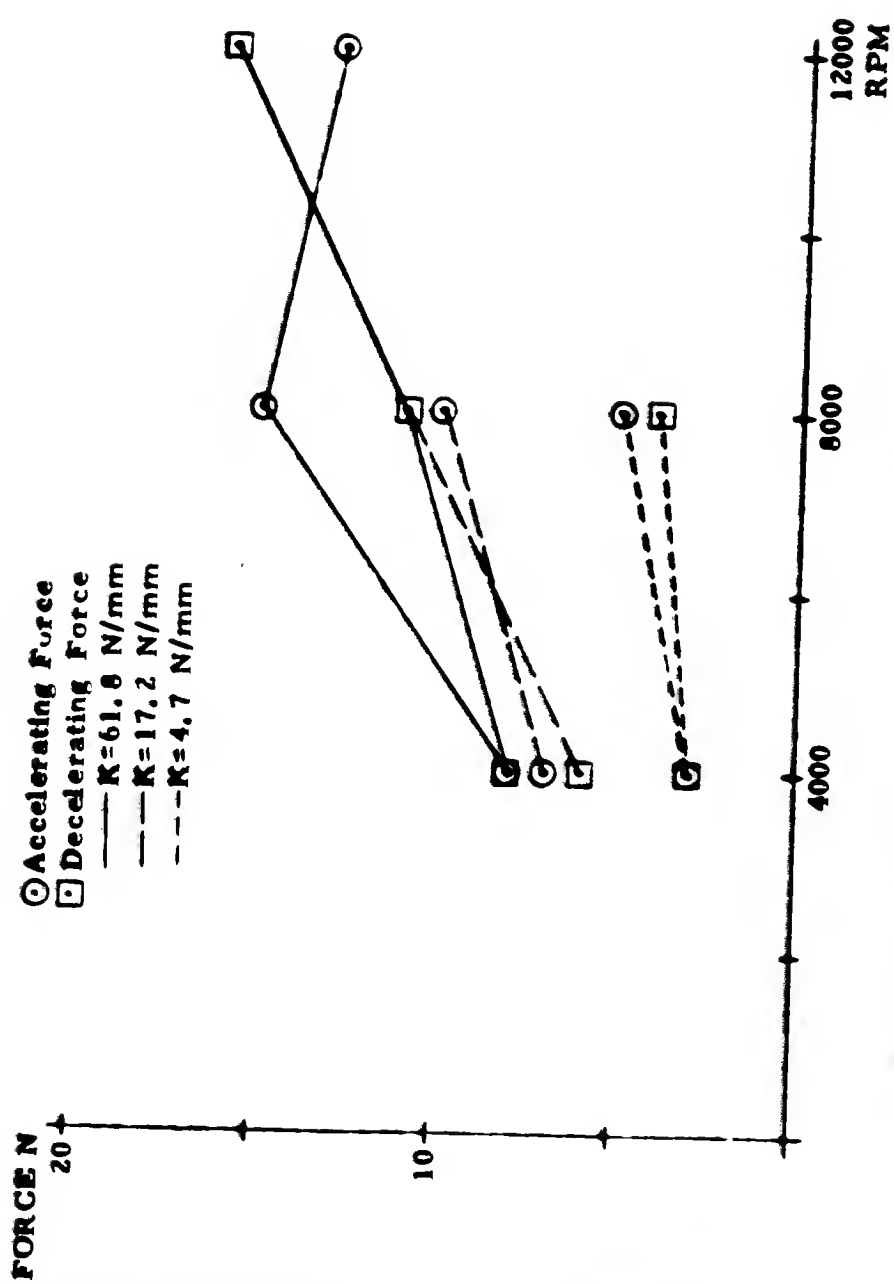


FIGURE 9b Cage Force Magnitude Versus Shaft Speed, 670 N Radial Load

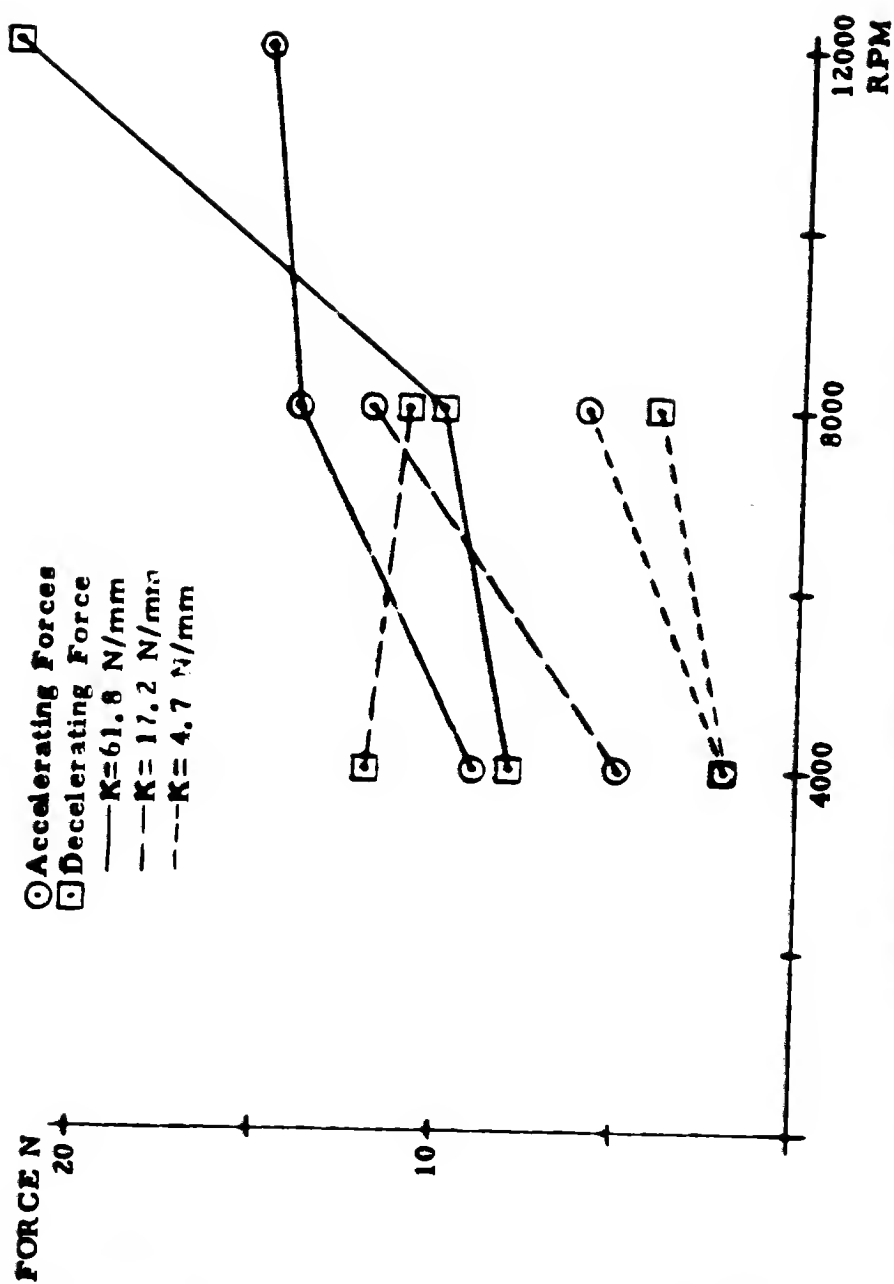
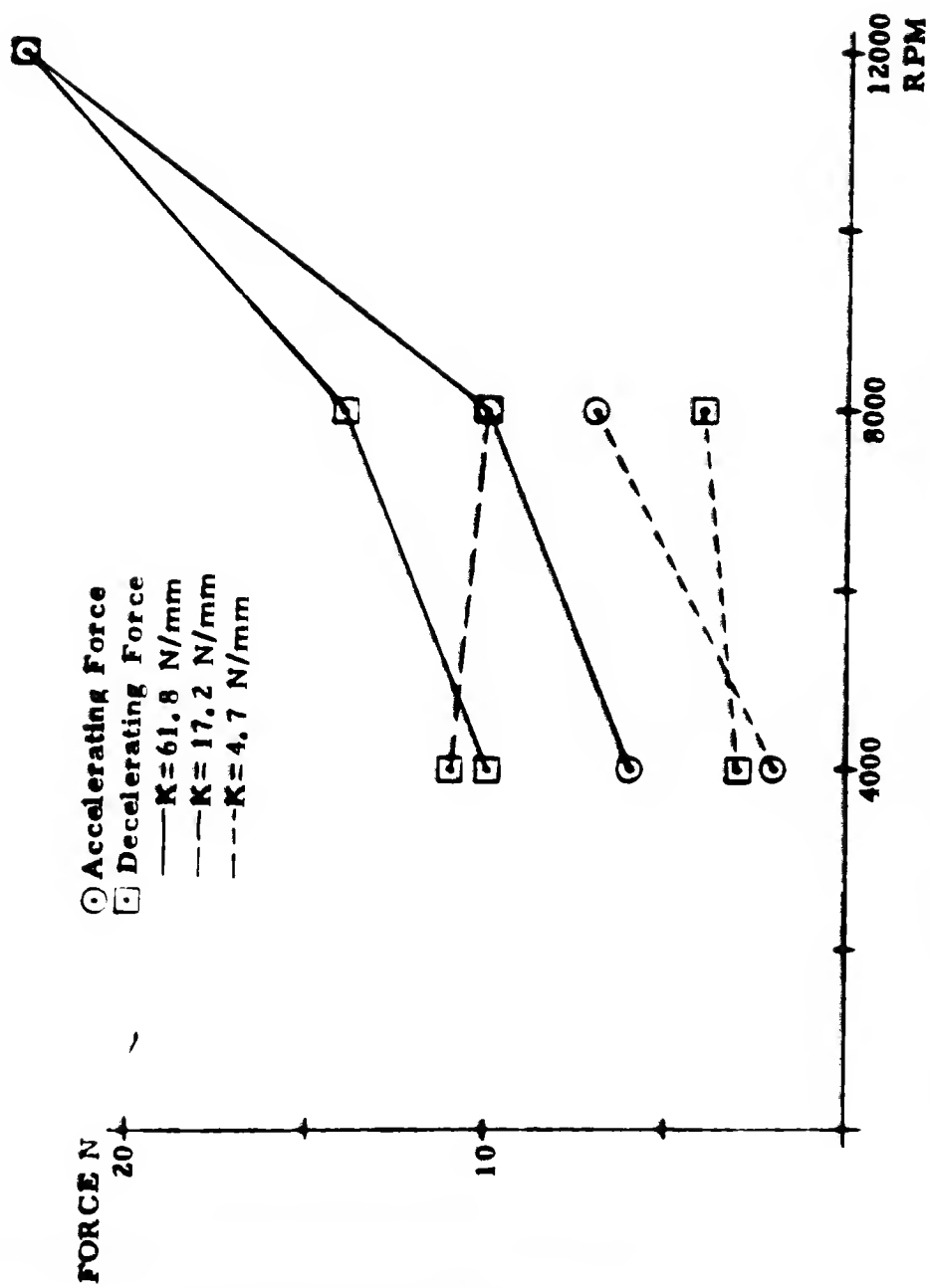


FIGURE 9c Cage Force Magnitude Versus Shaft Speed, 1330 N Radial Load



**FIGURE 9d Cage Force Magnitude Versus Shaft Speed, 4450 N Radial Load**

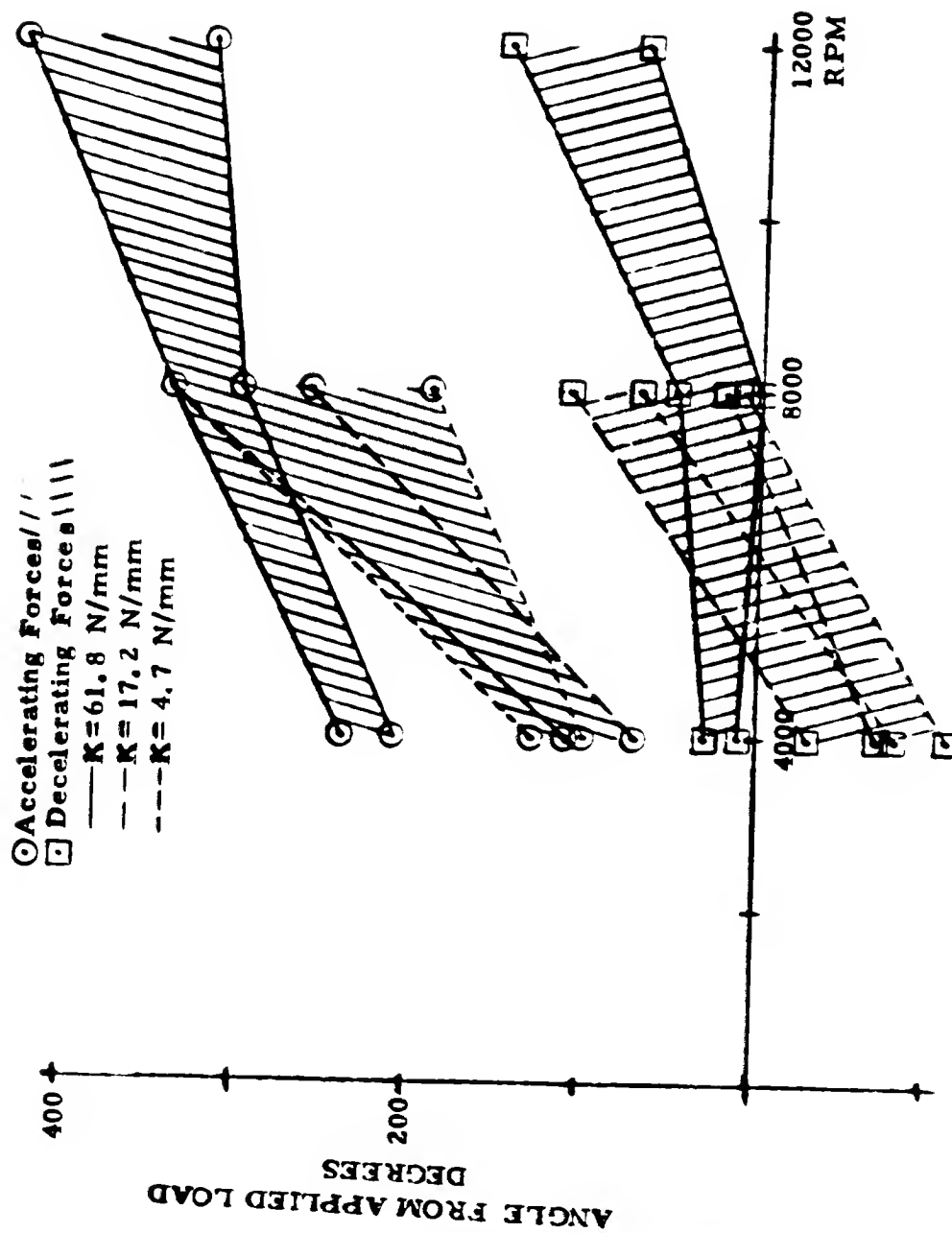


FIGURE 10a Locations of Accelerating and Decelerating Cage Forces as a Function of Shaft Speed, 360 N Radial Load

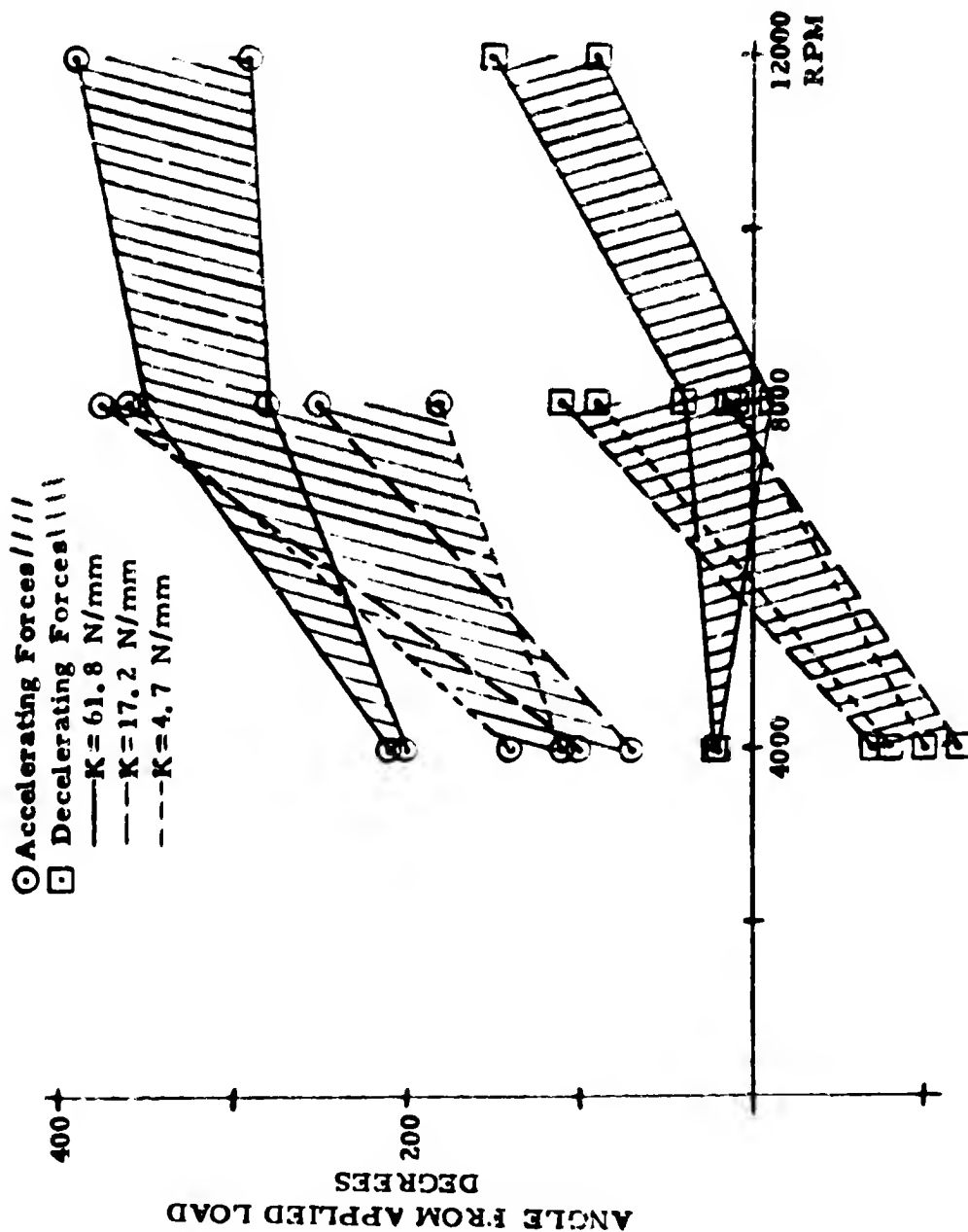


FIGURE 10b Locations of Accelerating and Decelerating Cage Forces as a Function of Shaft Speed, 670 N Radial Load

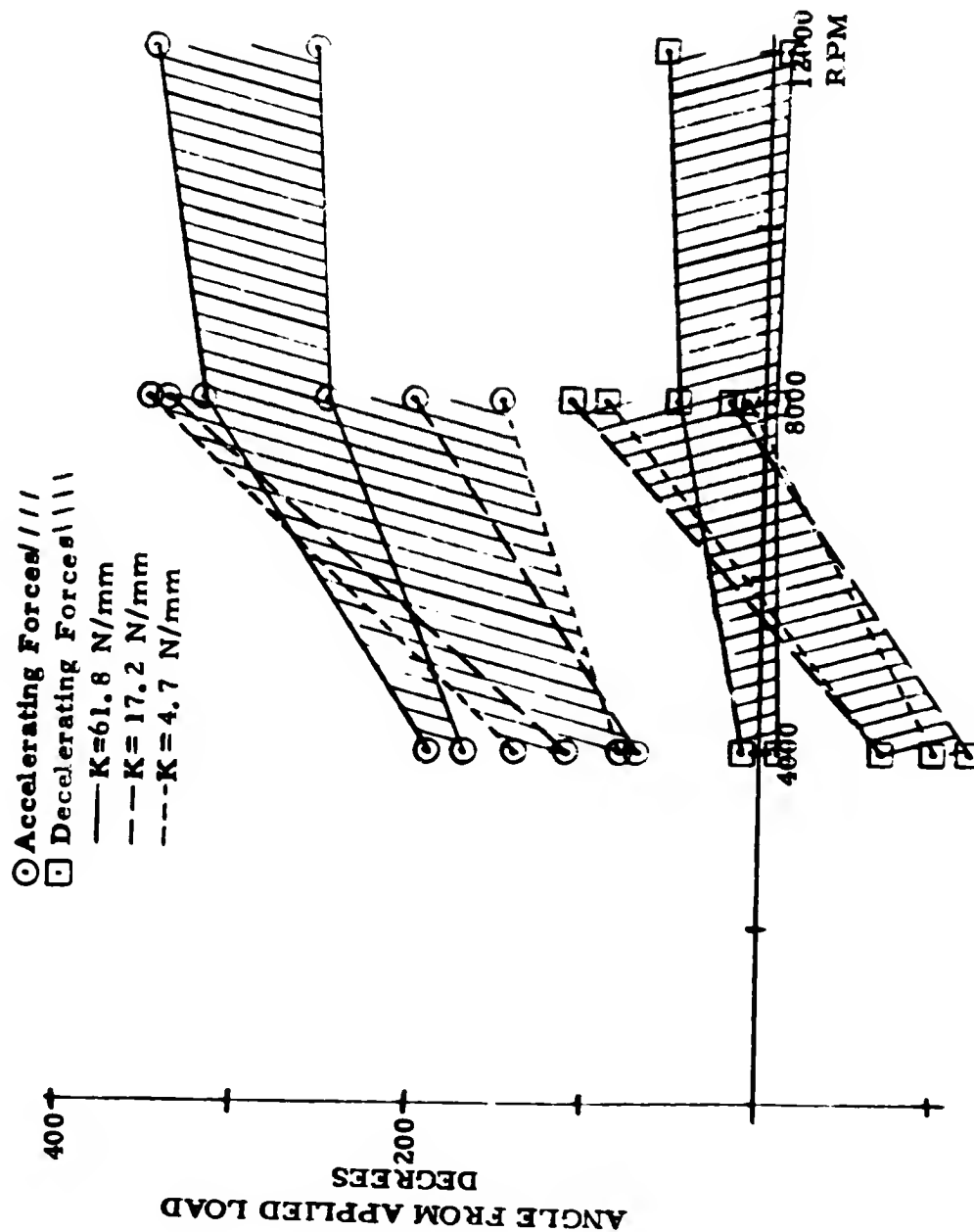
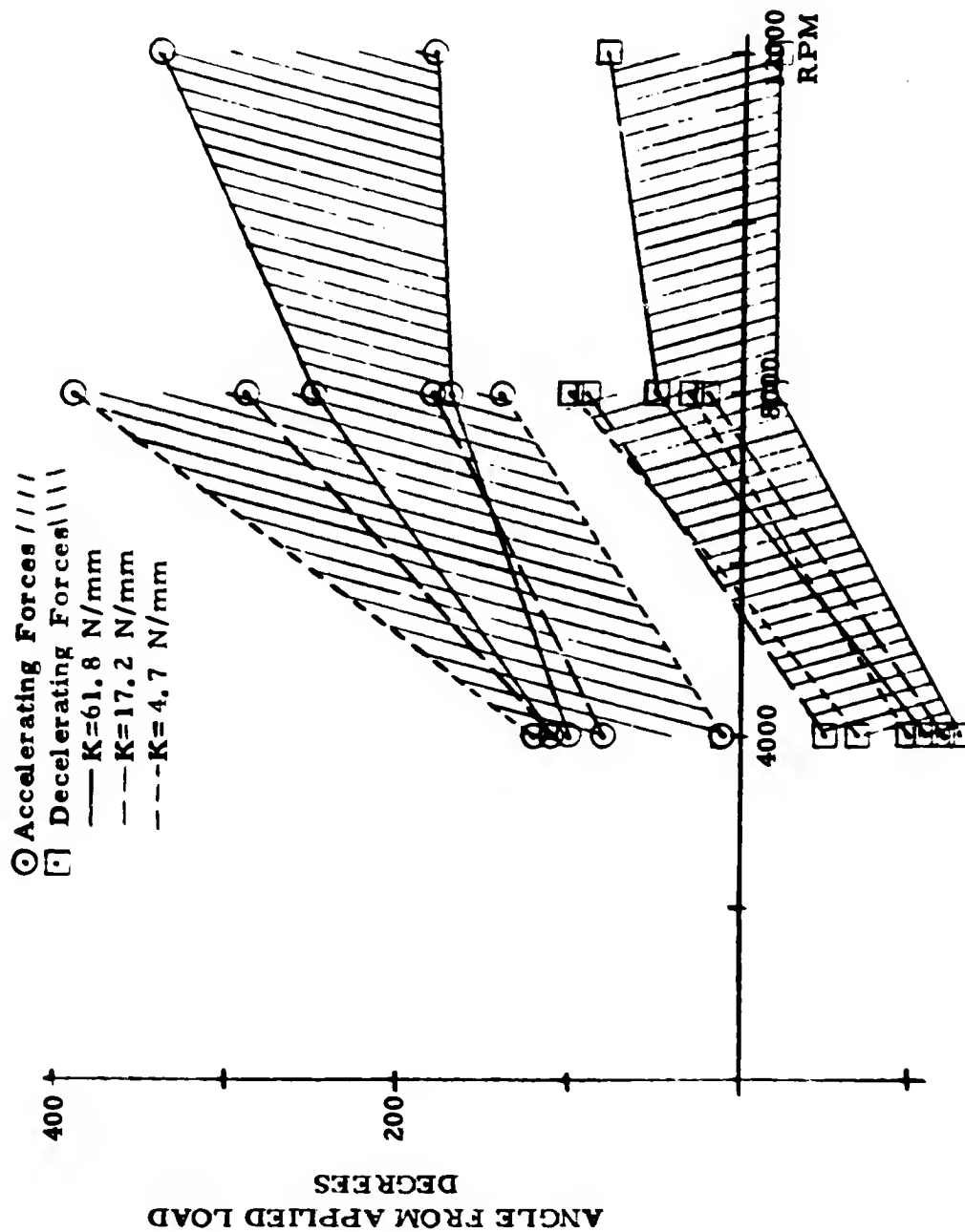


FIGURE 10c Locations of Accelerating and Decelerating Forces as a Function of Shaft Speed, 1330 N Radial Load

PRECEDING PAGE BLANK NOT FILMED.



**FIGURE 10d Locations of Accelerating and Decelerating Cage Forces as a Function of Shaft Speed, 4450 N Radial Load**



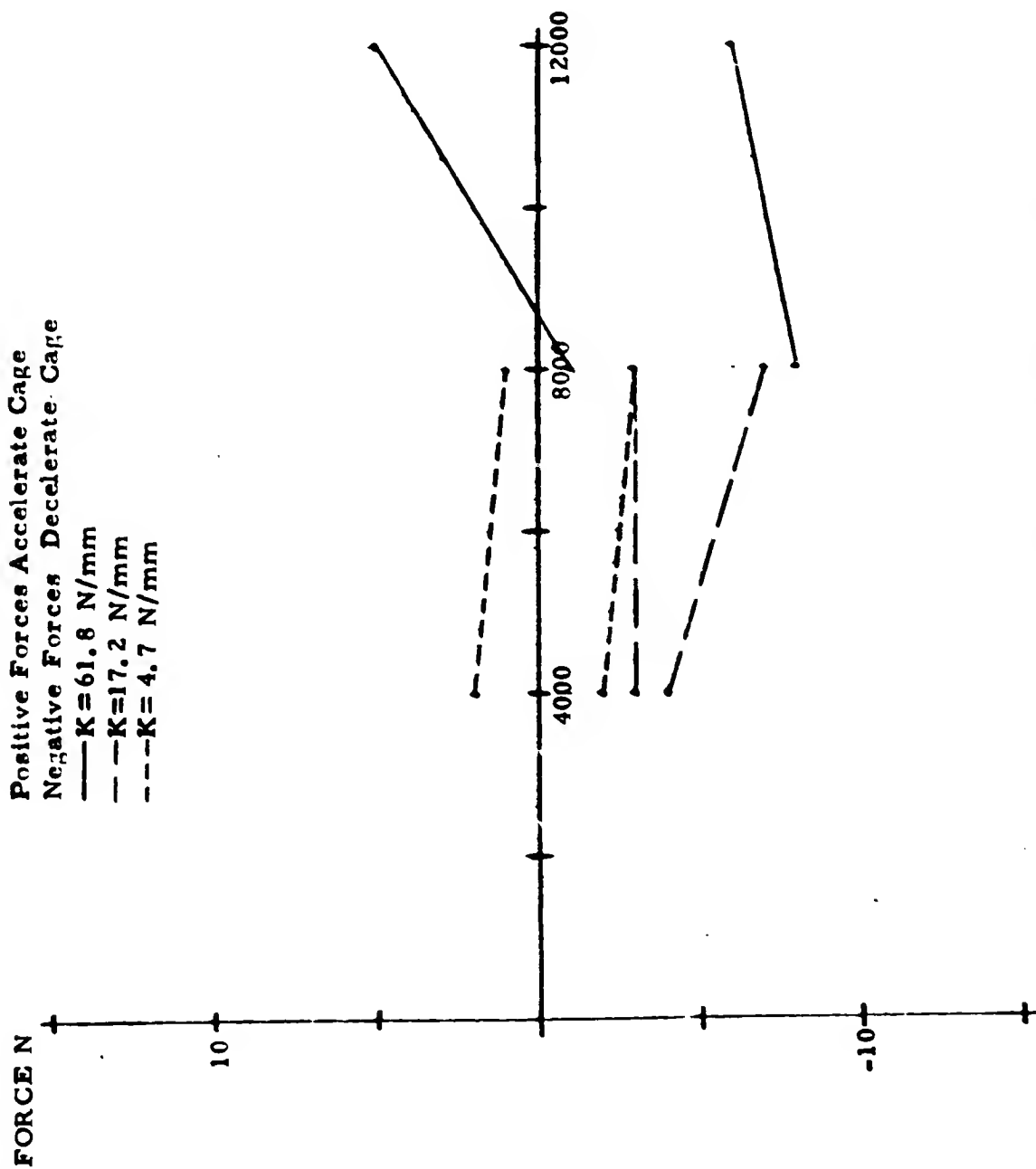


FIGURE 11a Cage Force Magnitude Range Versus Shaft Speed, 2220 N

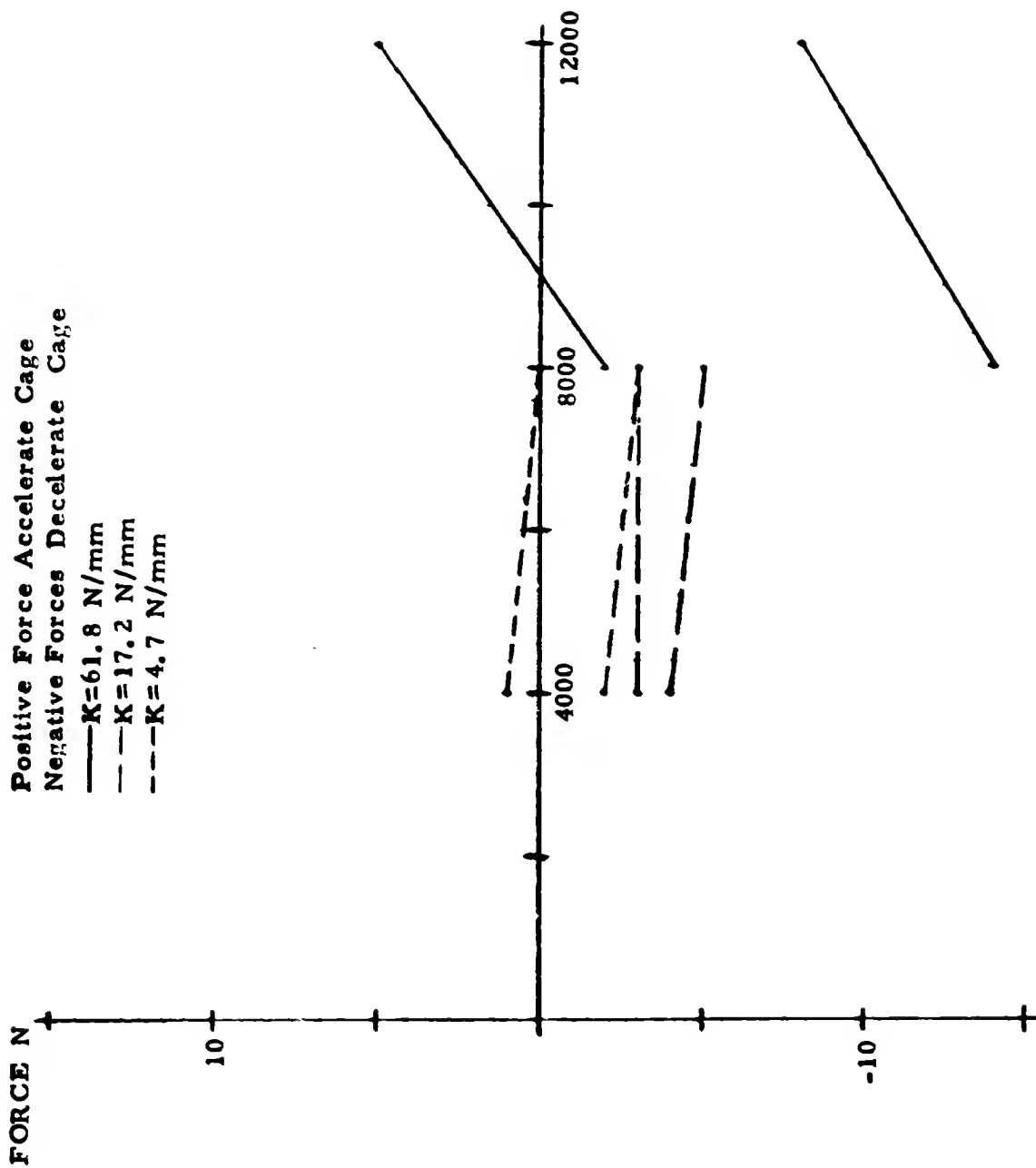


FIGURE 11b Cage Force Magnitude Range Versus Shaft Speed, 6670 N Thrust Load

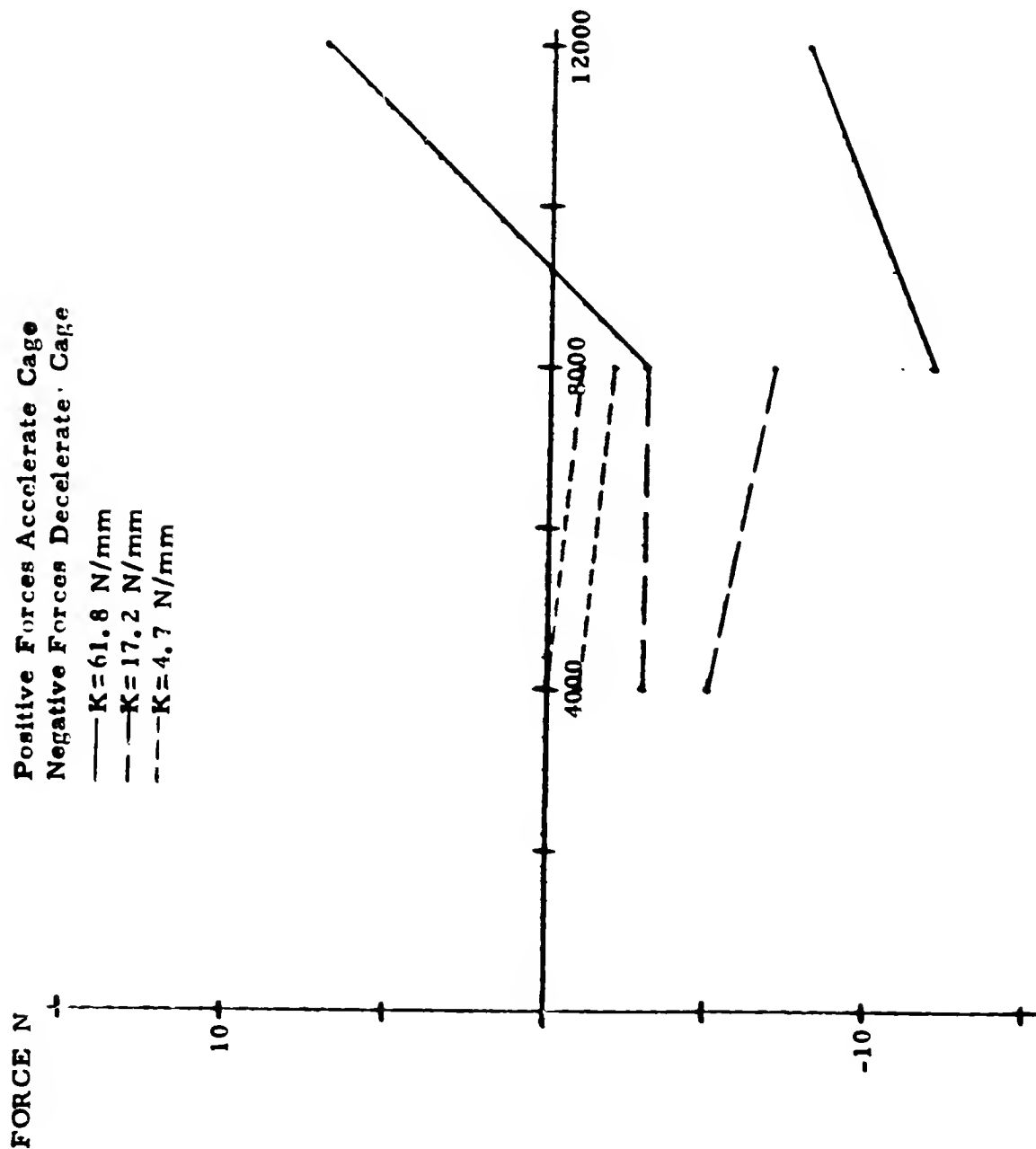


FIGURE 11c Cage Force Magnitude Range Versus Shaft Speed, 13330 N Thrust Load

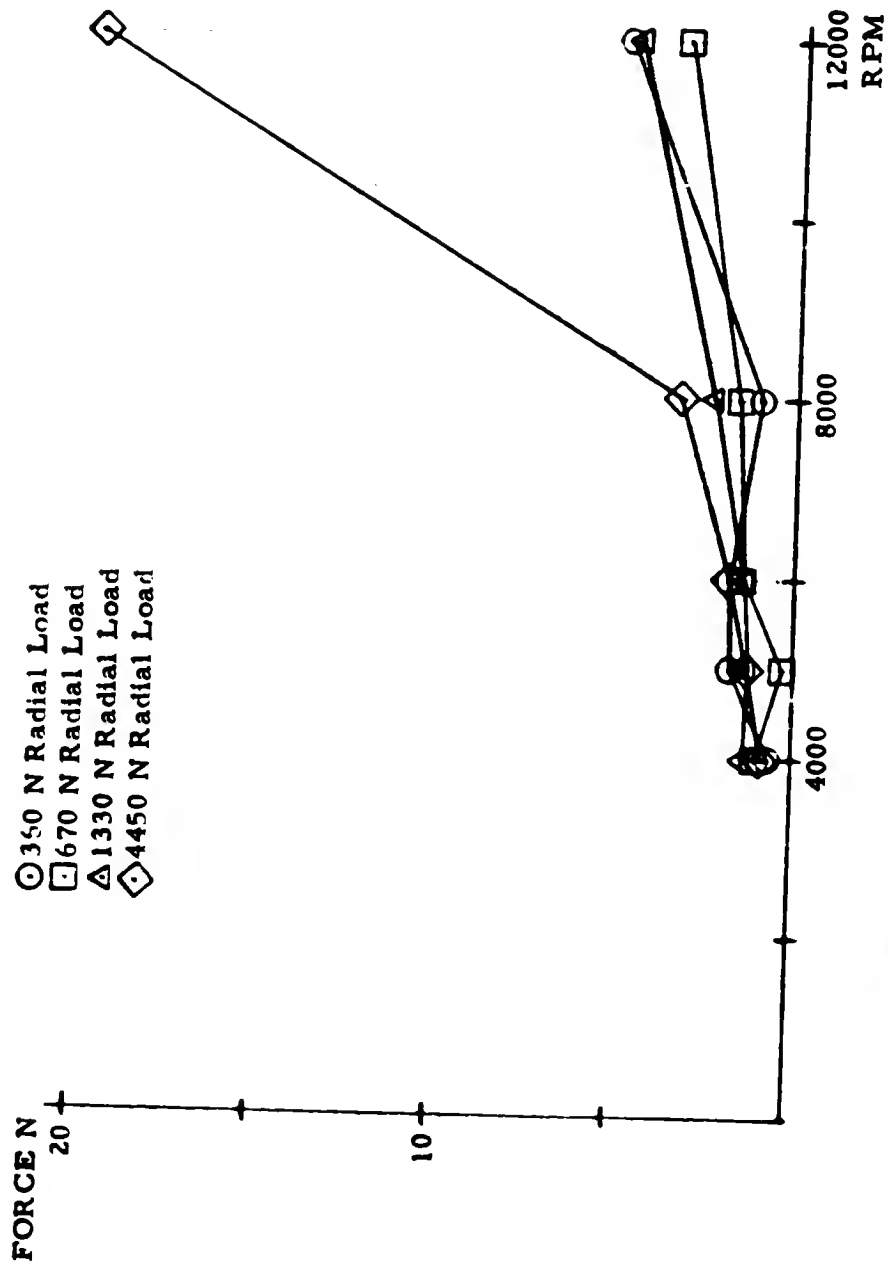


FIGURE 12a Resultant Cage Force Versus Shaft Speed

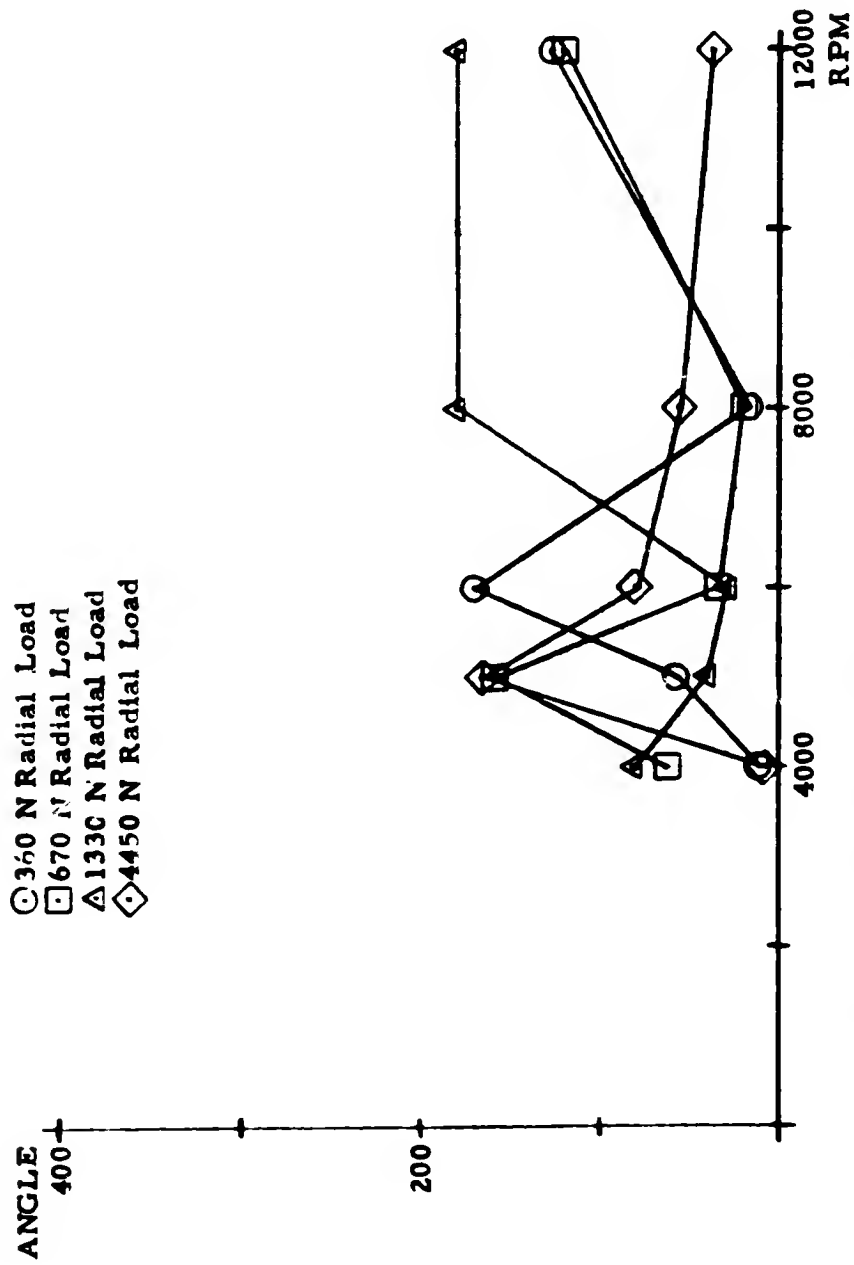


FIGURE 12b Resultant Cage Force Location Versus Shaft Speed

70090119NYF, N16 06/17/77

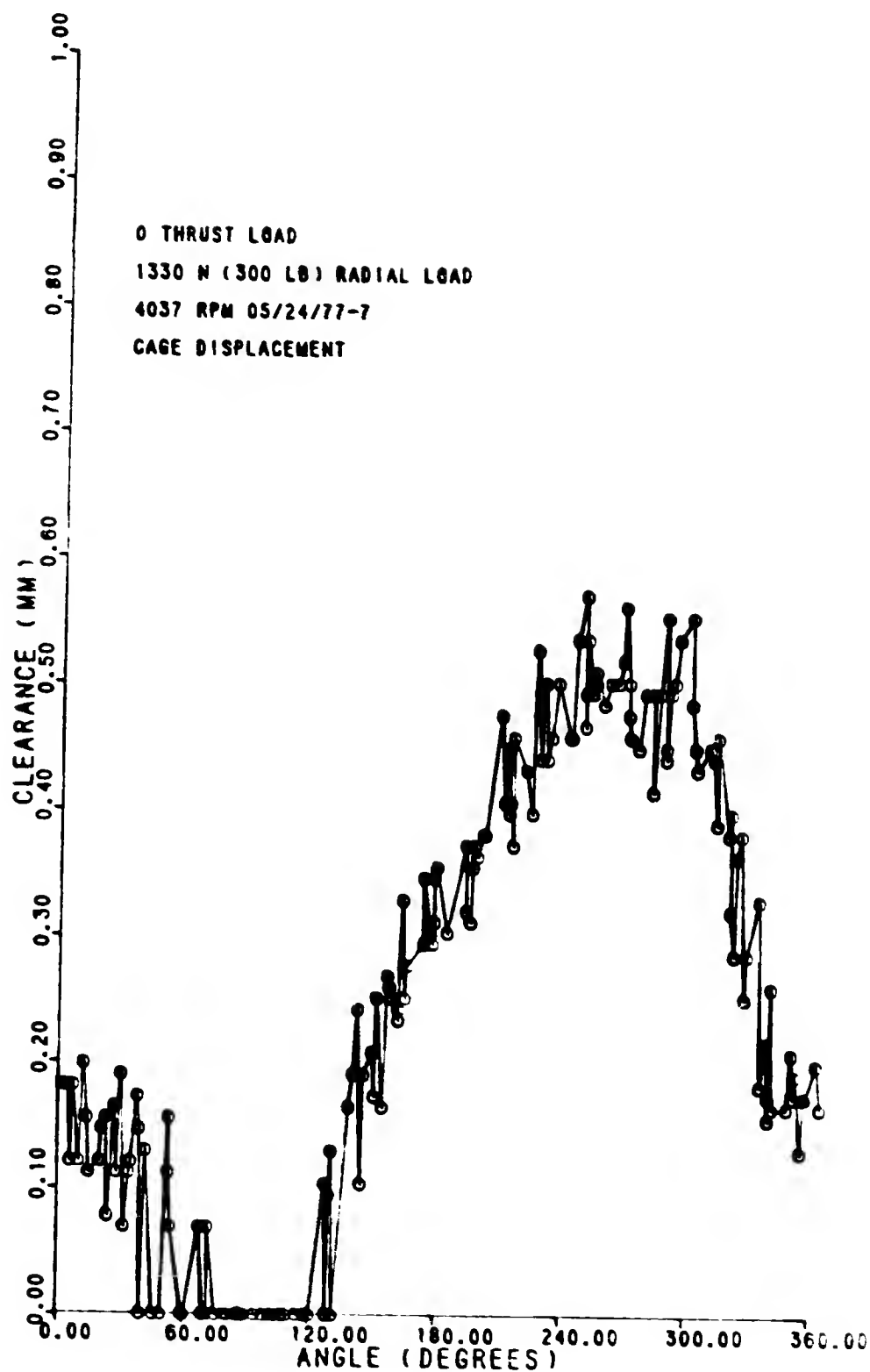


FIG. 13a

70090TTSNYPAN 06/09/77

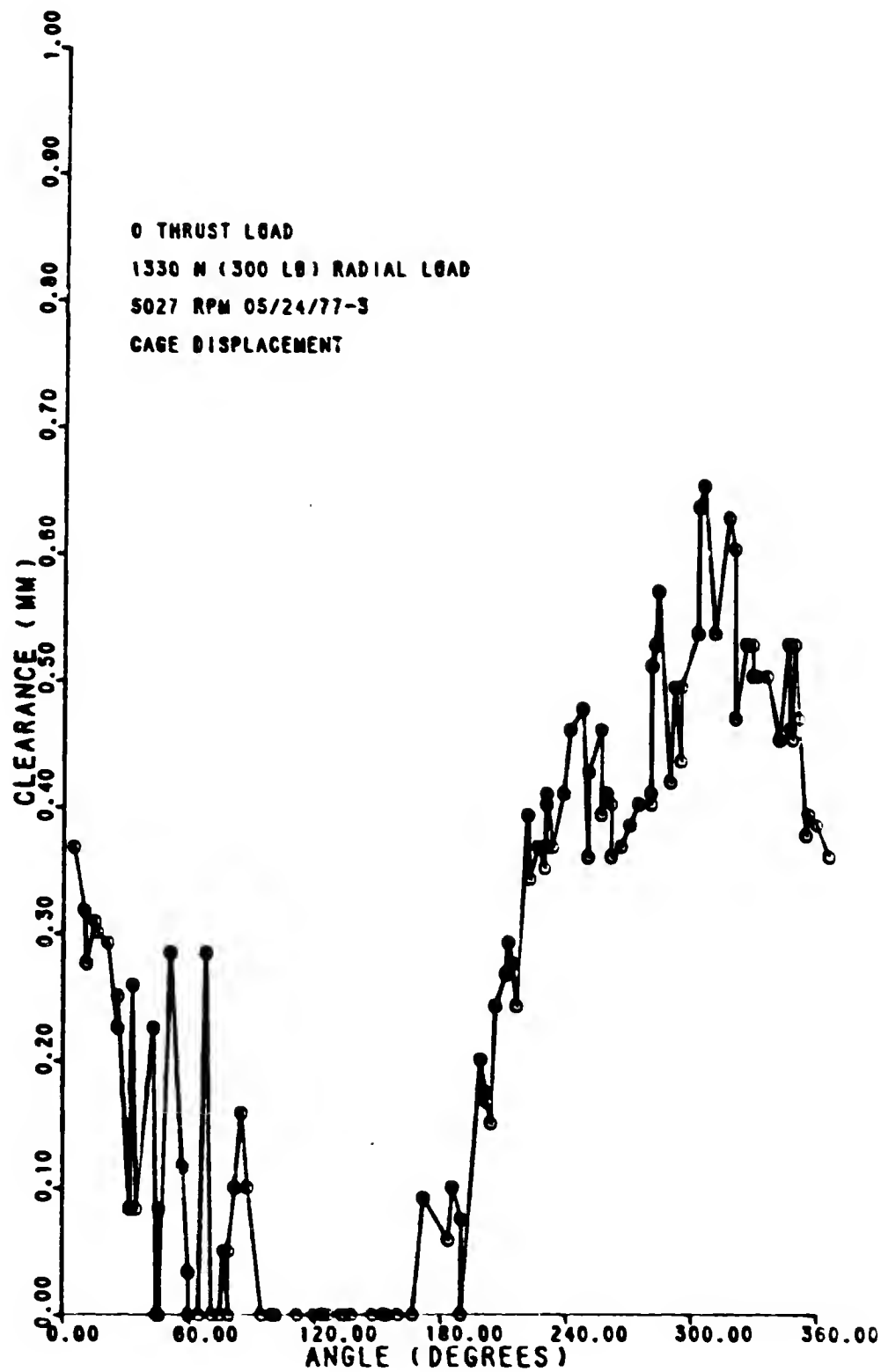
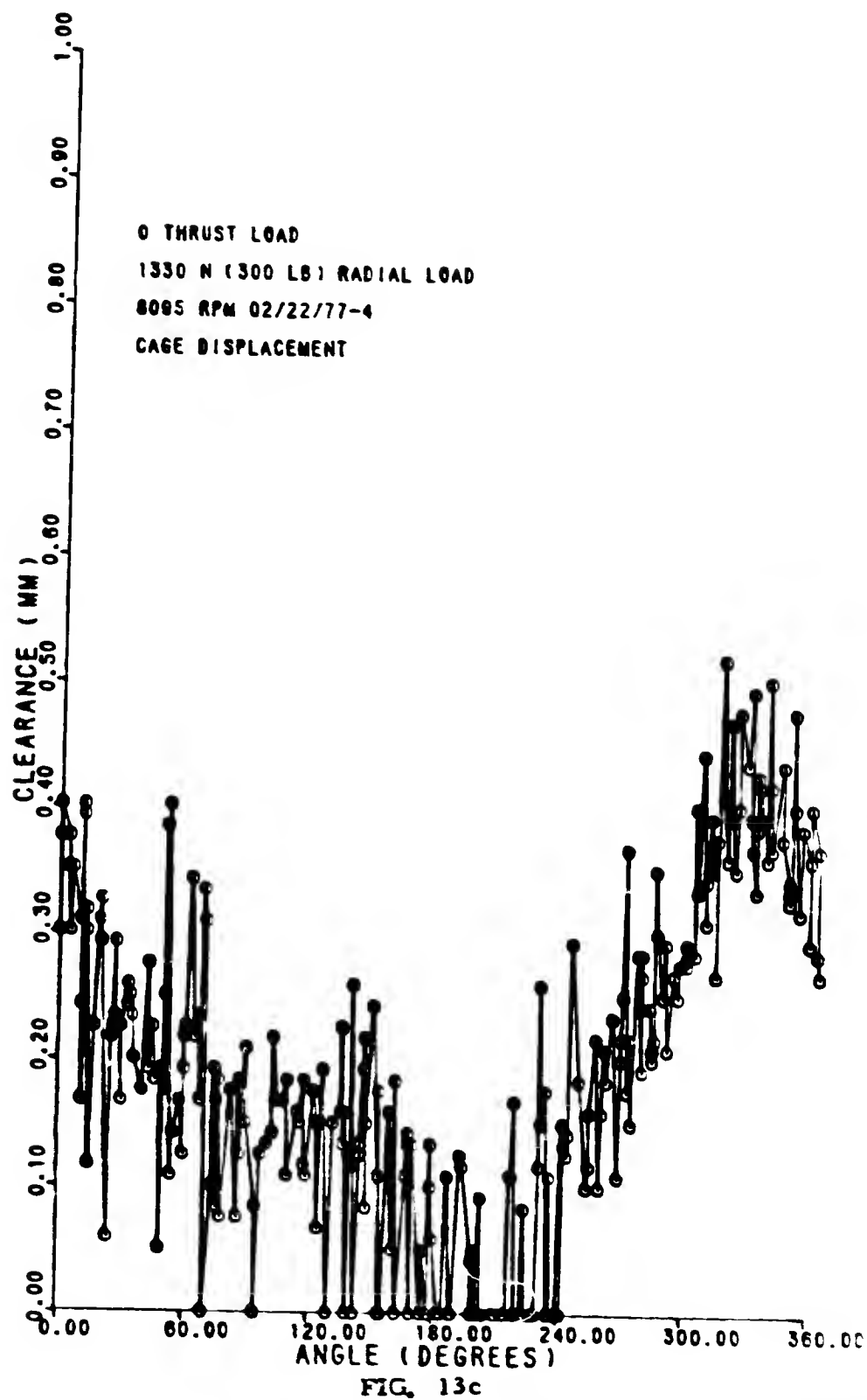


FIG. 13b

70090T9NYPANTT 06/09/77





70090119NYPAN9-06/09/77

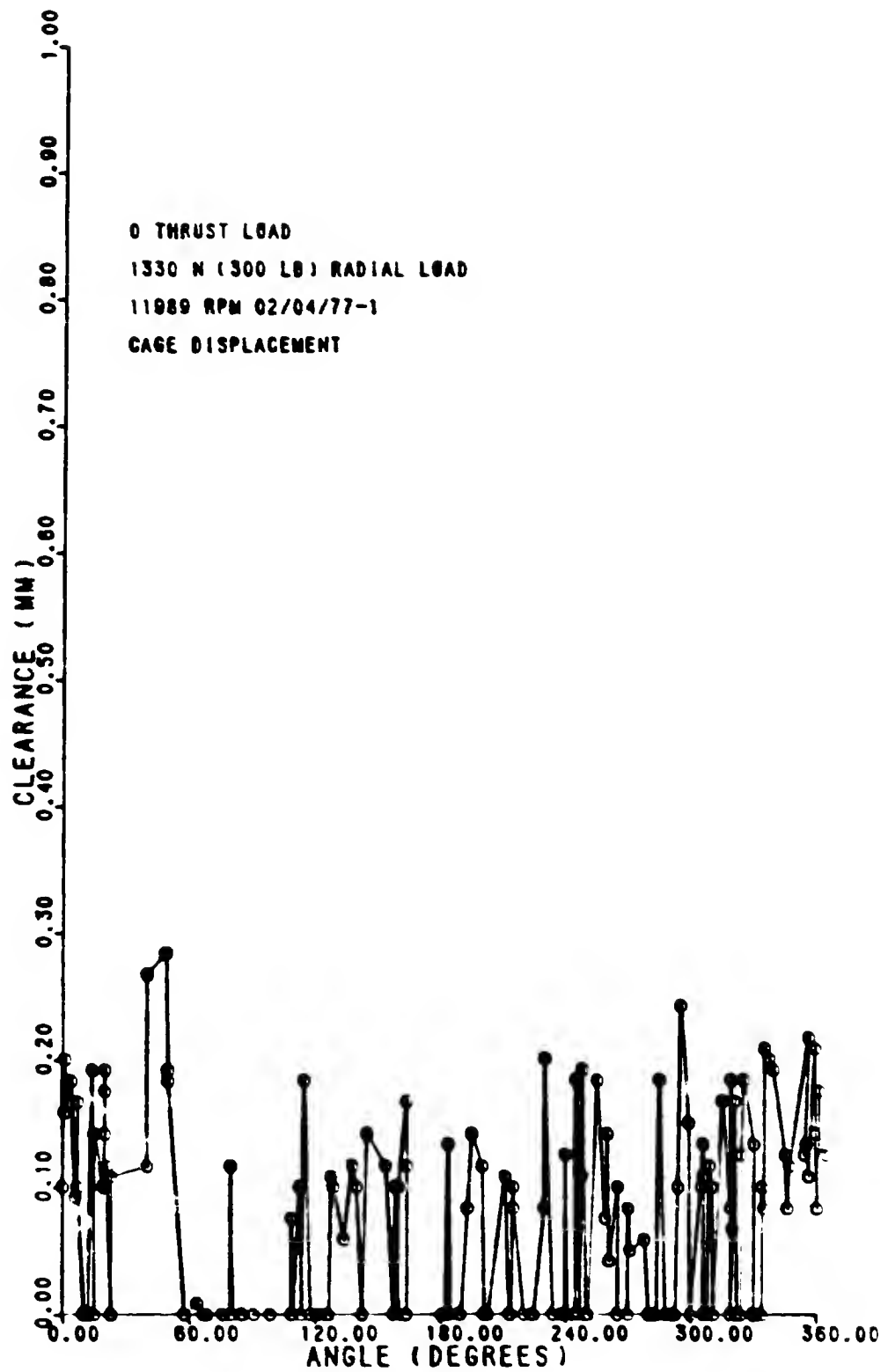


FIG. 13d

70050119NYPANIU

06/09/77

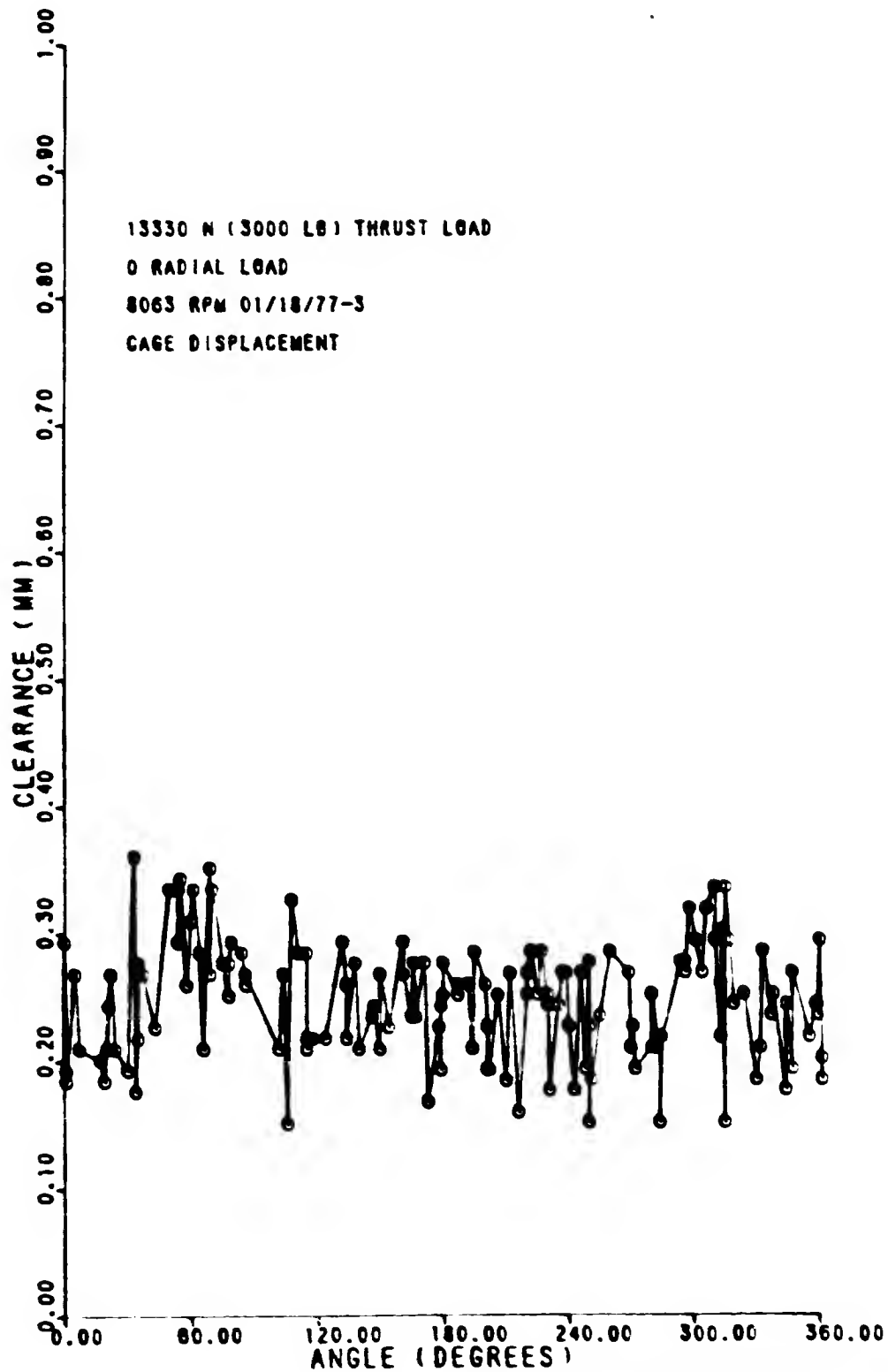


FIG. 13e

70090TTSNYPANT 3 06/30/77

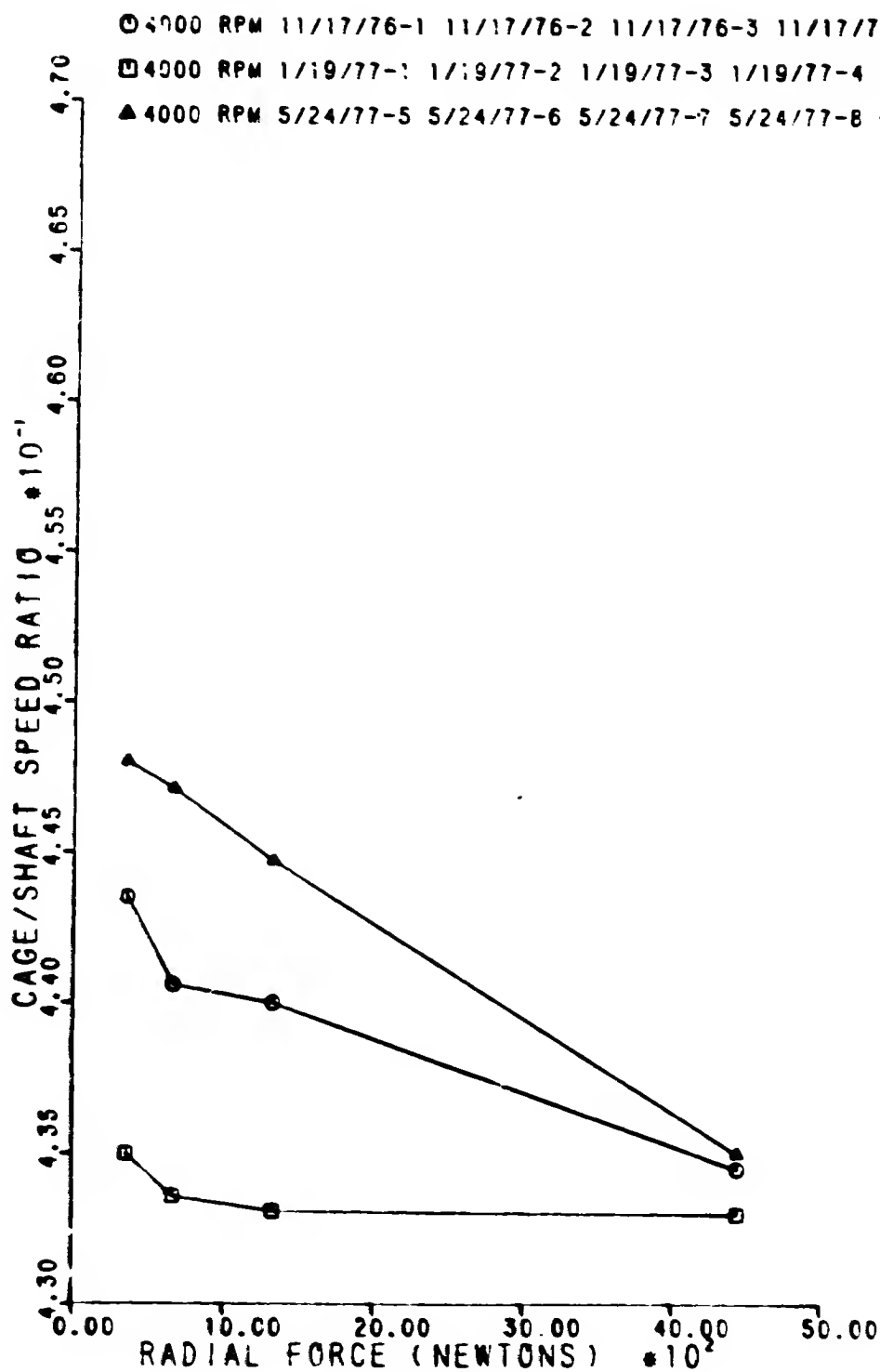


FIG. 14a

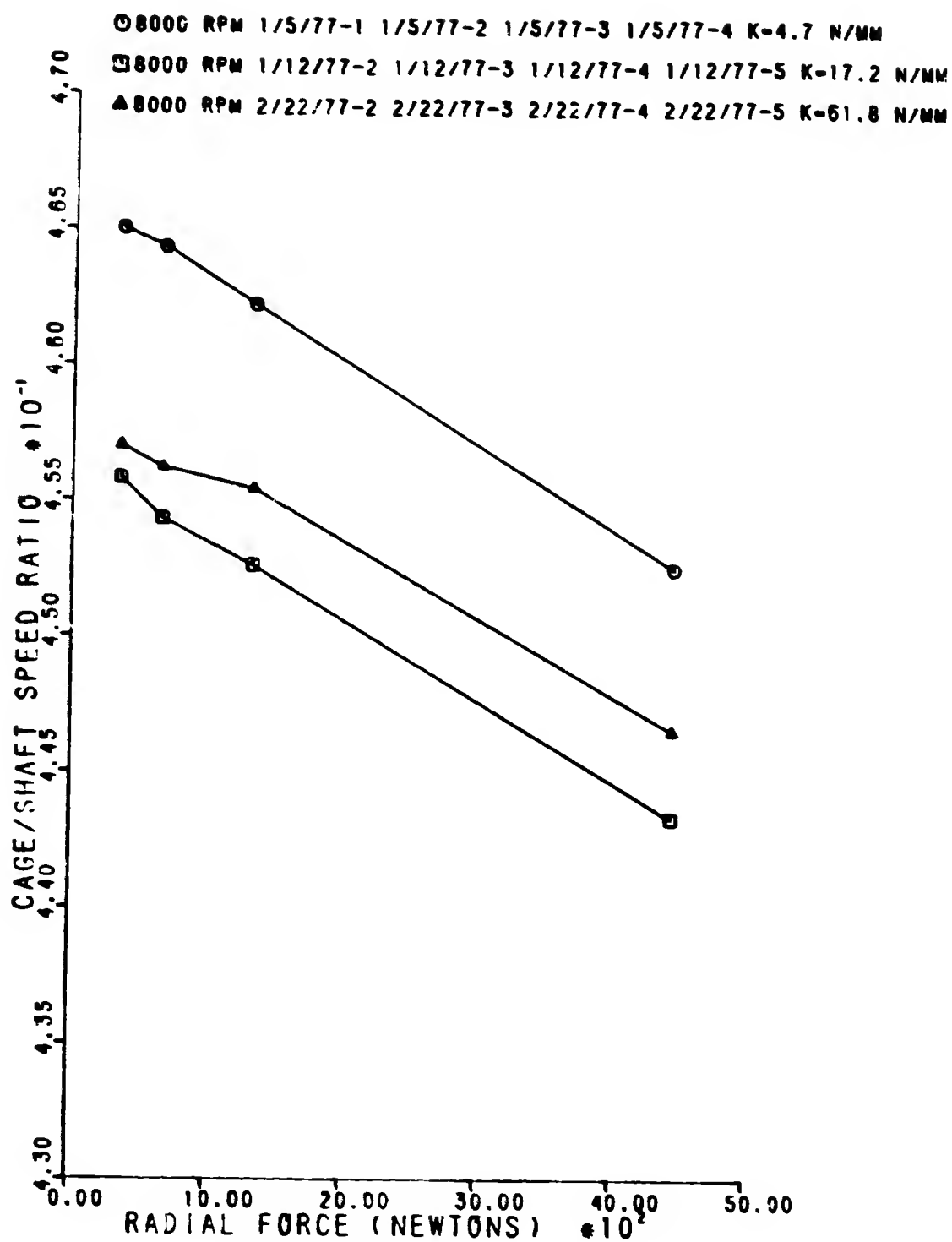


FIG. 14b

700901 1 5NYPAN13 - - 07/06/77

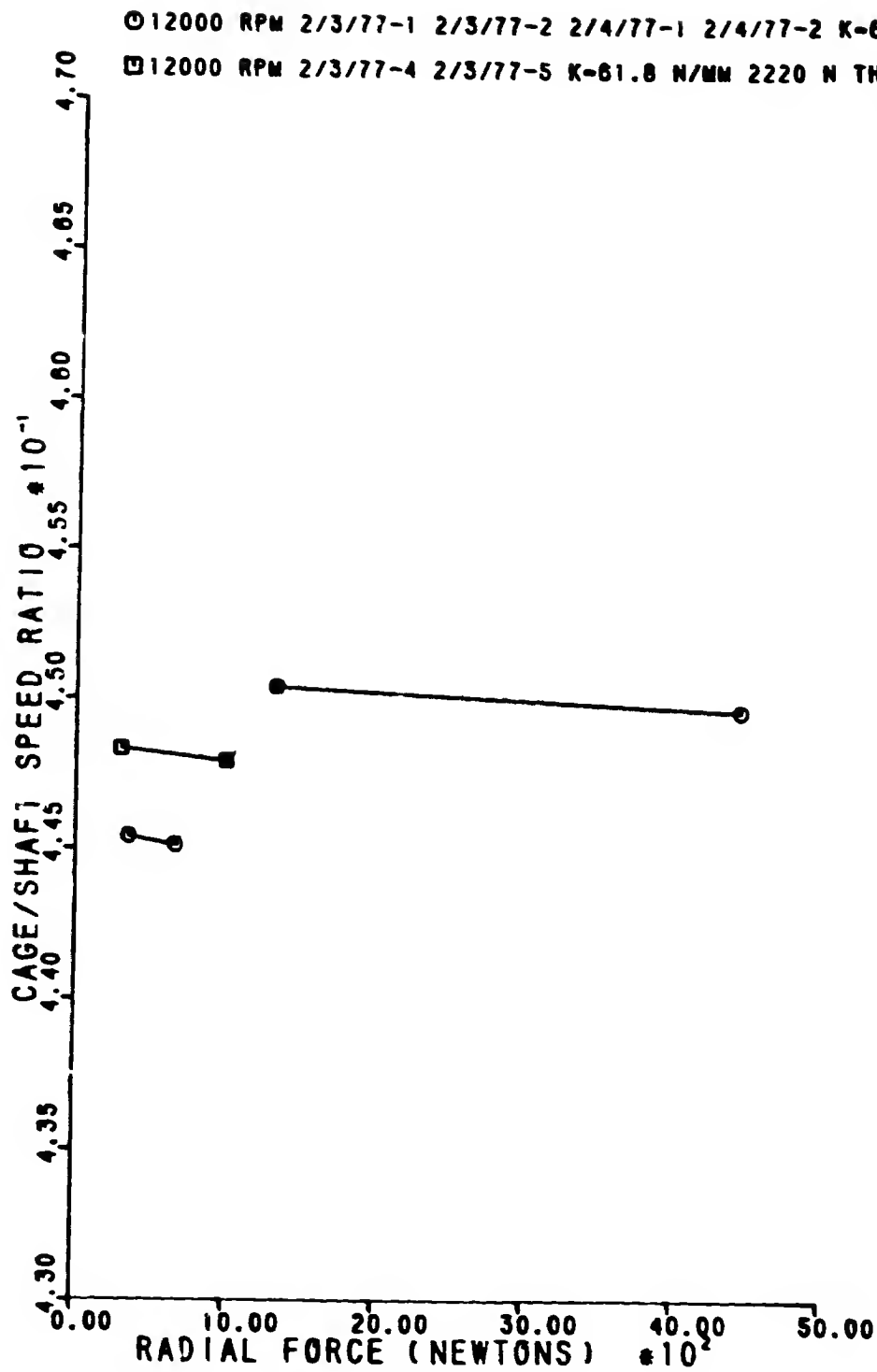
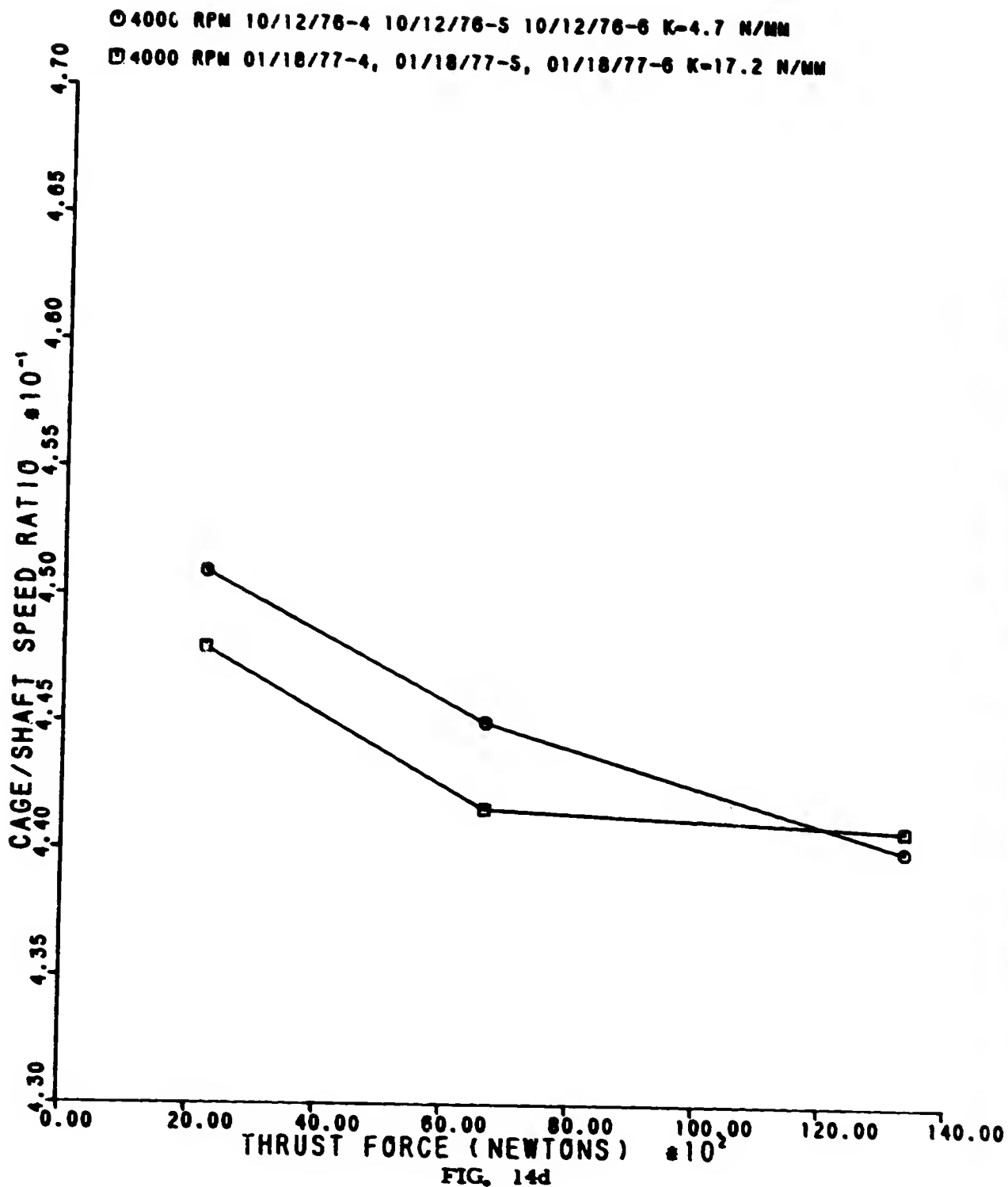
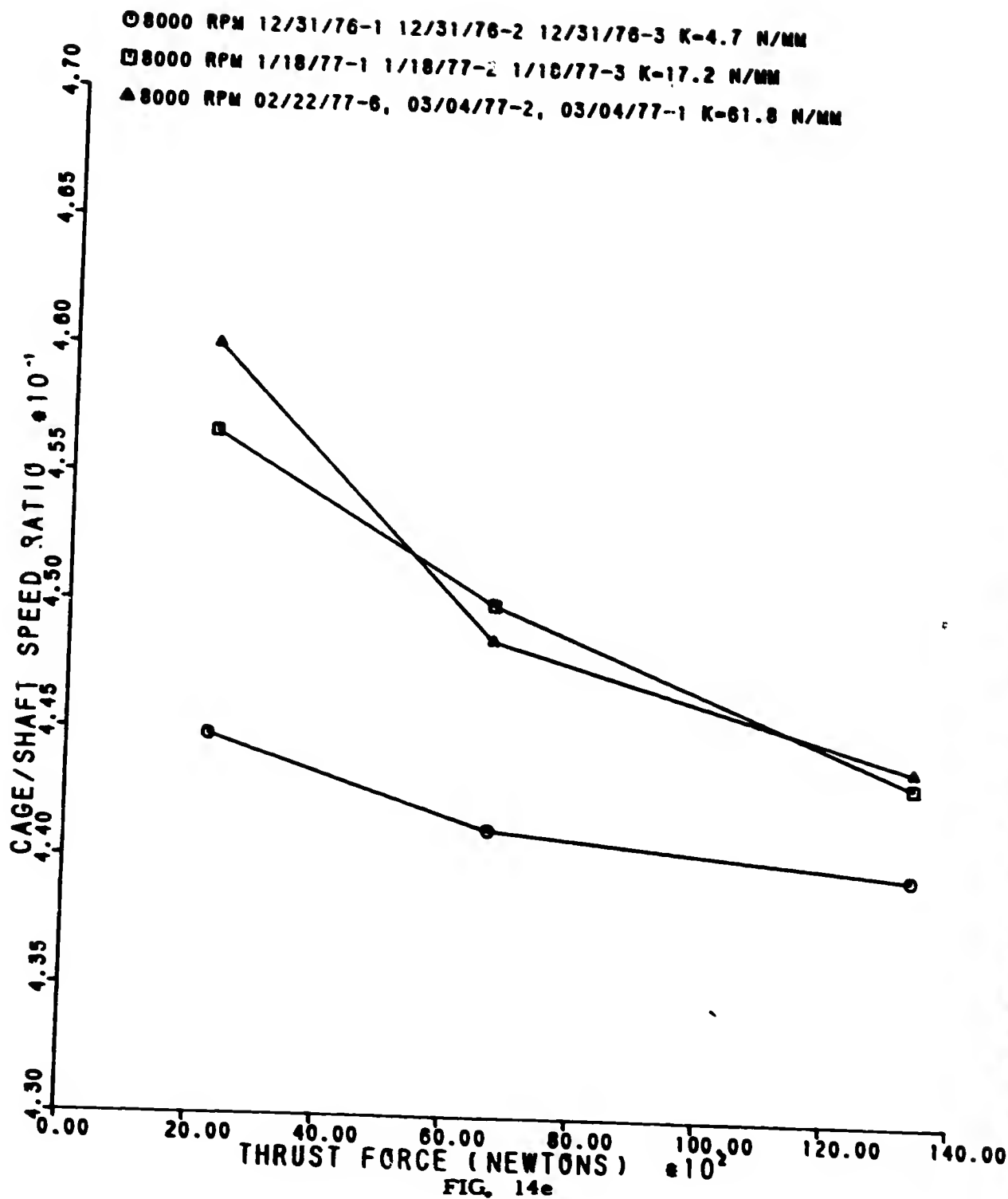


FIG. 14c

70501-13N1-1A1-1 07/06/77



7005019NY: PANT 07/06/77



70501-19NTPAN13-07/06/77

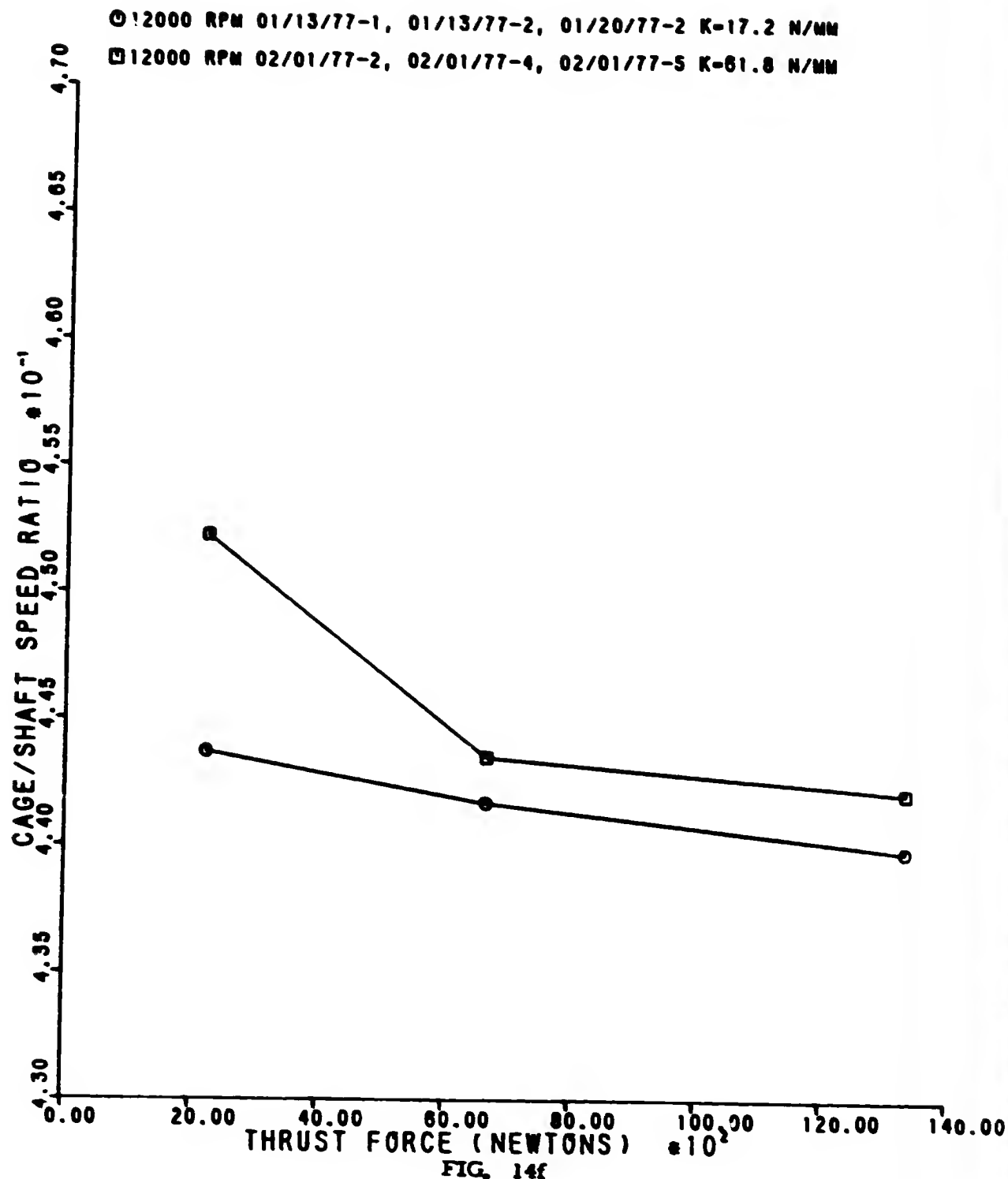




Table 1

Test Bearing Specifications

	<u>P/N 506110</u>	<u>P/N 506111</u>
Raceway Curvatures	52% Inner and Outer	52% Inner and Outer
Bearing Contact Angle	24°-27°**	24°-27°**
Bearing Mat'l, Races, Balls	CEVM-M-50-(R <sub>c</sub> 60 min)	CEVM-M-50 (R <sub>c</sub> 60 min)
Cage Mat'l	AMS-6415 (R <sub>c</sub> 28-33)	AMS-6415 (R <sub>c</sub> 28-33)
Cage Plating	Silver Plate Per AMS 2412	Silver Plate Per AMS 2412
Cage Plating Thickness, inches	.001-.002	.001-.002
Ball & Ring Stabili- zation Temp.	600°F	600°F
Balls		
Number	20	20
Nominal Dia., inches	0.750	0.750
Allowable Variation in Any Indiv. Ball Dia. & Sphericity, inches	0.000020 max.	0.000020 max.
Internal Radial Clearance*	.0048-.0060***	.0054-.0060 ***
Axial Play inches	.026 max.****	.024 max ****
Diametral Cage Clearance, in.	.016-.026	.019-.025
Bearing Inner Dia., inches	4.33070-4.33045	4.33070-4.33045
Bearing Outer Dia., inches	6.8898-6.8894	6.8898-6.8894
Inner Race Land Dia., inches	5.343 min.	5.334 min.
Outer Race Shoulder Dia., inches	6.077 max.	6.090 max.
Ball Pitch Dia., in.	5.650	5.635
Bearing Width	1.1811-1.1761	1.1811-1.1761

\*Same as Total Diametral Clearance

\*\*Measured Under 60 lb Thrust Load

\*\*\*Measured Under 33 lb Radial Load

\*\*\*\*Measured Under 22 lb Thrust Load

Table 2

SPEED, LOAD, AND SPRING CONSTANTSFigure 6  
4000 RPM Nominal Shaft Speed

Figure	Spring Constant	N/mm	N	Load (Lb)
6a	4.73	360	360	80 Radial
6a	17.2	360	360	80 Radial
6a	61.8	360	360	80 Radial
6b	4.73	667	667	150 Radial
6b	17.2	667	667	150 Radial
6b	61.8	667	667	150 Radial
6c	4.73	1330	1330	300 Radial
6c	17.2	1330	1330	300 Radial
6c	61.8	1330	1330	300 Radial
6d	4.73	4450	4450	1000 Radial
6d	17.2	4450	4450	1000 Radial
6d	61.8	4450	4450	1000 Radial
6e	4.73	2220	2220	500 Thrust
6e	17.2	2220	2220	500 Thrust
6f	4.73	6670	6670	1500 Thrust
6f	17.2	6670	6670	1500 Thrust
6g	4.73	13350	13350	3000 Thrust
6g	17.2	13350	13350	3000 Thrust
-	-	-	-	-

Figure 7  
8000 RPM Nominal Shaft Speed

Figure	Spring Constant	N/mm	N	Load (Lb)
7a	4.73	360	360	80 Radial
7a	17.2	360	360	80 Radial
7a	61.8	360	360	80 Radial
7b	4.73	667	667	150 Radial
7b	17.2	667	667	150 Radial
7b	61.8	667	667	150 Radial
7c	4.73	1330	1330	300 Radial
7c	17.2	1330	1330	300 Radial
7c	61.8	1330	1330	300 Radial
7d	4.73	4450	4450	1000 Radial
7d	17.2	4450	4450	1000 Radial
7d	61.8	4450	4450	1000 Radial
7e	4.73	2220	2220	500 Thrust
7e	17.2	2220	2220	500 Thrust
7e	61.8	2220	2220	500 Thrust
7f	4.73	6670	6670	1500 Thrust
7f	17.2	6670	6670	1500 Thrust
7f	61.8	6670	6670	1500 Thrust
7g	4.73	13350	13350	3000 Thrust
7g	17.2	13350	13350	3000 Thrust
7g	61.8	13350	13350	3000 Thrust

Figure 8  
12000 RPM Nominal Shaft Speed

Figure	Spring Constant	N/mm	N	Load (Lb)
-	-	-	-	-
-	-	-	-	-
8a	61.8	360	360	80 Radial
-	-	-	-	-
-	-	-	-	-
8b	61.8	667	667	150 Radial
-	-	-	-	-
-	-	-	-	-
8c	61.8	1330	1330	300 Radial
8c	61.8-2	1330	1330	300+2220N (500lb) (Thrust)
-	-	-	-	-
8d	61.8	4450	4450	1000 Radial
8d	61.8-2	4450	4450	1000+2220N (500lb) (Thrust)
-	-	-	-	-
8e	61.8	2220	2220	500 Thrust
-	-	-	-	-
-	-	-	-	-
8f	61.8	6670	6670	1500 Thrust
-	-	-	-	-
-	-	-	-	-
8g	61.8	13350	13350	3000 Thrust

Table 3

SPRING CONSTANTS AND BEARINGS USED

<u>Date Installed</u> <u>in Machine</u>	<u>Spring Constant</u>		<u>Bearing</u>
	<u>N/mm</u>	<u>Lb/in</u>	
June 1976	1.49	8.51	PWA 506110
August 18, 1976	4.73	27.0	PWA 506111
Jan. 12, 1977	17.2	98.2	PWA 506110
Jan. 28, 1977	61.8	353.0	PWA 506110

Table 4

CALCULATED NUMBER OF SHAFT REVOLUTIONS BETWEEN PHOTOGRAPHS

$\frac{\Delta\theta}{0} \text{ rev}$	$\frac{W}{s} = (\Delta\theta)_0 \frac{16 \times 60}{.441}$	$\frac{\Delta\theta}{s} \text{ rev}$	$\frac{W}{s} = (\Delta\theta)_s \frac{16 \times 60}{(-.559)}$
0 to 1	0 to 2,177 rpm	0 to -1	0 to 1,717 rpm
1 to 2	2,177 to 4,354	-1 to -2	1,717 to 3,435
2 to 3	4,354 to 6,531	-2 to -3	3,435 to 5,152
3 to 4	6,531 to 8,707	-3 to -4	5,152 to 6,869
4 to 5	8,707 to 10,884	-5 to -6	6,869 to 8,587
5 to 6	10,884 to 13,061	-6 to -7	8,587 to 10,304
		-7 to -8	10,304 to 12,021

\*For a cage to shaft speed ratio of 0.441

## Appendix J

```

00001 DIMENSION R(300,4),ANGLE(300),FORCE(300),ANGL(300)
00002 DIMENSION LINE1(8),LINE2(8),LINE3(6),LINE4(8)
00003 DIMENSION LINE5(4),FRM(300)
00004 DIMENSION XL(8),Y(8),YLB(20)
00005 INTEGER R,ANGLE
00006 ICN=0
00007 IC=0
00008 READ(5,30)S,AK,A
00009 30 FORMAT(2F10.0,I2)
00010 WRITE(6,31)S,AK
00011 31 FORMAT(1H1,8HNCICH = ,F6.0,7H AK = ,F6.4)
00012 WRITE(6,24)
00013 23 FORMAT(5X,110HZR1 ZR2 ZR3 ZR4 ZR2-ZR1 ZR3
00014 1-ZR1 ZR4-ZR1 ZR3-ZR2 ZR4-ZR3 ZR4-ZR2
00015 ZUR1=0.
00016 ZUR2=0.
00017 ZUR3=0.
00018 ZUR4=0.
00019 ZU1=0.
00020 ZU2=0.
00021 ZU3=0.
00022 ZU4=0.
00023 ZU5=0.
00024 ZU6=0.
00025 CO 21 I=1,N
00026 READ(5,11)IZR1,IZR2,IZR3,IZR4
00027 11 FORMAT(2X,I4,6X,I4,6X,I4,6X,I4)
00028 ZR1=IZR1
00029 ZR2=IZR2
00030 ZR3=IZR3
00031 ZR4=IZR4
00032 Z1=ZR2-ZR1
00033 Z2=ZR3-ZR1
00034 Z3=ZR4-ZR1
00035 Z4=ZR3-ZR2
00036 Z5=ZR4-ZR3
00037 Z6=ZR4-ZR2
00038 WRITE(6,24)ZR1,ZR2,ZR3,ZR4,Z1,Z2,Z3,Z4,Z5,Z6
00039 24 FORMAT(11F10.6)
00040 ZUR1=ZUR1+ZR1
00041 ZUR2=ZUR2+ZR2
00042 ZUR3=ZUR3+ZR3
00043 ZUR4=ZUR4+ZR4
00044 ZU1=ZU1+Z1
00045 ZU2=ZU2+Z2
00046 ZU3=ZU3+Z3
00047 ZU4=ZU4+Z4
00048 ZU5=ZU5+Z5
00049 ZU6=ZU6+Z6
00050 21 CONTINUE
00051 AZR1=ZUR1/FLOAT(N)
00052 AZR2=ZUR2/FLOAT(N)
00053 AZR3=ZUR3/FLOAT(N)
00054 AZR4=ZUR4/FLOAT(N)
00055 AZ1=ZU1/FLOAT(N)
00056 AZ2=ZU2/FLOAT(N)
00057 AZ3=ZU3/FLOAT(N)
00058 AZ4=ZU4/FLOAT(N)
00059 AZ5=ZU5/FLOAT(N)
00060 AZ6=ZU6/FLOAT(N)
00061 F1=S/AZ3
00062 SCZ1=AZ1*F1
00063 SCZ2=AZ2*F1
00064 SCZ3=AZ3*F1
00065 SCZ4=AZ4*F1
00066 SCZ5=AZ5*F1
00067 SCZ6=AZ6*F1
00068 WRITE(6,25)AZR1,AZR2,AZR3,AZR4,AZ1,AZ2,AZ3,AZ4,AZ5,AZ6
00069 25 FORMAT(1H0,11F10.3)
00070 WRITE(6,32)F1,AZ3
00071 32 FORMAT(1H0,5HFACTOR = ,F10.4,5X,8HNCICH = ,F6.0)
00072 WRITE(6,25)SCZ1,SCZ2,SCZ3,SCZ4,SCZ5,SCZ6
00073 READ(5,33)LINE3,LINE1,LINES
00074 33 FORMAT(6A4,8A4,4A4)
00075 READ(5,34)LINE2,LINE4
00076 34 FORMAT(8A4,8A4)

```

REPRODUCIBILITY OF THE  
ORIGINAL PAGE IS POOR

```

0077 WRITE(6,33) LINE3, LINE1
0078 WRITE(6,34) LINE2, LINE4
0079 WRITE(6,35) LINE5
0080 WRITE(6,26)
0081 26 FCRRAT(1H0, * R1 R2 R3 R4 R2-R1 R3-R1 R4-
0082 1R1 R3-R2 R4-R3 R4-R2 ANGLE D3-Z3 D4-Z4*)
0083 SU03=0.
0084 SU04=0.
0085 1001 IC=IC+1
0086 READ(5,18) R(IC,1), R(IC,2), R(IC,3), R(IC,4), ANGLE(IC)
0087 18 FORMAT(2X, I4, 6X, I4, 6X, I4, 6X, I4, 6X, I3)
0088 IF(1E0F(15), EQ, -1) GO TO 58
0089 ANGLE(IC)=ANGLE(IC)
0090 C1=R(IC,2)-R(IC,1)
0091 C2=R(IC,3)-R(IC,1)
0092 C3=R(IC,4)-R(IC,1)
0093 C4=R(IC,3)-R(IC,2)
0094 C5=R(IC,4)-R(IC,3)
0095 C6=R(IC,4)-R(IC,2)
0096 C7=D3-A23
0097 C8=D4-A24
0098 SLD3=SU03+D3
0099 SU04=SU04+D4
0100 GO TO 1001
0101 50 CONTINUE
0102 ID=IC-1
0103 AC3=SU03/FLCAT(IC)
0104 AD4=SU04/FLCAT(IC)
0105 F2=S/A03
0106 WRITE(6,35) F2, AD3, AD4
0107 35 FORMAT(1H0, 9HFACTOR = , F10.4, 5X, 2HNOTCH = , F6.0, 5X, 6HPIN = , F6.0)
0108 WRITE(6,26)
0109 20 FCRRAT(1H, * SC01 SC02 SC03 SC04 SC05 SC06 OI1 OI2
0110 1 OI3 OI4 AVER SOEV POLNCS NEWTON ANGLE D3-AC3 C4-AD4*)
0111 I=0
0112 XFORLB=0.
0113 YFORLB=0.
0114 ICOUNT=0
0115 SECTOR=18.
0116 CC 51 IC=1, ID
0117 G1=R(IC,2)-R(IC,1)
0118 G2=R(IC,3)-R(IC,1)
0119 G3=R(IC,4)-R(IC,1)
0120 G4=R(IC,3)-R(IC,2)
0121 G5=R(IC,4)-R(IC,3)
0122 G6=R(IC,4)-R(IC,2)
0123 C7=D3-AD3
0124 C8=D4-AD4
0125 SC01=G1*F2
0126 SC02=G2*F2
0127 SC03=G3*F2
0128 SC04=G4*F2
0129 SC05=G5*F2
0130 SC06=G6*F2
0131 C11=(SC01-SC02)
0132 C12=(SC02-SC03)
0133 C13=(SC03-SC05)
0134 C14=(SC05-SC06)
0135 AD=(OI1+OI2+OI3+OI4)/4.
0136 SOEV=SQRT(1+(OI1-AD)*(OI1-AD)+(OI2-AD)*(OI2-AD)+(OI3-AD)*(OI3-AD)+(OI4-AD)*(OI4-AD))/3.)
0137 FORCE(IC)=AD*AK*4.448
0138 FCRLB=AD*AK
0139 ANGLE=ANGLE(IC)
0140 IF (ANGLE.LE.SECTOR) GO TO 100
0141 I=I+1
0142 XLB(I)=XFCRLB/FLCAT(ICOUNT)
0143 YLB(I)=YFCRLB/FLCAT(ICOUNT)
0144 SECTOR=SECTOR+18.
0145 XFORLB=0.
0146 YFORLB=0.
0147 ICOUNT=0
0148 100 RANGLE=ANGLE(IC)*.017453
0149 XFORLB=(FCRLB*CCS(RANGLE))+XFCRLB
0150 YFORLB=(FCRLB*SIN(RANGLE))+YFCRLB
0151 ICOUNT=ICOUNT+1
0152

```

```

LA 0153 WRITE(6,22)SCD1,SCD2,SCD3,SCD4,SCD5,SCD6,CI1,CI2,CI3,CI4,AD,SDEV,
LA 0154 1FCR1B,FORCE(1C),ANGL(1C),DT,C9
LA 0155 22 FORMAT(1H,6F7.2,6F6.2,2F7.2,F5.0,2F8.0)
LA 0156 51 CONTINUE
LA 0157 WRITE(6,33)LINE3,LINE1
LA 0158 WRITE(6,34)LINE2,LINE4
LA 0159 WRITE(6,33)LINE5
LA 0160 TOTALX=0.
LA 0161 TOTALY=0.
LA 0162 SECTOR=0.
LA 0163 WRITE(6,101)
LA 0164 101 FORMAT(1H0,'SECTOR X FCRCES Y FCRCES')
LA 0165 CO 1G2 I=1,20
LA 0166 SECTOR=SECTOR+10.
LA 0167 WRITE(6,103)SECTOR,XLB(I),YLB(I)
LA 0168 103 FORMAT(1H0,F5.0,3X,F7.2,3X,F7.2)
LA 0169 TOTALX=TOTALX+XLB(I)
LA 0170 TOTALY=TOTALY+YLB(I)
LA 0171 102 CONTINUE
LA 0172 THETA=(ATAN(TOTALX/TOTALY))*57.2997
LA 0173 FCRC1=SQRT(TOTALX**2+TOTALY**2)
LA 0174 WRITE(6,104)THETA,FCRC1
LA 0175 104 FORMAT(1H0,'ANGLE=',F5.0,3X,'FCRC=',F7.2)
LA 0176 CALL PLOTS
LA 0177 CALL FLOT(1.5,5.5,-3)
LA 0178 CALL FACTCR(1.5)
LA 0179 ANGL(1C)=0.
LA 0180 ANGL(1C+1)=60.
LA 0181 CALL AXIS(0.,0.,15*ANGL(1C) (DEGREES),-15.0E.,0.,0.,E0. )
LA 0182 FORCE(1C)=0.
LA 0183 FORCE(1C+1)=5.
LA 0184 CALL AXIS(0.,-5.,15*FORCE(1C) (NEWTONS),-15.0E.,0.,0.,E0. )
LA 0185 CALL SYMBCL(-.6,-4.57,.10,105H-5.00 -4.00 -3.00 -2.00
LA 0186 1-1.00 0.00 1.00 2.00 3.00 4.00 5.00
LA 0187 2 .90.,105)
LA 0188 CALL SYMBCL(-.75,-1.06,.14,15*FORCE(1C) (POUNDS) .90.,15)
LA 0189 CALL SYMBCL(0.3,4.5,0.1 ,LINE1,0.0,32)
LA 0190 CALL SYMBCL(0.3,4.2,0.1 ,LINE2,0.0,32)
LA 0191 CALL SYMBCL(0.3,3.9,0.1 ,LINE3,0.0,24)
LA 0192 CALL SYMBCL(0.3,3.6,0.1 ,LINE4,0.0,32)
LA 0193 CALL SYMBCL(0.3,3.3,0.1 ,LINE5,0.0,16)
LA 0194 CALL PLOT(-.5,-4.45,3)
LA 0195 CALL PLOT(-.5,4.45,3)
LA 0196 CALL PLOT(-.56,-4.45,3)
LA 0197 CALL PLOT(-.5,-4.45,2)
LA 0198 CALL PLOT(-.56,-3.56,3)
LA 0199 CALL PLOT(-.5,-3.56,2)
LA 0200 CALL PLOT(-.56,-2.67,3)
LA 0201 CALL PLOT(-.5,-2.67,2)
LA 0202 CALL PLOT(-.56,-1.78,3)
LA 0203 CALL PLOT(-.5,-1.78,2)
LA 0204 CALL PLOT(-.56,-.89,3)
LA 0205 CALL PLOT(-.5,-.89,2)
LA 0206 CALL PLOT(-.56,0.,3)
LA 0207 CALL PLOT(-.5,0.,2)
LA 0208 CALL PLOT(-.56,0.89,3)
LA 0209 CALL PLOT(-.5,0.89,2)
LA 0210 CALL PLOT(-.56,1.78,3)
LA 0211 CALL PLOT(-.5,1.78,2)
LA 0212 CALL PLOT(-.56,2.67,3)
LA 0213 CALL PLOT(-.5,2.67,2)
LA 0214 CALL PLOT(-.56,3.56,3)
LA 0215 CALL PLOT(-.5,3.56,2)
LA 0216 CALL PLOT(-.56,4.45,3)
LA 0217 CALL PLOT(-.5,4.45,2)
LA 0218 NPTS=IC-1
LA 0219 CALL LINE (ANGL,FCRC,NPTS,1,1,1)
LA 0220 CALL PLOT(0.,0.,559)
LA 0221 END

```

REPRODUCED FROM  
ORIGINAL PAGE IS 100%

USASI FORTRAN DIAGNOSTIC RESULTS FOR FTN.MAIA

NO ERRORS  
(ALIB,CALCCNF,ALX-LIBRARY)

LEO

AME

**END**

**DATE**

**FILMED**

**OCT 12 1977**